

Evolutionary bursts drive morphological novelty in the world's largest skinks

5

Ian G. Brennan ^{*1,2}, David G. Chapple³,
J. Scott Keogh², Stephen Donnellan^{4,5}

¹Natural History Museum, Cromwell Road, London SW7 5BD, UK

²Division of Ecology & Evolution, Research School of Biology,
Australian National University, Canberra, ACT 2600 Australia

³School of Biological Sciences, Monash University
Clayton, VIC Australia

⁴ School of Biological Sciences, The University of Adelaide,
Adelaide, SA Australia

⁵South Australian Museum, North Terrace, Adelaide SA 5000 Australia

10 *Keywords:* Morphological evolution, Simpsonian, skink phylogenomics.

*Corresponding author: iangbrennan@gmail.com

Summary

Animal phenotypes evolve and diverge as a result of differing selective pressures and drift. These processes leave unique signatures in patterns of trait evolution, impacting the tempo and mode of morphological macroevolution. While there is a broad understanding of the history of some organismal traits (e.g. body size), there is little consensus about the evolutionary mode of most others. This includes the relative contribution of prolonged (Darwinian gradualist) and episodic (Simpsonian jump) changes towards the evolution of novel morphologies. Here we use new exon-capture and linear morphological datasets to investigate the tempo and mode of morphological evolution in Australo-Melanesian Tiliquini skinks. We generate a well-supported time-calibrated phylogenomic tree from ~400 single-copy nuclear markers for more than 100 specimens including undescribed diversity, and provide unprecedented resolution of the rapid Miocene diversification of these lizards. By collecting a morphological dataset that encompasses the lizard body plan (19 traits across the head, body, limb, and tail) we are able to identify that most traits evolve conservatively but infrequent evolutionary bursts result in morphological novelty. These phenotypic discontinuities occur via rapid rate increases along individual branches, inconsistent with both gradualistic and punctuated equilibrial evolutionary modes. Instead, this ‘punctuated gradualism’ has resulted in the rapid evolution of blue-tongued giants and armored dwarves in the ~20 million years since colonizing Australia. These results outline the evolutionary pathway towards new morphologies and highlight the heterogeneity of evolutionary tempo and mode, even within individual traits.

Introduction

Great variations in organismal morphology are expected to accumulate over long periods of time and reflect the varied requirements of different species^{1,2}. Some organisms are very small and some are very large, others are brightly colored and others cryptic, and through drift and selection, traits respond and diverge from common forms. Despite the dramatic variety we see in nature, on deep timescales, measures of these differences (variance, disparity, *et al.*) often fail to exceed the expectation of a neutral model where the accumulation of variation is the result of a random evolutionary walk through time (Brownian Motion)^{3,4}. In other words, Earth's flora and fauna realize only a fraction of all possible shapes and sizes⁵. This diversity undershoot suggests bounds on phenotypes as a result of genetic, functional, or developmental constraints^{6,7}. If constant and gradual processes are unlikely explanations for the accumulation of trait diversity at deep timescales, then how important are heterogeneous processes at shallower ones?

When traits are assumed to evolve under an unbiased random walk (Brownian Motion), trait variance (v) is proportional to evolutionary rate (σ^2), and the accumulation of variance is dictated by elapsed time (t ; so $v=\sigma^2 t$). This exploration of trait space (diffusion) is characterized by trait change along branches drawn from a normal (Gaussian) distribution, and assumes a flat adaptive landscape^{8,9}. Given observed trait limits, correlations among traits, and the “clumpiness” of extant morphological diversity, this seems an unlikely expectation^{2,10}. In practice, morphological evolution is often concentrated on one or a small number of major axes. The primary axis serves as a ‘line of least resistance’¹¹ providing a pool of variation on which selection can act. However evolution is not limited to the major axis, and trajectories along minor axes may also pave a path towards new phenotypes. These competing processes are sometimes called “elaboration” (*along* major axis) and “innovation” (*away* from major axis)^{12,13}. However their relative contributions towards organismal macroevolution and the evolution of novel forms has been largely overlooked^{13–15}.

Almost 80 years ago G.G. Simpson suggested novelty arose by rapid “jumps” to new adaptive zones across an uneven landscape¹⁶. To explore this landscape, one potential path requires relaxing our assumption that traits evolve consistently across lineages—changing the *mode* of evolution. Proposed alternative evolutionary models such as pulsed or punctuated processes account for rapid jumps in just such a way—by deviating only in the evolutionary *mode*—leaving variance to accumulate as under BM. Another pathway however requires relaxing our assumption that traits evolve via constant rates through time—changing the *tempo* of evolution. These relaxed-rate methods are implemented in Variable Rates or Multi-Regime models of trait evolution. Traditionally, jumps have been difficult to identify without fossil data. This is due in part to the limited information content at internal nodes of a phylogenetic tree, however, even in fossil studies debate has continued about gradual versus pulsed/punctuated evolution^{17,18}. Recent advances in phylogenetic comparative methods however, provide the tools to distinguish between gradual and punctuated evolutionary modes, and suggest that pulsed evolution and rate heterogeneity may be common processes^{19–24}. Investigating these patterns and processes in extant systems provides a potentially valuable comparison against the paleontological foundation on which many of these ideas were built.

When studying the morphological evolution of any empirical group differences in evolu-

tionary mode and tempo are potentially compounded by mosaic evolution—which suggests that processes may vary widely across individual traits and the modules they make up. So when looking for macroevolutionary shifts towards new phenotypes, changes may be temporally, phylogenetically, or regionally (across the body) heterogeneous. Just a century ago 80 these complications seemed impossible to address: “To select a few of the great number of structural differences for measurement would be almost certainly misleading; to average them all would entail many thousands of measurements for each species or genus compared”²⁵. Modern comparative methods however, have made these comparisons possible^{26–28}. Here we investigate the relative roles these sources of variation play, by focusing on the Tiliquini 85 skinks. Tiliquines consist of ~62 species with varied ecologies, high levels of sociality^{29,30}, and highly imbalanced biogeographic richness. The majority of species (~48 spp.) are endemic to Australia where their distributions span the continent’s highest alpine peaks and most inhospitable deserts. To survive in such varied climes, tiliquines have diverged into herbivorous giants that roam the treetops, spiky socialites that live communally in rock 90 crevices or complex burrows, and elongate long-lived slow-movers that wander across open lands. These ecotypes have diagnosable morphologies, and the modest species richness of the group allows high-dimensional macroevolutionary study to be computationally tractable. Additionally, tiliquines are ideally suited for studies of the tempo and pace of morphological evolution because they have been suggested to show a morphological gradient with highly 95 derived phenotypes nested deeply within a generally conserved body plan^{30,31}.

But to what degree are these morphological deviations *remarkable*, and what tempo and mode have they evolved by? To answer these questions we started by generating an exon-capture dataset for Tiliquini skinks and reconstructing the phylogenetic relationships of this group. To look at morphological evolution we collected an extensive phenotypic dataset of 19 100 linear measurements which summarize broad axes of variation across the head, body, limbs, and tail. Finally we incorporate these data into a multivariate framework for comparing evolutionary rates and disparity of traits (and the modules they compose) relative to a neutral BM model of evolution. From this we are able to show that (1) most traits show heterogeneous—not neutral or incremental—evolutionary histories, (2) evolutionary bursts 105 are temporally and phylogenetically distributed but uncommon, and (3) these jumps result in morphological novelty that can exceed uncorrelated trait expectations.

Results

Phylogenetic Analyses and Divergence Dating

We present a well-resolved phylogeny that provides unprecedented resolution of Tiliquini 110 skinks representing all genera and 63 taxa (102 samples) across this continental lizard radiation. Concatenated (Fig.S16) and coalescent-consistent species trees (Fig.1) return broadly similar topologies with the exception of a handful of extremely short internal branches (Fig.S17). Discordant branches fall within the anomaly zone³² in which concatenation is likely to be mislead by the contribution of a large number of anomalous gene trees. In support of this, these nodes as represented in our coalescent species tree generally have low gene 115 concordance factors (gCFs) and equivocal site concordance factors (sCFs), but are strongly

supported by individual topology tests (see Supplementary Materials [Topology Tests](#)). Of these contentious nodes, two have taxonomic implications. *Lissolepis* is not recovered as monophyletic, with *L. coventryi* estimated as sister to *Liopholis*, and *L. luctuosa* more closely related to the remaining tiliquines (*Cyclodomorphus*, *Tiliqua*, *Bellatorias*, *Egernia*). We also find *Cyclodomorphus* to be non-monophyletic, with the *C. gerrardii* group more closely allied with *Tiliqua* than with the *C. maximus* group.

Branches that define many of the inter-generic relationships among Australian tiliquines are the result of a series of rapid speciation events occurring 15–21 mya. Most of these branches are shorter than a million years long, and several of which are less than 500k years long. These rapid divergences contrast with the deep splits between Australian tiliquines and their sister taxon *Corucia* (30 mya; 95% HPD: 27–35 mya), as well as the preceding split from *Tribolonotus* (60 mya; 95% HPD: 55–64 mya) (Fig.1,[S1](#)).

Phenotypic Analyses

Modularity and integration model selection in *EMMLi*³³ identified a four module model with separate within module correlations (intramodule integration varies among modules) and separate among module correlations (intermodule integration varies among modules) as the best fit to our data.

15 of 19 morphological traits are best fit by variable rate or pulsed models (Fig.[S14](#)) as well as the summary trait encapsulating size. The abundant preference for heterogeneous evolutionary models encouraged us to focus on the evolution of traits and modules under the Variable Rates model for all further analyses. The major axis of morphological variation (elaboration; PC1) across the Tiliquini and across each genus is primarily explained by tail length (Fig.[S28](#)—[S30](#)). The major axis of morphological innovation (PC2) varies when considering the clade as a whole (interlimb length) or individual genera (primarily size and/or interlimb length). The relationship between elaboration and innovation, however, varies among genera. We visualize this through varied slopes between our first two PC axes, highlighting different paths to phenotypic novelty (Fig.2).

Comparing the slopes of disparity accumulation curves highlights periods of significant morphological conservatism (tail module 20–15 mya) and expansion (body and limb modules 18–14 mya; tail module 3 mya–present). Periods of expansion generally—but not always—coincide with periods of increased mean evolutionary rates (Fig.3). Little information can be extracted from the early evolution of this group (75–30 mya), as estimates along bare branches leading to *Tribolonotus* and *Corucia* likely do not reflect the evolution of extinct unsampled lineages along these edges. Discretizing morphological change as primarily elaborative or innovative allows us to identify that both processes happen at clade and species-level scales (Fig.2).

Averaging rates however, hides pulses of extreme rate variation (Fig.4). We identified pulses by isolating branches with at least twice the background evolutionary rate (mean scalar $r \geq 2$) that were shifted in at least 70% of the sampling posterior. Across 19 focal traits, roughly 13% branches exhibited a significant rate pulse, with more than 3% showing major shifts in evolutionary rate (mean scalar $r > 10$) (Fig.[S11](#)). Major shifts were primarily concentrated in head width, interlimb length, tail length and width, and upper arm length. In modules, nearly 16% of branches exhibited significant rate pulses, with 2% showing major

¹⁶⁰ shifts, concentrated in tail and body modules. Many rate increases are concentrated in the *Cyclodomorphus*–*Tiliqua* clade, with particularly rapid rates among *Cyclodomorphus michaeli*, *casuarinae*, and *praealtus*. Body and tail traits also commonly show rate pulses in the crevice dwelling *Egernia stokesii* and *depressa* clades. Under relaxed-rate models rate pulses transfer into bursts in morphological change. We are able to visualize these ¹⁶⁵ morphological jumps along individual branches (Fig.6), highlighting instances which lead to novel phenotypes.

¹⁷⁰ Simulations under uncorrelated and correlated Brownian Motion show differences in the accumulation of trait combinations. This highlights how evolution can be biased along particular axes (Fig.5, S6). Empirical traits generally conform to BM expectations, however extreme phenotypes exceeding BM predictions have evolved in the feet of *Tiliqua* and tails of some *Egernia* (Fig.5, S18–S22).

Discussion

The variety of organismal forms provides a rich source of data for macroevolutionary biologists investigating the timing and accumulation of morphological diversity. Whether ¹⁷⁵ morphological disparity has accumulated early¹, uniformly³⁴, or via intermittent pulses^{2,20,23} remains a contested topic at varied evolutionary scales. Here we investigate the morphological evolution of the tiliquine skink body by looking across time, phylogeny, and body regions to better understand the modes by which traits evolve. We provide evidence for Tiliquini skinks that most traits evolve conservatively, but morphological novelty accumulates through extreme punctuations—jumps into new trait space. Our findings are consistent with evidence from the fossil record that major transitions to new phenotypes may occur over short intervals^{14–16}. In Tiliquini skinks these jumps are uncommon (0.003–0.05 jumps/my), do not follow an established morphological order³⁵, and can be nested to develop new trait combinations.

¹⁸⁵ Phylogenomics of the Tiliquini

Skinks are one of the most species-rich reptile groups, making up roughly 25% of all lizard diversity (1700+ species). The largest and most impressive skinks belong to the tribe Tiliquini which are primarily distributed across Australia with a small number of species found in Indonesia, Papua New Guinea, and the Solomon Islands. Despite their importance as models ¹⁹⁰ of reptilian sociality^{29,36} and recent fossil discoveries^{31,37,38}, phylogenetic hypotheses for the Tiliquini have relied on a handful of molecular markers and limited species sampling^{30,39,40}. Our exon capture dataset provides a well supported estimate of the relationships among all eight Tiliquini genera and 85% of described species. In agreement with previous estimates we recover the Tiliquini as members of the Lygosominae alongside the Sphenomorphini, ¹⁹⁵ Eugongylini, and Mabuyini (Fig.S1), suggesting an Asian origin for the subfamily⁴¹.

Living tiliquines are divided into three clades, comprising the enigmatic Crocodile Skinks *Tribolonotus*, the monotypic Solomon Islands endemic *Corucia*, and an Australian radiation. Splits among these groups are old (~60 & ~30 mya), and followed by the rapid Miocene divergence of all Australian Tiliquini genera (23–15 mya). These rapid speciation events result

200 in short internal branches that prove difficult to resolve on a per-locus basis (Fig.1,S26). However, most of these difficult nodes are resolved by leveraging our ~400 loci in ASTRAL, investigating summary statistics, and applying topology tests. Our new phylogenetic hypotheses of these nodes has necessitated that we propose taxonomic changes for two genera, which we provide in the attached Appendix ([Taxonomic Implications and Changes](#)). Some
205 splits remain intractable however. The branching patterns among major *Egernia* clades, and the series of splits among *Lissolepis luctuosa*, *Liopholis*, and the remaining Australian tiliquines have splits so short (300–400ky) that they exist at the limits of phylogenetic reconstruction. Regardless of resolution of these difficult branches, the radiation of Australian Tiliquini into divergent ecologies and morphologies happened rapidly and in concert across
210 open landscapes, closed forests, deserts, and mountain peaks.

Evolving Novel Phenotypes by Bursts

Earth's incredible biodiversity of forms and functions have evolved over hundreds of millions of years. Growing evidence suggests that much of this diversity accumulated via short periods of rapid phenotypic change, not by incremental divergence²³. If this is true and pulsed
215 morphological evolution is common, then it is important to understand how it contributes to the development of morphological novelty and diversity. To do this we identified how pulses are distributed through time, across the phylogeny, and among morphological axes. We provide evidence of highly heterogeneous patterns of morphological trait evolution in Tiliquini skinks, with truly novel phenotypes resulting from rapid episodic changes.

220 Much of modern macroevolutionary thinking relies on Simpson's (1944) idea of adaptive zones. The varied adaptive landscape accumulates diversity as lineages traverse into new adaptive zones that are centered around fitness peaks. Lineages move into new zones by evolutionary jumps—rapid movement across suboptimal space. In comparative studies the idea of a multipeak morphological landscape is often described by multi-optima OU
225 models^{44–46}. While these models account for the clustering of species around discrete trait values (evolutionary ‘clumpiness’) they do not explain well the process of movement across the landscape to occupy new peaks. Our analysis of the tiliquine lizard body plan provides evidence that pulses in evolutionary rate and coincident phenotypic change are common across many morphological traits (preferred in 15 of 19 traits), but are likely rare events
230 relative to slower background evolution. This suggests that large distances of trait space can be quickly traversed to reach new morphological realms, and these realms are likely wide. When comparing modeled empirical data to gradualist simulations, jumps are observable as large trait changes along individual branches (Fig.6). However, the accumulation of morphological disparity does not appear to be dictated solely by rare jumps, or to occur explicitly
235 at speciation, as in the punctuated equilibrium model of Eldredge & Gould⁴⁷. Instead, we find broad support for a model in which the background process of evolution by a random walk (Brownian Motion) is punctuated by bursts in evolution that result in jumps to new adaptive zones. We consider this process more akin to the “punctuated gradualism” model of Malmgren et al. (1983)⁴⁸. While we recognize that our inferred process is not entirely
240 consistent with the original description which proposed punctuations between evolutionary *stasis* and gradualism, we suggest that these distinctions may instead be indicative of similar processes occurring at different scales along the micro-to-macroevolutionary continuum. At

both scales, a heterogeneous mode driven by an increase in evolutionary rates facilitates the evolution of novel and divergent morphologies (Fig. 4)—in the case of these lizards, this
245 occurs against a background morphological diffusion process. In this way we attempt to find common ground for both Darwinian and Simpsonian evolution.

In the Variable Rates model branch-specific shifts are indicative of an increase in evolutionary rate but remain a parameter of a random walk (Brownian) process. So, increasing the evolutionary rate suggests an increase in the *evolvability* and ultimately the potential variance of a lineage⁴⁹. An alternative interpretation of our identification of rate bursts could instead be a directional (biased) trend towards distinct trait values. A recently designed method for addressing this—the *fabric* model of *BayesTraits*⁵⁰—proposes that excess rate estimates could instead be absorbed by a biased walk to new trait space. Importantly, this does not fundamentally change the outcome that evolution has veered into a new morphological lane, but it does suggest a difference in the evolutionary mode. Whereas a rate pulse suggests a rapid, random exploration of trait space that lands in a new zone, directional trends elicit a guided evolutionary walk (e.g. via selection) towards a new area of trait space. Because a guided walk is directional the evolutionary rate need not be rapid. Regardless, the jump in trait value along a branch, and evolution of a new phenotype remains the same.
250
255 This provides an appealing explanation for scenarios where selection might be particularly effective, such as in small populations or those with high trait variances.

Importantly, inferred phenotypic jumps happen along both the primary morphological axis—where they exaggerate existing variance (elaboration)—and along minor morphological axes—where they develop novel trait combinations (innovation). Along both major
260 and minor axes relatively uncommon but major discontinuities result in unusual and novel morphologies, as seen in birds⁵¹ and fish⁵². In Tiliquini skinks, the most obviously novel phenotypes belong to the Bluetongue lizards *Cyclodomorphus* and *Tiliqua*. Bluetongues concurrently underwent dramatic shifts in limb and body modules, extending the length of the body and shortening the limbs. Subsequent jumps in head and tail modules resulted
265 in further temporally staggered morphological bursts. These nested morphological pulses gave rise to broad heads and bodies, dwarfed extremities and stumpy tails in *Tiliqua*, highlighting that truly new morphologies can arise from rapid exploration of multiple body axes. However, some of the most dramatic changes have happened on the shortest timescales. In the *Cyclodomorphus michaeli* clade (*C. casuarinae*, *C. michaeli*, *C. praealtus*) which we estimate at less than 4 million years old, we identify jumps in tail, limb, and body traits.
270 These result in the rapid shortening of the interlimb, tail, and leg lengths in *C. praealtus*, and lengthening of these traits in *C. casuarinae* and *C. michaeli*. Interestingly, these changes are potentially driven not by mechanistic morphological reasons but instead by physiological ones. *C. praealtus* lives at high elevations where shortened extremities may be advantageous
275 to maintain thermal mass following Allen’s Rule⁵³.

Occasionally independent evolutionary trajectories arrive at similar adaptive zones, a process usually called morphological convergence. We identify convergence in the spiny crevice-dwelling clades of *Egernia* (*E. stokesii* and *E. depressa*). These clades have undergone rapid shortening and widening of the tail from non-armored, long-tailed ancestors (Fig. 4).
280 Amazingly, these clades have both arrived at this novel phenotype via rate increases of roughly ten times the background rate. The repeated evolution of a distinct phenotype like highly modified tails suggests strong selective pressures shaping some morphological

axes⁵⁴. Another example of the strength of selection concerns the only clade of primarily crepuscular and nocturnal tiliquines the *Liopholis kintorei–inornata* group. This clade is broadly distributed across arid and semi-arid Australia, living in burrows they dig in loose soil or sand. However, the transition of these skinks towards a nocturnal lifestyle does not appear to have driven exceptional morphological differentiation from other *Liopholis*, except for the size of their eyes. The transition in diel activity is coincident with a jump in eye diameter and even the evolution of vertical pupils in the Night skink *Liopholis striata* (Fig. S11). Despite the evolution of novel morphologies by phenotypic bursts, truly exceptional morphologies (those exceeding Brownian expectations) are rare. In a few cases, such as the feet of some *Tiliqua* and the tails of some *Egernia*, contemporary trait values fall outside what we expect under a uncorrelated random walk model. These instances provide the strongest cases for active selection driving the evolution of phenotypes (Fig. 5).

300 **Conclusions**

Animal bodies are made up of many morphological traits which in their myriad combinations contribute to Earth's amazing biodiversity. Our study of gross lizard morphology provides evidence that trait evolution is heterogeneous, and is structured phylogenetically, temporally, and across the body-plan. This adds to a growing body of evidence that morphological traits diverge through evolutionarily discontinuous processes. These discontinuities contribute substantially towards the evolution of novel morphologies, and we suggest that this may be a common process in morphological diversification across animals that helps reconcile Darwinian and Simpsonian evolution.

Acknowledgments

310 A considerable thank you to the curators and staff of the many Australian museums and databases for access to tissues and locality data that made this work possible. We greatly appreciate the assistance of Emily Lemmon Moriarty, Alan Lemmon, and Michelle Kortyna in generating AHE data for this project. We thank Mark Hutchinson, Kailah Thorn, and Mike Lee for sharing their expertise in Tiliquini skinks, and colleagues in Natalie Cooper's lab at the NHM for their insight. JSK, SCD, and DGC thank the Australian Research Council for ongoing support, including grants LP170100012 and FT200100108 to DGC. IGB is supported by a Marie Skłodowska-Curie Fellowship funded by the European Commission. We appreciate the constructive assessments of three anonymous reviewers who challenged us to improve this research.

320 **Author Contributions**

Conceptualization, IGB, JSK, SD; sampling, JSK, SD.; analysis, IGB; funding acquisition/resources, JSK, SD, DCG; data curation, DCG, IGB; writing—original draft, IGB; writing—reviewing & editing, all authors.

Competing Interests

- ³²⁵ The authors recognize no conflicts of interest, either direct or indirect, that might bias the conclusions, implications, or opinions stated in this work.

Figures

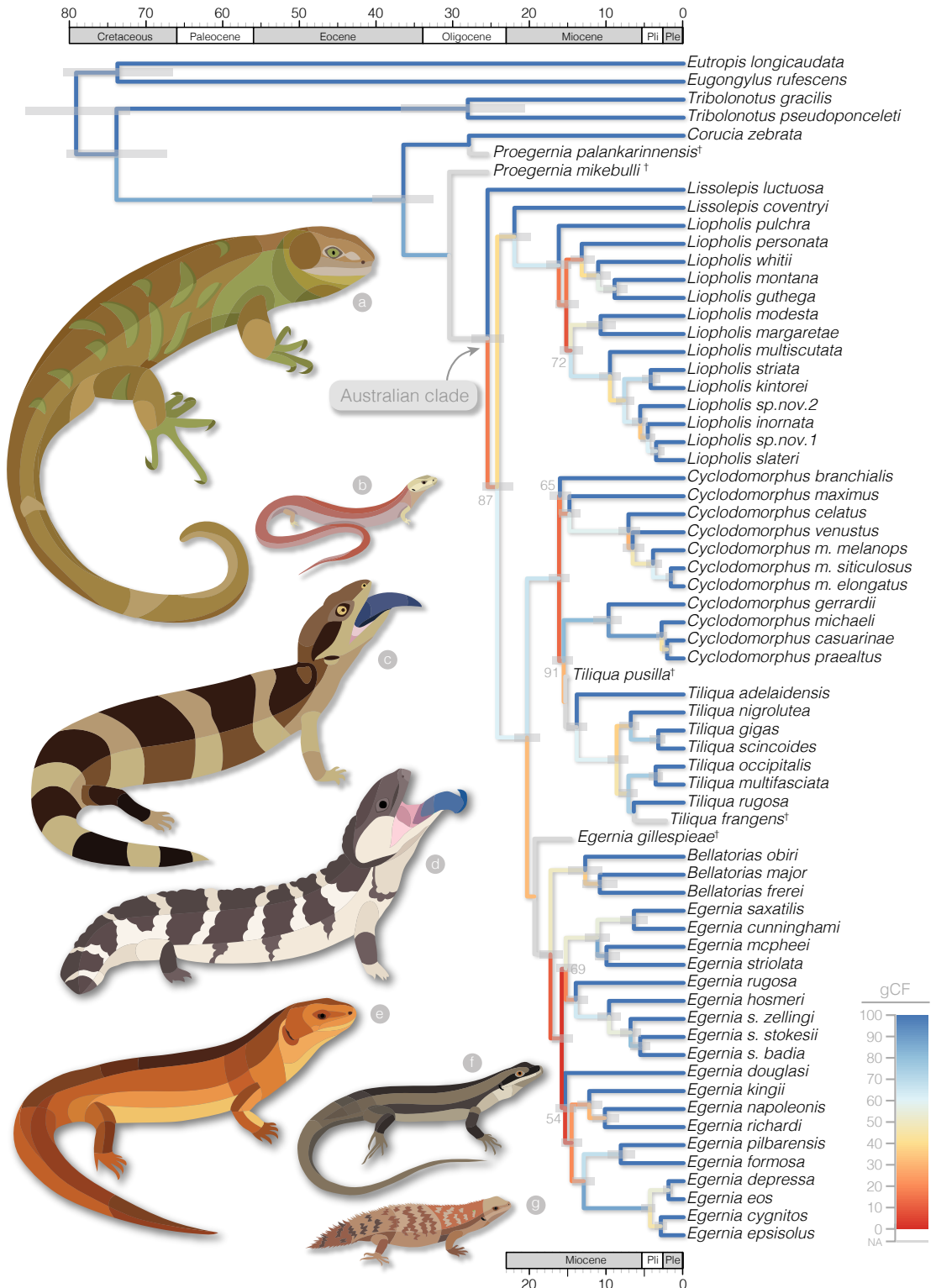


Figure 1: Species tree caption below.

Figure 1. Species tree estimated with ASTRAL and time-calibrated with MCMCTree shows late Oligocene or early Miocene divergences of most major Australian Tiliquini skinks, in contrast to a Cretaceous divergence from *Tribolonotus* and late Eocene divergence from the monotypic *Corucia*. Local posterior supports for all nodes are 100, except where indicated by grey numbers at nodes. Branches are colored according to gene concordance factors (gCF)—the proportion of gene trees which support the given bifurcation—to highlight areas of discordance among genetrees. For illustrative purposes fossil taxa (†) have been placed in the dated molecular tree following a combined evidence analysis in BEAST. Animals illustrate the diversity of size and shape across the Tiliquini: (a) *Corucia zebra*, (b) *Cyclodomorphus michaeli*, (c) *Tiliqua occipitalis*, (d) *Tiliqua rugosa*, (e) *Egernia rugosa*, (f) *Egernia striolata*, (f) *Egernia depressa*.

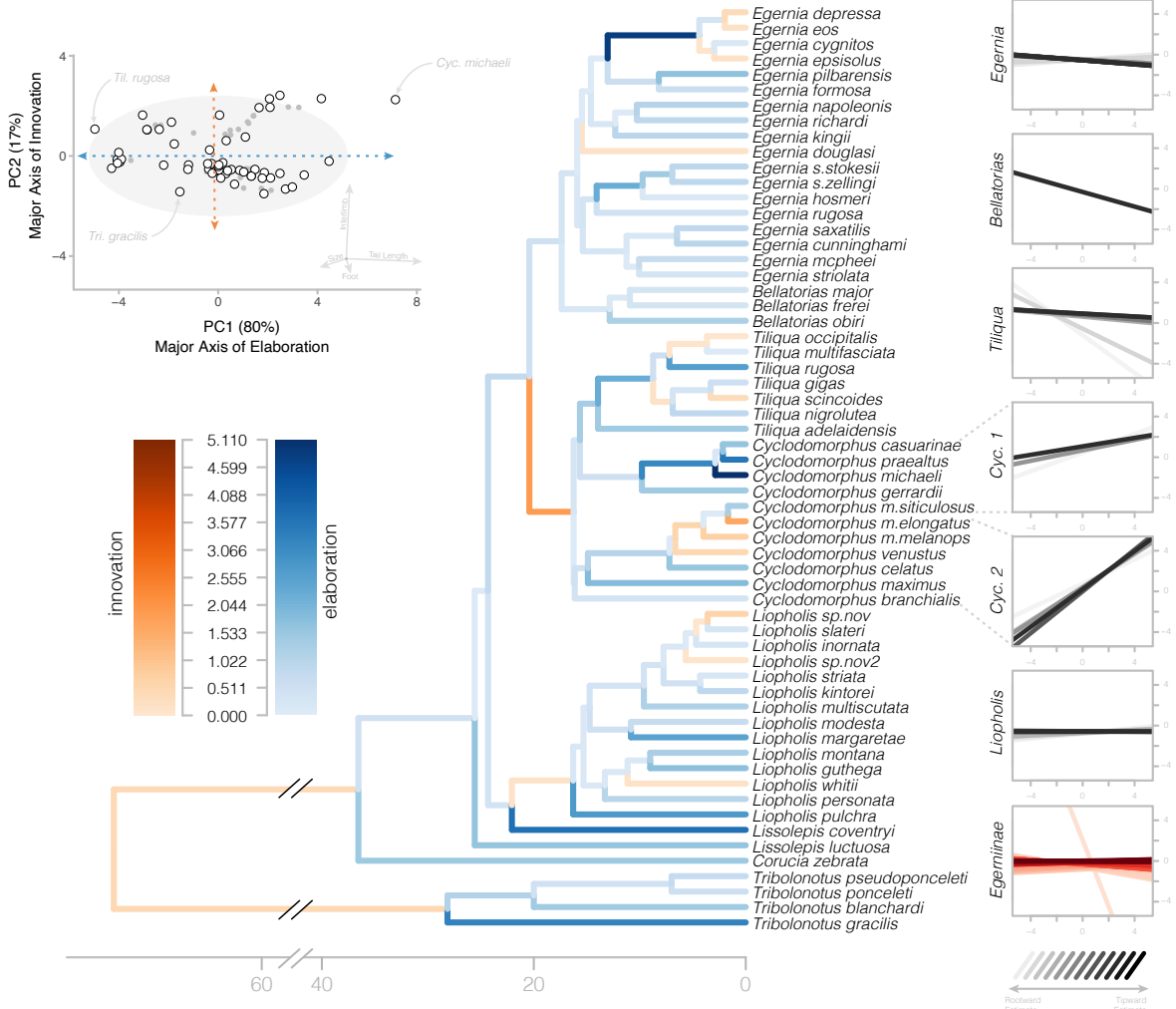


Figure 2: Major and minor axes of morphological change allow us to identify periods of elaboration (along PC1-blues) and innovation (along PC2-oranges) in Tiliquini skinks. Top left—biplot of first two principal components show the distribution of observed species (white circles with black outlines) and estimated ancestors (grey circles) along the major axis of elaboration and innovation. Colored branches on the tree at center indicate the primary direction of morphological change from ancestor to descendant node. Blue branches indicate principally elaborative change, while orange branches indicate principally innovative change. Color saturation (light to dark) indicates the Euclidean distance travelled in PC space along that branch. At right we visualize the varied relationships between these axes among groups. For each clade (genera and group as a whole) we plot the evolution of the relationship between elaborative and innovative axes through time from the root of the clade (lightest regression) to the tips (darkest regression). Regression plots highlight the varied patterns of subclades, including strong conservatism of *Liopholis* and novelty of *Cyclodomorphus*.

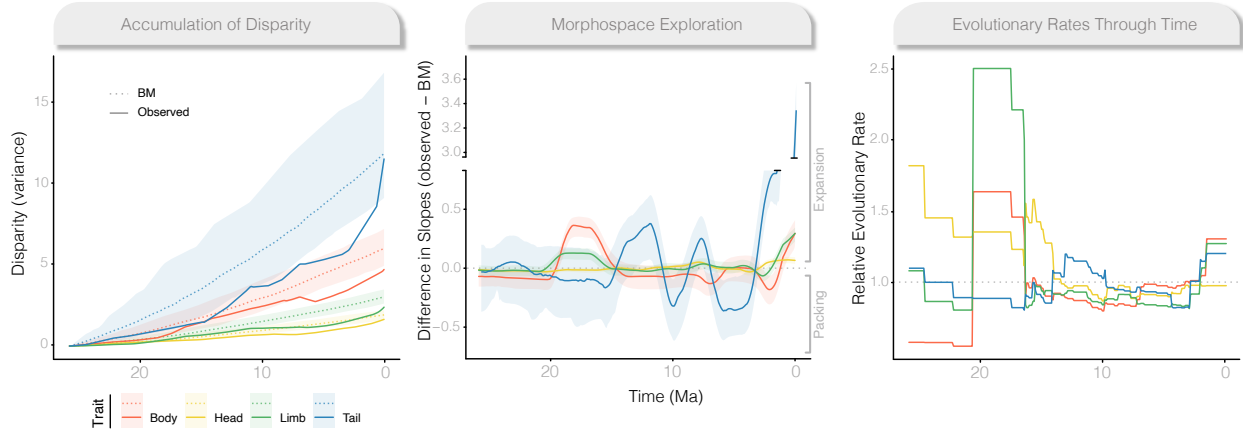


Figure 3: Evolutionary trajectories vary widely across modules and through time. (left) Accumulation of multivariate disparity (as variance) through time for each module (solid lines) compared to Brownian Motion (dotted lines). (center) The comparison of slopes of each module to BM highlights periods of morphological expansion (values greater than 0) and conservatism (values less than 0). (right) Evolutionary rates across modules are highly heterogeneous (see three different scales for y axis), showing periods of temporal variability, as well as high variances within modules and among traits (Fig.S23–S25). Figures represent analyses of the Australian clade alone to avoid bias in estimated rates and diversity as a result of long bare branches leading to *Corucia* and *Tribolonomotus*. For comparison with patterns estimated from data including these taxa, see Fig.S31.

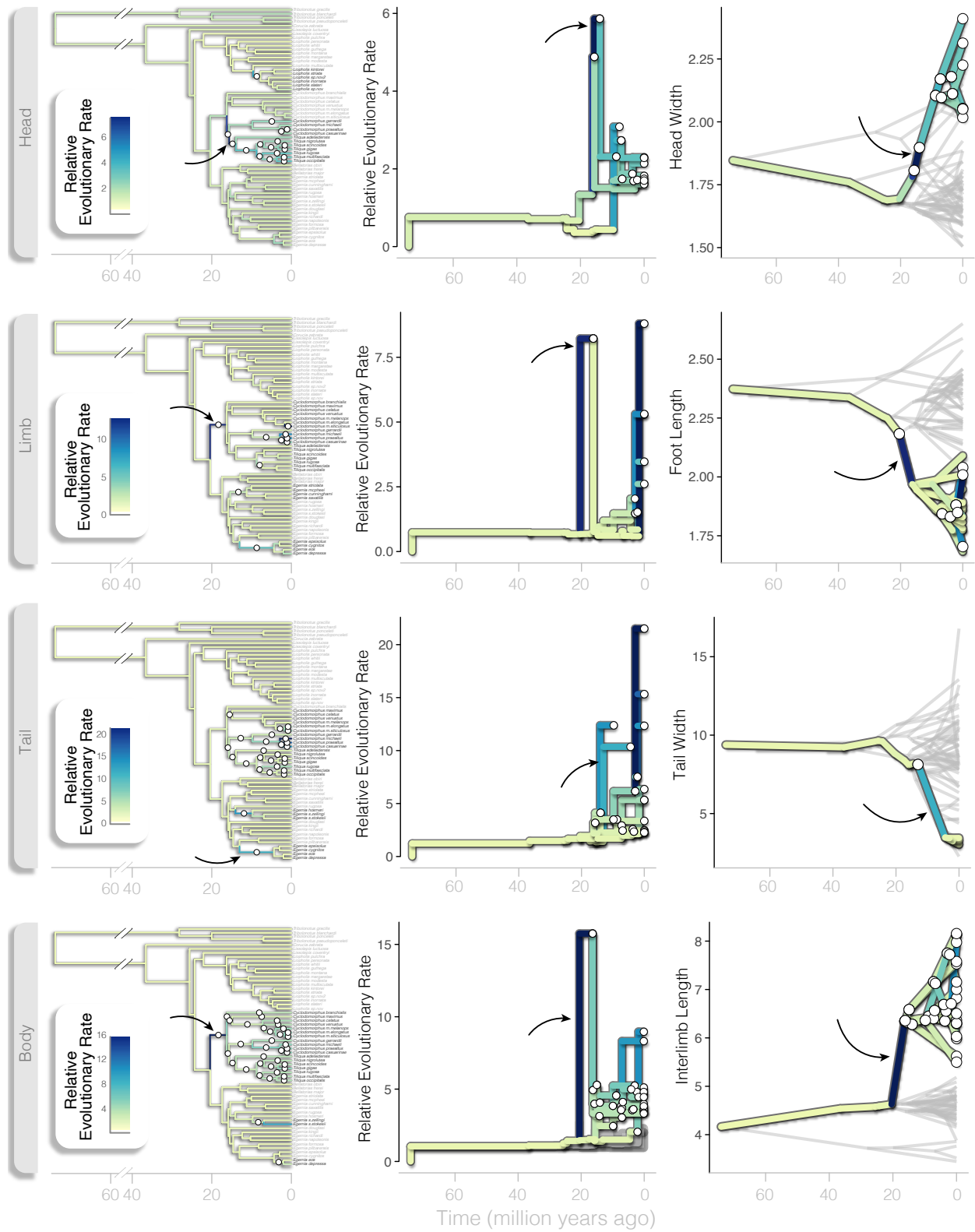


Figure 4: Rates caption below.

Figure 4. Bursts in rates of phenotypic evolution are distributed across the Tiliquini tree and exhibit strong departures from background rates. Rows represent morphological modules. In all plots branch colors correspond to estimated multivariate evolutionary rates, with significant rate changes noted by white circles at nodes or along branches. (left column) Tiliquini species trees highlighting the location of multivariate rate pulses. (center column) Branch rate trajectories plotted from the root node to nodes that show significant rate shifts (estimated rate scalar $r > 2$). Solid grey envelope contains 95% quantiles of background evolutionary rates (estimated rate scalar $r < 2$) with the mean plotted in dark grey. (right column) Phenograms of an individual trait from each module showing the evolution of extreme phenotypes driven by bursts in evolutionary rate. In each row, a black arrow highlights a single branch of interest across all three plots.

340
345

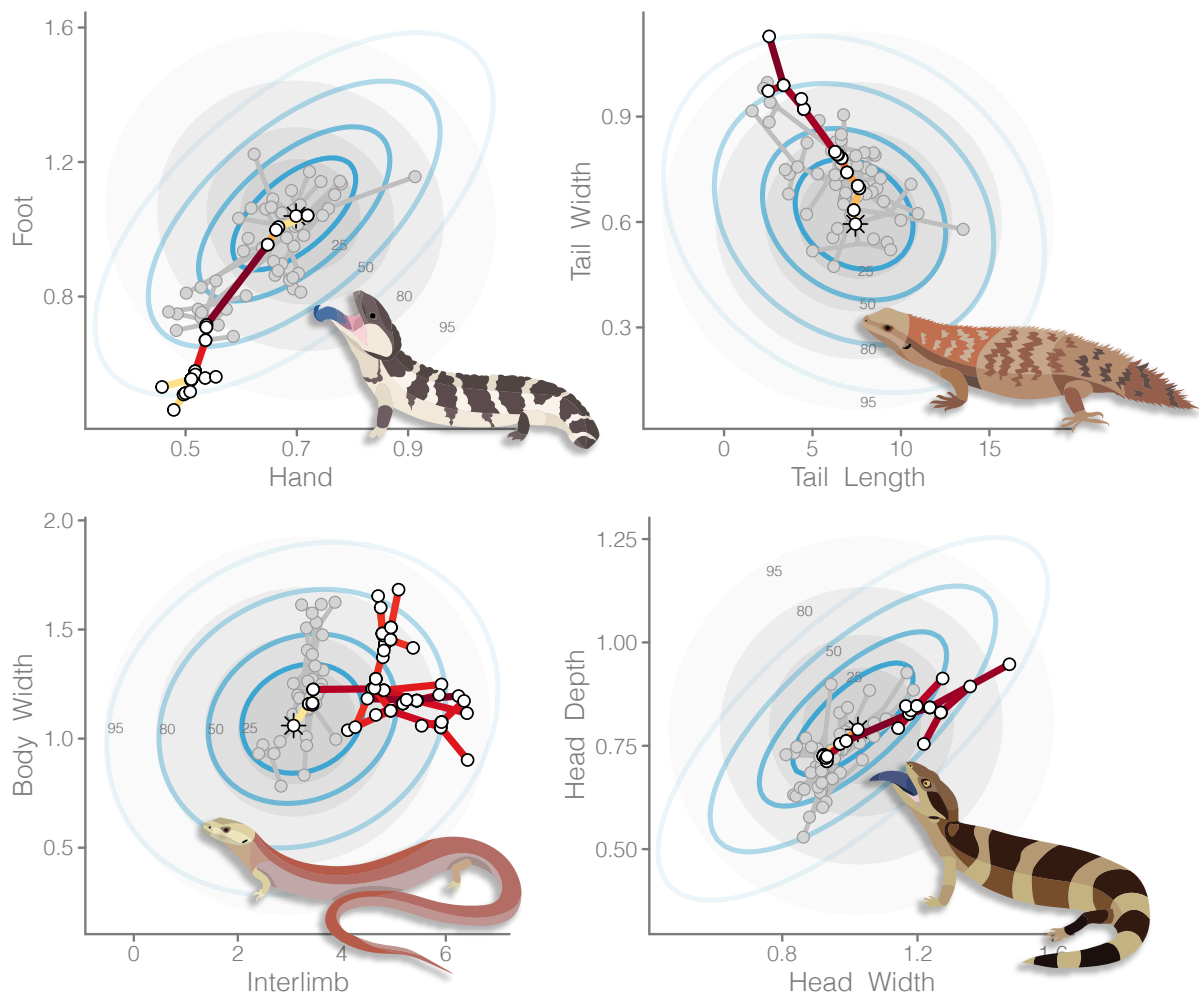


Figure 5: Novel morphologies exceed expectations of uncorrelated trait evolution. Bivariate plots show a phylomorphospace (species points connected by a phylogeny) of the Tiliquini. Each plot isolates a single clade within the group to highlight morphological extremes. Branches of the highlighted clade are colored according to evolutionary rates, with remaining species and branches in grey. In the background are ellipses containing 25/50/80/95% of traits simulated under empirical rates for uncorrelated (grey) and correlated (blue rings) Brownian Motion. Highlighted clades are (clockwise from top left: *Tiliqua*; *Egernia stokesii*–*E.hosmeri*, *Tiliqua rugosa*–*T.gigas*, *Cyclodomorphus*–*Tiliqua*).

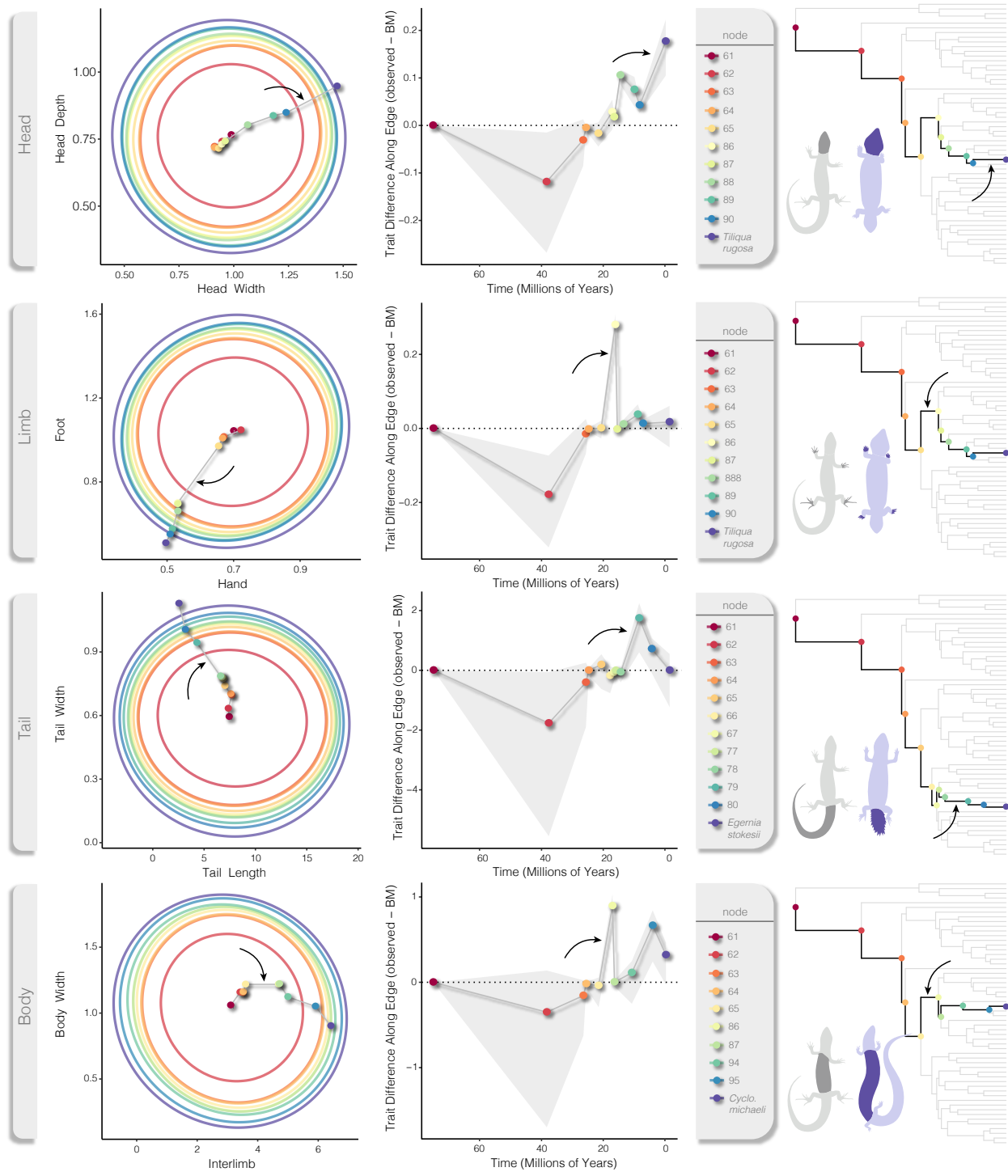


Figure 6: Phenotypic jumps caption below.

Figure 6. Phenotypic jumps are visible as greater than expected trait changes along branches, as estimated under the Variable Rates model and compared to Brownian Motion. Rows correspond to morphological modules, noted in grey at far left. Both circular (left column) and line plots (center column) show the evolutionary trajectory of focal traits from the root of the Tiliquinis

tree (node 57, dark red) to a single tip (dark purple) that has exhibited one or more rate bursts. (left) Large colored rings represent the simulated distribution of trait values under uncorrelated Brownian Motion at each node along the root-to-tip trajectory. Small colored points represent observed and ancestral trait values as estimated under Variable Rates as they traverse the path root-to-tip connected by a grey line. (center) The line plot indicates the trait difference of nodes as (observed - simulated) values with 95% quantiles shown in light grey. Nodes that fall above the dotted line (0) show greater than expected trait change along the branch that leads to that node, visible as greater distances between points in the plots at left. Nodes falling below the dotted line show less trait change than expected. Trees at right serve as a guide for the root-to-tip path of each example, with nodes colored accordingly. Examples of divergent morphologies are illustrated (purple) against a more ‘typical’ scincid body plan (*Liopholis*—grey). Black arrows in each row indicate the greatest jump in phenotype compared to expectations. References to node numbers can be seen in Fig. S27.

³⁶⁵ **Materials and Methods**

Walkthroughs of the data, code, analyses, and results are currently available in the *Supplementary Material* on GitHub at www.github.com/IanGBrennan/Tiliquini.

Data Collection

We assembled an exon-capture dataset across 77 Tiliquini skinks representing 53 of 62 currently recognized species, with a focus on Australian taxa (47 of 48 spp.). This sampling covers all 8 genera, as well as many recognized subspecies ([Table S1](#)). We included outgroup representatives from all subfamilies and most tribes, generated as part of broader look at squamate phylogenetics⁴¹. Nuclear exons were targeted and sequenced using the Anchored Hybrid Enrichment approach⁵⁵, and resulted in 379 loci (average coverage 367 loci, min = 362, max = 375) totaling ~600 kbp per sample ([Fig.S3](#)). Rough alignments were compiled using MAFFT⁵⁶ and refined using MACSE⁵⁷, alignment parameters are specified in the supplementary materials. Per locus information content is summarized in [Fig.S4](#).

We collected 21 linear measurements for 61 Tiliquini skink species from 650 museum samples (average 10 per spp., min.=2, max.=134). These linear measurements aimed to capture the gross morphology of the lizard body plan and are distributed across the head, body, limbs, and tail ([Fig.S5](#)). From the initial 21 measurements some were further divided (e.g. snout-vent length) or dropped to arrive at a set of 19 non-overlapping morphological traits that are summarized in the Supplemental Material ([Morphological Measurements](#)).

Phylogenetic Analyses and Divergence Dating

We reconstructed individual genealogies for our exon-capture data (n=379) under maximum-likelihood in IQ-TREE 2⁵⁸, allowing the program to assign the best fitting substitution model using ModelFinder⁵⁹, then perform 1,000 ultrafast bootstraps⁶⁰. We then estimated the species tree using the shortcut coalescent method ASTRAL III⁶¹, with IQ-TREE gene trees as input. For comparison we estimated a locus-partitioned concatenated species tree in IQ-TREE and investigated differing species tree topologies by delimiting the anomaly zone (see Supplement: [Anomaly Zone](#)). To estimate divergence times among taxa we applied a series of fossil and secondary calibrations in MCMCTree⁶² and as outlined in [Table S2](#) and informed by a combined-evidence morphology and molecular dating estimation in BEAST⁶³, further described in the Supplementary Materials (section: [Timetree](#)).

³⁹⁵ **Phenotypic Analyses**

Our interest is in identifying the tempo and mode of evolution that produces morphological novelty and so we focus on the dynamics of morphological diversification in the Tiliquini radiation. Our approach is based on a novel dataset that summarizes the lizard body plan. We started by generating mean trait values per species and removed the effect of absolute size by transforming our trait values into log-shape ratios. To identify independently evolving morphological modules we designed module models that ranged from highly specialized (head, limbs, body, and tail traits evolve independently) to highly integrated (null model in which all traits belong to a single module), see Supplementary Material for details. We

compared model likelihoods and estimated correlation coefficients using *EMMLi*³³ and used
405 the preferred model to designate module-specific datasets.

To identify the evolutionary mode of individual morphological traits we fit a series of models ranging from a basic unbiased random walk to entirely punctuated. These allowed phenotypes to evolve through incremental change (Brownian Motion—BM), incremental change around an optimum (Ornstein Uhlenbeck), decreasing change with time (Early Burst)—akin
410 to an adaptive radiation scenario, two “pulse” or “jump” models which allow change in instantaneous bursts (Jump Normal, Normal Inverse Gaussian), and a Variable Rates model in which rates of change vary across individual branches of the tree—in principle a multirate BM model similar to the relaxed clock model of timetree estimation. For consistency we fit the BM, OU, EB, JN, and NIG models in *pulsR*²³. We fit the VR model in *Bayes Traits V4*⁶⁴
415 and processed the output using the standalone *PPPostProcess* software. We compared model fit by AIC scores. *Bayes Traits* implements an MCMC algorithm so to estimate a maximum likelihood for the VR model we transformed the input tree by the estimated median rate scalar, then fit the observed data to the transformed tree using BM in *pulsR*. We obtained an AIC value by penalizing the likelihood for each scaled branch of the transformed tree
420 with mean scalar r greater than two, in addition to the estimation of the rate parameter and root state. We then calculated AICw for each model and identified a preferred model if its AICw was greater than twice the next best model.

To understand the temporal and phylogenetic heterogeneity of evolution we estimated ancestral states for each trait under the rate heterogeneous VR model by optimizing Brownian Motion on the VR rate-transformed trees in *phytools*⁶⁵. We extrapolated trait values linearly along branches given start and end values at nodes and a constant evolutionary rate. We did this from the root to the tips in 0.1 million year windows across all branches. To summarize the standing morphological variation across the same temporal windows we calculated disparity as both the variance and the average squared Euclidean distance among
425 all pairs of contemporaneous taxa. Similarly we extracted the mean evolutionary rate in 0.1 million year windows for each trait and module. To determine if our observed patterns follow a null expectation of the accumulation of disparity through time we simulated univariate and uncorrelated and correlated multivariate datasets for each trait and module applying parameter estimates from observed data for theta, sigma, and covariance. We carried out
430 the same disparity and rate through time extraction methods in 0.1 million year windows. To understand the relative contribution of niche expansion and niche packing to the accumulation of disparity through time we compared slopes of the accumulation of variance of observed traits and modules to simulated data. We plotted the trends in variance, rate, and slopes using custom functions found in the scripts included in the supplement.

440 Lastly, to summarize the major avenues of morphological change we ran PCA on (1) all traits jointly across all species and across (2) individual modules and (3) clades separately, then fit linear models to the first 2 PC axes (always accounting for $\geq 90\%$ of variance). This allowed us to identify the major axes of elaboration (PC1) and innovation (PC2) following the language of¹² and¹³. Tracking the angle (slope of regression) and extent of trait change
445 between individual nodes enabled us to qualitatively identify periods of primarily innovation or elaboration on a branch-by-branch basis.

References

1. Foote, M. (1997). The evolution of morphological diversity. *Annual Review of Ecology and Systematics* *28*, 129–152.
- 450 2. Deline, B., Greenwood, J.M., Clark, J.W., Puttick, M.N., Peterson, K.J., and Donoghue, P.C. (2018). Evolution of metazoan morphological disparity. *Proceedings of the National Academy of Sciences* *115*, E8909–E8918.
3. Lynch, M. (1990). The rate of morphological evolution in mammals from the stand-point of the neutral expectation. *The American Naturalist* *136*, 727–741.
4. Hansen, T.F., and Houle, O. (2004). Evolvability, stabilizing selection, and the problem. Phenotypic integration: Studying the ecology and evolution of complex phenotypes, 130.
- 455 5. Hall, B.K. (1996). Bauplane, phylotypic stages, and constraint-why there are so few types of animals. *Evolutionary Biology*, Vol *29* *29*, 215–261.
6. Vermeij, G.J. (2015). Forbidden phenotypes and the limits of evolution. *Interface Focus* *5*, 20150028.
- 460 7. Galis, F., Metz, J.A., and Alphen, J.J. van (2018). Development and evolutionary constraints in animals. *Annual Review of Ecology, Evolution, and Systematics* *49*, 499–522.
8. Arnold, S.J., Pfrender, M.E., and Jones, A.G. (2001). The adaptive landscape as a conceptual bridge between micro-and macroevolution. Microevolution rate, pattern, process, 9–32.
9. Hansen, T.F., and Martins, E.P. (1996). Translating between microevolutionary process and macroevolutionary patterns: The correlation structure of interspecific data. *Evolution* *50*, 1404–1417.
- 465 10. Felsenstein, J. (1988). Phylogenies and quantitative characters. *Annual Review of Ecology and Systematics* *19*, 445–471.
11. Schlüter, D. (1996). Ecological causes of adaptive radiation. *The American Naturalist* *148*, S40–S64.
- 470 12. Endler, J.A., Westcott, D.A., Madden, J.R., and Robson, T. (2005). Animal visual systems and the evolution of color patterns: Sensory processing illuminates signal evolution. *Evolution* *59*, 1795–1818.
13. Guillerme, T., Bright, J.A., Cooney, C.R., Hughes, E.C., Varley, Z.K., Cooper, N., Beckerman, A.P., and Thomas, G.H. (2023). Innovation and elaboration on the avian tree of life. *bioRxiv*, 2022–2008.
14. Erwin, D.H. (2015). Novelty and innovation in the history of life. *Current Biology* *25*, R930–R940.
- 475 15. Simões, T.R., Vernygora, O., Caldwell, M.W., and Pierce, S.E. (2020). Megaevolutionary dynamics and the timing of evolutionary innovation in reptiles. *Nature Communications* *11*, 3322.
16. Simpson, G.G. (1944). *Tempo and mode in evolution* (Columbia University Press).

- 480 17. Hunt, G. (2008). Gradual or pulsed evolution: When should punctuational explanations be preferred? *Paleobiology* *34*, 360–377.
18. Hunt, G., Hopkins, M.J., and Lidgard, S. (2015). Simple versus complex models of trait evolution and stasis as a response to environmental change. *Proceedings of the National Academy of Sciences* *112*, 4885–4890.
- 485 19. Venditti, C., Meade, A., and Pagel, M. (2011). Multiple routes to mammalian diversity. *Nature* *479*, 393–396.
20. Uyeda, J.C., Hansen, T.F., Arnold, S.J., and Pienaar, J. (2011). The million-year wait for macroevolutionary bursts. *Proceedings of the National Academy of Sciences* *108*, 15908–15913.
21. Landis, M.J., Schraiber, J.G., and Liang, M. (2013). Phylogenetic analysis using lévy processes: Finding jumps in the evolution of continuous traits. *Systematic biology* *62*, 193–204.
- 490 22. Baker, J., Meade, A., Pagel, M., and Venditti, C. (2016). Positive phenotypic selection inferred from phylogenies. *Biological Journal of the Linnean Society* *118*, 95–115.
23. Landis, M.J., and Schraiber, J.G. (2017). Pulsed evolution shaped modern vertebrate body sizes. *Proceedings of the National Academy of Sciences* *114*, 13224–13229.
- 495 24. Bastide, P., and Didier, G. (2023). The cauchy process on phylogenies: A tractable model for pulsed evolution. *bioRxiv*, 2023–2004.
25. Matthew, W.D. (1914). Time ratios in the evolution of mammalian phyla. A contribution to the problem of the age of the earth. *Science* *40*, 232–235.
26. Felice, R.N., and Goswami, A. (2018). Developmental origins of mosaic evolution in the avian cranium. *Proceedings of the National Academy of Sciences* *115*, 555–560.
- 500 27. Watanabe, A., Fabre, A.-C., Felice, R.N., Maisano, J.A., Müller, J., Herrel, A., and Goswami, A. (2019). Ecomorphological diversification in squamates from conserved pattern of cranial integration. *Proceedings of the National Academy of Sciences* *116*, 14688–14697.
28. Goswami, A., Noirault, E., Coombs, E.J., Clavel, J., Fabre, A.-C., Halliday, T.J., Churchill, M., Curtis, A., Watanabe, A., Simmons, N.B., et al. (2022). Attenuated evolution of mammals through the cenozoic. *Science* *378*, 377–383.
29. Chapple, D.G. (2003). Ecology, life-history, and behavior in the australian scincid genus egernia, with comments on the evolution of complex sociality in lizards. *Herpetological Monographs* *17*, 145–180.
- 505 30. Gardner, M.G., Hugall, A.F., Donnellan, S.C., Hutchinson, M.N., and Foster, R. (2008). Molecular systematics of social skinks: Phylogeny and taxonomy of the egernia group (reptilia: scincidae). *Zoological Journal of the Linnean Society* *154*, 781–794.
31. Thorn, K., Hutchinson, M., Lee, M., Brown, N., Camens, A., and Worthy, T. (2021). A new species of proegernia from the namba formation in south australia and the early evolution and environment of australian egerniine skinks. *Royal Society Open Science* *8*, 201686.

- 510 32. Linkem, C.W., Minin, V.N., and Leaché, A.D. (2016). Detecting the anomaly zone
in species trees and evidence for a misleading signal in higher-level skink phylogeny
(squamata: scincidae). *Systematic biology* *65*, 465–477.
33. Goswami, A., and Finarelli, J.A. (2016). EMMLi: A maximum likelihood approach
to the analysis of modularity. *Evolution* *70*, 1622–1637.
- 515 34. Imfeld, T.S., and Barker, F.K. (2022). Songbirds of the americas show uniform mor-
phological evolution despite heterogeneous diversification. *Journal of evolutionary
biology* *35*, 1335–1351.
35. Sallan, L.C., and Friedman, M. (2012). Heads or tails: Staged diversification in
vertebrate evolutionary radiations. *Proceedings of the Royal Society B: Biological
Sciences* *279*, 2025–2032.
36. Gardner, M.G., Pearson, S.K., Johnston, G.R., and Schwarz, M.P. (2016). Group
living in squamate reptiles: A review of evidence for stable aggregations. *Biological
Reviews* *91*, 925–936.
- 520 37. Thorn, K.M., Hutchinson, M.N., Archer, M., and Lee, M.S. (2019). A new scincid
lizard from the miocene of northern australia, and the evolutionary history of social
skinks (scincidae: egerniinae). *Journal of Vertebrate Paleontology* *39*, e1577873.
38. Thorn, K.M., Fusco, D.A., Hutchinson, M.N., Gardner, M.G., Clayton, J.L.,
Prideaux, G.J., and Lee, M.S. (2023). A giant armoured skink from australia ex-
pands lizard morphospace and the scope of the pleistocene extinctions. *Proceedings
of the Royal Society B* *290*, 20230704.
- 525 39. Chapple, D.G., Keogh, J.S., and Hutchinson, M.N. (2004). Molecular phylogeography
and systematics of the arid-zone members of the egernia whitii (lacertilia: Scincidae)
species group. *Molecular phylogenetics and evolution* *33*, 549–561.
40. Chapple, D.G., and Keogh, J.S. (2006). Group structure and stability in social ag-
gregations of white's skink, egernia whitii. *Ethology* *112*, 247–257.
41. Burbrink, F.T., Graziotin, F.G., Pyron, R.A., Cundall, D., Donnellan, S., Irish,
F., Keogh, J.S., Kraus, F., Murphy, R.W., Noonan, B., et al. (2020). Interrogating
genomic-scale data for squamata (lizards, snakes, and amphisbaenians) shows no sup-
port for key traditional morphological relationships. *Systematic biology* *69*, 502–520.
- 530 42. Leslie, A.B., Simpson, C., and Mander, L. (2021). Reproductive innovations and
pulsed rise in plant complexity. *Science* *373*, 1368–1372.
43. Novack-Gottshall, P.M., Sultan, A., Smith, N.S., Purcell, J., Hanson, K.E., Lively,
R., Ranjha, I., Collins, C., Parker, R., Sumrall, C.D., et al. (2022). Morphological
volatility precedes ecological innovation in early echinoderms. *Nature Ecology &
Evolution* *6*, 263–272.
44. Hansen, T.F. (1997). Stabilizing selection and the comparative analysis of adaptation.
Evolution *51*, 1341–1351.
- 535 45. Beaulieu, J.M., Jhwueng, D.-C., Boettiger, C., and O'Meara, B.C. (2012). Modeling
stabilizing selection: Expanding the ornstein–uhlenbeck model of adaptive evolution.
Evolution *66*, 2369–2383.

46. Burin, G., Park, T., James, T.D., Slater, G.J., and Cooper, N. (2023). The dynamic adaptive landscape of cetacean body size. *Current Biology* *33*, 1787–1794.
- 540 47. Gould, S.J., and Eldredge, N. (1972). Punctuated equilibria: An alternative to phyletic gradualism. *Models in paleobiology* *1972*, 82–115.
48. Malmgren, B.A., Berggren, W.A., and Lohmann, G. (1983). Evidence for punctuated gradualism in the late neogene *globorotalia tumida* lineage of planktonic foraminifera. *Paleobiology* *9*, 377–389.
- 545 49. Holstad, A., Voje, K.L., Opedal, Ø.H., Bolstad, G.H., Bourg, S., Hansen, T.F., and Pélabon, C. (2024). Evolvability predicts macroevolution under fluctuating selection. *Science* *384*, 688–693.
50. Pagel, M., O'Donovan, C., and Meade, A. (2022). General statistical model shows that macroevolutionary patterns and processes are consistent with darwinian gradualism. *Nature communications*, 1113.
- 550 51. Cooney, C.R., Bright, J.A., Capp, E.J., Chira, A.M., Hughes, E.C., Moody, C.J., Nouri, L.O., Varley, Z.K., and Thomas, G.H. (2017). Mega-evolutionary dynamics of the adaptive radiation of birds. *Nature* *542*, 344–347.
52. Ronco, F., Matschiner, M., Böhne, A., Boila, A., Büscher, H.H., El Taher, A., Indermaur, A., Malinsky, M., Ricci, V., Kahmen, A., et al. (2021). Drivers and dynamics of a massive adaptive radiation in cichlid fishes. *Nature* *589*, 76–81.
- 555 53. Alho, J., Herczeg, G., Laugen, A., Räsänen, K., Laurila, A., and Merilä, J. (2011). Allen's rule revisited: Quantitative genetics of extremity length in the common frog along a latitudinal gradient. *Journal of evolutionary biology* *24*, 59–70.
54. Ramm, T., Roycroft, E.J., and Müller, J. (2020). Convergent evolution of tail spines in squamate reptiles driven by microhabitat use. *Biology Letters* *16*, 20190848.
55. Lemmon, A.R., Emme, S.A., and Lemmon, E.M. (2012). Anchored hybrid enrichment for massively high-throughput phylogenomics. *Syst Biol* *61*, 727–744. <https://doi.org/10.1093/sysbio/sys049>.
56. Katoh, K., and Standley, D.M. (2013). MAFFT multiple sequence alignment software version 7: Improvements in performance and usability. *Molecular biology and evolution* *30*, 772–780.
- 560 57. Ranwez, V., Douzery, E.J., Cambon, C., Chantret, N., and Delsuc, F. (2018). MACSE v2: Toolkit for the alignment of coding sequences accounting for frameshifts and stop codons. *Molecular biology and evolution* *35*, 2582–2584.
58. Minh, B.Q., Schmidt, H.A., Chernomor, O., Schrempf, D., Woodhams, M.D., Von Haeseler, A., and Lanfear, R. (2020). IQ-TREE 2: New models and efficient methods for phylogenetic inference in the genomic era. *Molecular biology and evolution* *37*, 1530–1534.
59. Kalyaanamoorthy, S., Minh, B.Q., Wong, T.K., Von Haeseler, A., and Jermiin, L.S. (2017). ModelFinder: Fast model selection for accurate phylogenetic estimates. *Nature methods* *14*, 587–589.

60. Haeseler, A. von, Minh, B.Q., and Nguyen, M.A.T. (2013). Ultrafast approximation
for phylogenetic bootstrap. *Molecular Biology and Evolution* *30*, 1188–1195. <https://doi.org/10.1093/molbev/mst024>.
61. Zhang, C., Sayyari, E., and Mirarab, S. (2017). ASTRAL-III: Increased scalability
and impacts of contracting low support branches. *53–75*.
- 570 62. Rannala, B., and Yang, Z. (2007). Inferring speciation times under an episodic molec-
ular clock. *Systematic biology* *56*, 453–466.
63. Suchard, M.A., Lemey, P., Baele, G., Ayres, D.L., Drummond, A.J., and Rambaut,
A. (2018). Bayesian phylogenetic and phylodynamic data integration using BEAST
1.10. *Virus evolution* *4*, vey016.
64. Venditti, C., Meade, A., and Pagel, M. (2011). Multiple routes to mammalian diver-
575 sity. *Nature* *479*, 393–396.
65. Revell, L.J. (2012). Phytools: An r package for phylogenetic comparative biology
(and other things). *Methods in ecology and evolution*, 217–223.
66. Borowiec, M.L. (2016). AMAS: A fast tool for alignment manipulation and computing
of summary statistics. *PeerJ* *4*, e1660.
- 580 67. Reis, M. dos, and Yang, Z. (2011). Approximate likelihood calculation on a phylogeny
for bayesian estimation of divergence times. *Molecular biology and evolution* *28*,
2161–2172.

Appendix

Taxonomic Implications and Changes

As a result of our phylogenetic investigation, some taxonomic issues must be addressed and others will unfortunately remain outstanding until more focused sampling can be achieved.
585 We comment on both cases below.

(1) Paraphyly of *Lissolepis*: Phylogenetic estimation and topology testing do not support
590 the monophyly of *Lissolepis*. The type species of *Lissolepis* is *L.luctuosa* (Peters 1866), and despite *L.coventryi* (Storr 1978) forming a clade with *Liopholis*, these taxa are morphologically distinct. We feel that to acknowledge the distinctiveness of *L.coventryi* the best course of action is to erect a new genus to contain this species.

595 *Paluarius* gen. nov. Brennan, Chapple, Keogh & Donnellan

Egernia Storr 1978
Lissolepis Gardner 2008

600 **Type species:** *Egernia coventryi* Storr 1978

Diagnosis and definition: Currently a monotypic genus comprising a single medium sized ($\bar{x} = 80$ mm; max = 100 mm) skink with four well developed limbs each with five digits and fourth toe much longer than third. Lower eyelid movable and without a transparent ‘window’. Parietal and nasal scales both narrowly separated. Nasal scales in contact, or 605 if separated—narrowly. Ear aperture small and with two anterior lobules. 20–24 mid-body scale rows, dorsal scales faintly striated. 17–22 lamellae under the fourth toe. 5–7 supraciliaries.

Comparison: Distinguished from *Lissolepis* by broad geographic separation (southwest WA for *Lis.*; extreme southeast SA and coastal VIC for *Pal.*), continuous striped (*Paluarius*) 610 rather than spotty (*Lissolepis*) dorsal patterning, shorter and blunter head (head length 15% of SVL in *Pal.*, 20% in *Lis.*), fewer midbody scale rows (20–24 in *Pal.*, 22–28 in *Lis.*), longer postnasal crease that runs to the top of the nasal scale, interparietal narrower (*Pal.*) than frontal (vs. as wide as frontal in *Lis.*), fewer supraciliaries (5–7 *Pal.*, 7–9 *Lis.*), fewer lamellae under fourth toe (17–22 *Pal.*, 21–28 *Lis.*), shorter tail (150% of SVL *Pal.*, 200% in *Lis.*), and 615 smaller size (80–100 mm *Pal.* vs. 100–129mm *Lis.*).

Etymology: This skink lives among swamps, heaths, and marshes in far southeastern Australia. In allusion to its preferred habitat, from latin ‘palus’—swamp and ‘-arius’—where things are kept, together meaning ‘keeper of the swamp’.

Contents: *Paluarius coventryi* comb. nov. (Storr 1978)

(2) Paraphyly of *Cyclodomorphus*: Phylogenetic estimates and topology testing do not support the monophyly of *Cyclodomorphus* (Fitzinger 1843). The type species of *Cyclodomorphus* is *C. casuarinae* (Dumeril & Bibron 1839), which along with the species 625 *gerrardii*, *michaeli*, and *praealtus* form a clade with *Tiliqua*. We propose a new generic name to contain the taxa more closely related to *C. maximus* than to *C. gerrardii*.

Caerulingua gen. nov. Brennan, Chapple, Keogh & Donnellan

630 *Cyclodus* Dumeril & Bibron 1839
Hinula Gunther 1867
Lygosoma Hardwicke & Gray 1828
Tiliqua Gray 1825
Omolepida Gray 1845
635 *Cyclodomorphus* Fitzinger 1843

Type species: *Omolepida maxima* Storr 1976

Diagnosis and definition: A genus of moderate to large, elongate skinks characterized by long interlimb (trunk) lengths and relatively short limbs, each with five digits. Many 640 scalation characters are shared with *Cyclodomorphus*, and so make distinguishing the two difficult. Starting from the snout, nasals are in contact with one another and broadly contact the frontonasal which widely separates the prefrontals. There are no subocular scales, but three supraocular scales, the anterior two of which contact the frontal. Eyelid movable and no transparent ‘window’. Parietal scales are widely separated by an interparietal scale. Ear 645 opening small, with small anterior lobules (usually 2).

Etymology: From the Latin ‘caeruleus’ for blue and ‘lingua’ for tongue, meaning ‘blue tongue’, alluding to their common name of ‘little bluetongues’ relative to the larger ‘bluetongues’ in *Tiliqua*.

Contents: *Caerulingua branchialis* comb. nov. (Gunther 1867); *Caerulingua celatus* 650 comb. nov. (Shea & Miller 1995); *Caerulingua maximus* comb. nov. (Storr 1976); *Caerulingua melanops elongatus* comb. nov. (Shea & Miller 1995); *Caerulingua melanops melanops* comb. nov. (Stirling & Zietz 1893); *Caerulingua melanops siticulosus* comb. nov. (Shea & Miller 1995); *Caerulingua venustus* comb. nov. (Shea & Miller 1995).

Comment: Wells (2007) proposed splitting *Cyclodomorphus*, reallocating *C. gerrardii* 655 to *Hemisphaeriodon* and creating a new generic name for the *Cyclodomorphus maximus* clade. In following the best practices in herpetological nomenclature outlined by Kaiser et al. (2013) and adopted by the Australian Society of Herpetologists in their Position Statement on Taxonomy (2022) we do not recognize the name proposed by Wells (2007) and instead provide *Caerulingua* as the generic name for this clade of tiliquine skinks.

660

(3) Synonymizing *Liopholis pulchra* ssp.: The southwestern Australian species *Liopholis pulchra* currently comprises two taxa *L.p.pulchra* and *L.p.longicauda*. As recognized, the

nominate subspecies ranges across the extreme southwest of Western Australia, and sub-
665 species *longicauda* is confined to a series of small islands off the coast of Jurien Bay. In the
description of the subspecies *longicauda* (Ford, 1963; *The Western Australian Naturalist* (9)
25–29), it is apparent that in almost all characters, specifically scalation, the two subspecies
overlap. Molecular comparison of the subspecies has to date been limited, however. Our
exon capture data suggests that *longicauda* is nested within *pulchra*, with a sample of *pulchra*
670 from Berry Reserve more closely related to samples from Whitlock, Favorite, and Escape
Islands, than to another *pulchra* from D'Entrecasteaux National Park. This provides context
for the clinal variation seen in this species. Additionally, the sample collected from Berry
Reserve (in 2022 by Jari Cornelis and Robert Audcent) showed extensive orange flush on the
ventral surfaces—a character deemed apomorphic for the ssp. *longicauda* by Ford (1963).
675 For other characters it fits the description of *L.p.pulchra* (7 upper labial scales, nasal scales
separated by rostral, 3 ear lobules). **As a result**, we synonymize the subspecies *Liopholis*
pulchra longicauda with *Liopholis pulchra*.

680 (4) *Cyclodomorphous melanops*: Our limited sampling suggests species-level divergences
among the three subspecies of *C. melanops* (~4mya, 2mya), however unpublished mtDNA
data shows more complicated genetic history among these taxa and the closely related *C.*
venustus, *C. celatus*, and *C. branchialis*. In light of these results we take the conservative
685 stance of retaining the subspecies as is, and suggest a more focused study with greater
sampling would provide better understanding of this morphologically conservative clade.

(5) *Egernia stokesii*: Similarly, the divergence between *E. stokesii* subspecies *E.s.stokesii*,
E.s.badia, and *E.s.zellingi* are comparatively deep (>5mya), but our sampling remains lim-
ited. Unpublished mtDNA data suggests low divergence or introgression between subspecies
690 *E.s.stokesii* and *E.s.badia*, and so without more extensive population level sampling we re-
frain from making taxonomic changes to this complex.

(6) Paraphyly of *Liopholis inornata*: Our sampling of *L. inornata* and sister taxa *L.*
slateri, *L. sp. nov.* from Purnululu NP, and *L. sp. nov.2* from the North West Cape, WA
695 highlight a complicated phylogenetic history. As currently understood, *L. inornata* is a wide
ranging species found across much of arid WA, SA, NSW, and QLD. This range overlaps
entirely with *L. slateri* with which it could potentially be confused, but remains allopatric
from two additional taxa. We highlight this clade as another group which needs a much
more thorough population genetic assessment to resolve.

Supplementary Material

Supplementary material included below consists of additional figures, tables, and extended methods to complement the main text.

Table S1. Taxon sampling: Ingroup Tiliquini sampling is listed in upper table, with outgroup sampling following.

Genus	Species	Subspecies	Specimen Registration	ABTC No.	Locality	State	Country
<i>Bellatorias</i>	<i>frerei</i>	—	AMS R.113970	10881	Bunya Mountains	QLD	Australia
<i>Bellatorias</i>	<i>frerei</i>	—	AMS R.96317	11439	Heathlands	QLD	Australia
<i>Bellatorias</i>	<i>frerei</i>	—	SAMA R21133	—	—	QLD	Australia
<i>Bellatorias</i>	<i>major</i>	—	SAMA R33412	4115	Whian Whian SF	NSW	Australia
<i>Bellatorias</i>	<i>obiri</i>	—	AMS R.100018	11440	Jabiluka	NT	Australia
<i>Corucia</i>	<i>zebrata</i>	—	—	50418	Levaleva Choiseul Island	—	Solomon Islands
<i>Corucia</i>	<i>zebrata</i>	—	UMFS 11250	—	—	—	Solomon Islands
<i>Cyclodomorphus</i>	<i>branchialis</i>	—	WAM R156771	—	—	WA	Australia
<i>Cyclodomorphus</i>	<i>casuarinae</i>	—	SAMA R22957	54924	Mount Victoria	NSW	Australia
<i>Cyclodomorphus</i>	<i>casuarinae</i>	—	SAMA R63333	101476	—	TAS	Australia
<i>Cyclodomorphus</i>	<i>celatus</i>	—	SAMA R22873	54920	Burns Beach	WA	Australia
<i>Cyclodomorphus</i>	<i>gerrardii</i>	—	SAMA R34884	16792	Paluma	QLD	Australia
<i>Cyclodomorphus</i>	<i>maximus</i>	—	WAM R168816	135574	Middle Osborn Island	WA	Australia
<i>Cyclodomorphus</i>	<i>melanops</i>	elongatus	MAGNT R20662	29413	Finke Gorge NP	NT	Australia
<i>Cyclodomorphus</i>	<i>melanops</i>	melanops	SAMA R34056	11739	Mount Stuart Homestead	WA	Australia
<i>Cyclodomorphus</i>	<i>melanops</i>	siticulusus	SAMA R52374	58905	St. Francis Island	SA	Australia
<i>Cyclodomorphus</i>	<i>melanops</i>	siticulusus	SAMA R26399	—	Nullarbor Stn	SA	Australia
<i>Cyclodomorphus</i>	<i>praecaltus</i>	—	—	97283	Bogong High Plains	VIC	Australia
<i>Cyclodomorphus</i>	<i>venustus</i>	—	SAMA R18869	54897	Port Germein Dump	SA	Australia
<i>Egernia</i>	<i>cunninghami</i>	—	AMS R.112873	11398	Yetman	NSW	Australia
<i>Egernia</i>	<i>cunninghami</i>	—	AMS R.118939	14392	Kanangra Walls	NSW	Australia
<i>Egernia</i>	<i>depressa</i>	—	SAMA R22856	53933	Python Pool	WA	Australia
<i>Egernia</i>	<i>depressa</i>	—	WAM R120631	63425	Mardathuna	WA	Australia
<i>Egernia</i>	<i>depressa</i>	—	CUMV 14263	63425	—	WA	Australia
<i>Egernia</i>	<i>douglasi</i>	—	ABTC 141482	141482	Beverley Springs Homestead	WA	Australia
<i>Egernia</i>	<i>eos</i>	—	WAM R98079	23913	Ainsley Gorge	WA	Australia
<i>Egernia</i>	<i>episisolus</i>	—	WAM R90897	63515	Woodstock	WA	Australia
<i>Egernia</i>	<i>formosa</i>	—	SAMA R29267	53997	Yalgo	WA	Australia
<i>Egernia</i>	<i>formosa</i>	—	WAM R103993	61869	Woodstock Station	WA	Australia
<i>Egernia</i>	<i>hosmeri</i>	—	SAMA R36707	17065	Mount Isa	QLD	Australia
<i>Egernia</i>	<i>kingii</i>	—	SAMA R29444	54006	Mount Clarence	WA	Australia
<i>Egernia</i>	<i>mcpheei</i>	—	SAMA R33649	—	—	NSW	Australia
<i>Egernia</i>	<i>napoleonis</i>	—	SAMA R23080	53949	Denmark	WA	Australia
<i>Egernia</i>	<i>pilbarensis</i>	—	WAM R132519	63479	Burrup Peninsula	WA	Australia
<i>Egernia</i>	<i>richardi</i>	—	SAMA R26315	40639	Koonalda Station	SA	Australia
<i>Egernia</i>	<i>richardi</i>	—	SAMA R63272	112886	Merdayerrah Sandpatch	SA	Australia
<i>Egernia</i>	<i>rugosa</i>	—	—	108820	Charleville	QLD	Australia
<i>Egernia</i>	<i>rugosa</i>	—	—	108823	Charleville	QLD	Australia
<i>Egernia</i>	<i>saxatilis</i>	intermedia	SAMA R44004	12812	The Grampians	VIC	Australia
<i>Egernia</i>	<i>stokesii</i>	zellingi	SAMA R42897	9143	Stonehenge	QLD	Australia
<i>Egernia</i>	<i>stokesii</i>	zellingi	SAMA R45053	35026	Toopawarinna Hill	SA	Australia
<i>Egernia</i>	<i>stokesii</i>	zellingi	SAMA R44127	57871	Pernatty Station	SA	Australia
<i>Egernia</i>	<i>stokesii</i>	badia	WAM R135193	63511	Walycatchem	WA	Australia
<i>Egernia</i>	<i>stokesii</i>	badia	WAM R152997	92933	Walga Rock	WA	Australia

Genus	Species	Subspecies	Specimen Registration	ABTC No.	Locality	State	Country
<i>Egernia</i>	<i>stokesii</i>	badia	WAM R152998	92934	Walga Rock	WA	Australia
<i>Egernia</i>	<i>stokesii</i>	stokesii	WAM R135166	—	West Wallabi Island	WA	Australia
<i>Egernia</i>	<i>stokesii</i>	stokesii	WAM R135167	—	West Wallabi Island	WA	Australia
<i>Egernia</i>	<i>striolata</i>	—	AMS R.126116	1150	Denham	NSW	Australia
<i>Egernia</i>	<i>striolata</i>	—	SAMA R53262	70470	Telowie	SA	Australia
<i>Egernia</i>	<i>striolata</i>	—	SAMA R55661	76988	Moorrinya NP	QLD	Australia
<i>Egernia</i>	<i>striolata</i>	—	QM J86594	100573	Durikai SF	QLD	Australia
<i>Eutropis</i>	<i>longicaudata</i>	—	SAMA R38916	57273	—	—	Malaysia
<i>Liopholis</i>	<i>guthega</i>	—	SAMA R37781	16273	Kosciusko NP	NSW	Australia
<i>Liopholis</i>	<i>inornata</i>	—	SAMA R45219	58081	Mootatunga	SA	Australia
<i>Liopholis</i>	<i>inornata</i>	—	SAMA R49140	58604	Eyre Peninsula	SA	Australia
<i>Liopholis</i>	<i>inornata</i>	—	NMV D65868	61607	Buningtonia Springs	WA	Australia
<i>Liopholis</i>	<i>inornata</i>	—	—	101744	—	—	Australia
<i>Liopholis</i>	<i>inornata</i>	—	UMMZ244330	—	—	WA	Australia
<i>Liopholis</i>	<i>inornata cf.</i>	—	AMS R.106840	—	Widgee Downs	NSW	Australia
<i>Liopholis</i>	<i>inornata cf.</i>	—	SMZ 1494	—	Selwyn	QLD	Australia
<i>Liopholis</i>	<i>kintorei</i>	—	WAM R131047	63449	—	WA	Australia
<i>Liopholis</i>	<i>margaretae</i>	margaretae	SAMA R51590	42404	Amata	SA	Australia
<i>Liopholis</i>	<i>margaretae</i>	personata	SAMA R24815	53965	Mount Remarkable NP	SA	Australia
<i>Liopholis</i>	<i>modesta</i>	—	SAMA R39172	12411	Retreat	NSW	Australia
<i>Liopholis</i>	<i>montana</i>	—	SAMA R37768	16389	Mount Gingera	ACT	Australia
<i>Liopholis</i>	<i>montana</i>	—	SAMA R56033	—	Davies Plain/Kings Plain	VIC	Australia
<i>Liopholis</i>	<i>montana</i>	—	SAMA R56034	—	Davies Plain/Kings Plain	VIC	Australia
<i>Liopholis</i>	<i>multiscutata</i>	—	SAMA R63458	126142	—	SA	Australia
<i>Liopholis</i>	<i>pulchra</i>	pulchra	WAM R132054	63464	D'Entrecasteaux NP	WA	Australia
<i>Liopholis</i>	<i>pulchra</i>	pulchra	WAM TR2206	—	Berry Reserve	WA	Australia
<i>Liopholis</i>	<i>pulchra</i>	longicauda	WAM R145186	—	Jurien Bay Islands	WA	Australia
<i>Liopholis</i>	<i>pulchra</i>	longicauda	WAM R151766	—	Jurien Bay Islands	WA	Australia
<i>Liopholis</i>	<i>pulchra</i>	longicauda	WAM R152970	—	Jurien Bay Islands	WA	Australia
<i>Liopholis</i>	sp. nov.	—	WAM R156715	85105	Purnululu NP	WA	Australia
<i>Liopholis</i>	sp. nov.2	—	WAM R156453	—	Learmouth	WA	Australia
<i>Liopholis</i>	<i>slateri</i>	slateri	—	99920	Finke River	NT	Australia
<i>Liopholis</i>	<i>slateri</i>	slateri	MAGNT R20673	29437	Finke Gorge NP	NT	Australia
<i>Liopholis</i>	<i>slateri</i>	slateri	—	150946	—	—	Australia
<i>Liopholis</i>	<i>striata</i>	—	SAMA R45402	58180	Ampeinna Hills	SA	Australia
<i>Liopholis</i>	<i>whitii</i>	—	SAMA R53588	94846	Spring Mount	SA	Australia
<i>Lissolepis</i>	<i>coventryi</i>	—	SAMA R45916	58241	Nelson	SA	Australia
<i>Lissolepis</i>	<i>luctuosa</i>	—	WAM R90386	135575	Walpole	WA	Australia
<i>Lissolepis</i>	<i>luctuosa</i>	—	WAM R90226	135576	Lake Wilson	WA	Australia
<i>Lissolepis</i>	<i>luctuosa</i>	—	WAM R131278	—	—	WA	Australia
<i>Tiliqua</i>	<i>adelaidensis</i>	—	SAMA R42426	57682	Burra	SA	Australia
<i>Tiliqua</i>	<i>gigas</i>	gigas	AMS R.124720	48811	Usino	Madang	Papua New Guinea
<i>Tiliqua</i>	<i>gigas</i>	gigas	AMS R.124721	48812	Usino	Madang	Papua New Guinea
<i>Tiliqua</i>	<i>gigas</i>	evanescens	AMS R.129710	50170	Guleguleu Normanby Island	Milne Bay	Papua New Guinea
<i>Tiliqua</i>	<i>multifasciata</i>	—	SAMA R49974	37896	Purni Bore	SA	Australia
<i>Tiliqua</i>	<i>multifasciata</i>	—	UMMZ 244405	—	—	SA	Australia
<i>Tiliqua</i>	<i>nigrolutea</i>	—	SAMA R33410	4114	Clarkefield	VIC	Australia

Genus	Species	Subspecies	Specimen Registration	ABTC No.	Locality	State	Country
<i>Tiliqua</i>	<i>occipitalis</i>	—	SAMA R28391	54961	Iron Knob	SA	Australia
<i>Tiliqua</i>	<i>occipitalis</i>	—	UMMZ 244408	—	—	WA	Australia
<i>Tiliqua</i>	<i>rugosa</i>	<i>rugosa</i>	SAMA R18978	55216	Bremer Bay	WA	Australia
<i>Tiliqua</i>	<i>rugosa</i>	<i>aspera</i>	SAMA R20587	55264	Cowell	SA	Australia
<i>Tiliqua</i>	<i>rugosa</i>	—	—	—	—	—	Australia
<i>Tiliqua</i>	<i>rugosa</i>	—	UMMZ 244409	—	—	—	Australia
<i>Tiliqua</i>	<i>scincoides</i>	<i>intermedia</i>	QM J51107	24812	Cape Flattery	QLD	Australia
<i>Tiliqua</i>	<i>scincoides</i>	<i>chimaera</i>	WAM R112258	101416	Latdalam	—	Indonesia
<i>Tiliqua</i>	<i>scincoides</i>	<i>scincoides</i>	SAMA R28511	54968	Minnipa	SA	Australia
<i>Tiliqua</i>	<i>scincoides</i>	<i>intermedia</i>	SAMA R53937	70143	Tunnel Creek Gorge	WA	Australia
<i>Tribolonus</i>	<i>gracilis</i>	—	AMS R.122119	14359	Karkar Island	—	Papua New Guinea
<i>Tribolonus</i>	<i>pseudoponceleti</i>	—	—	156097	—	—	Solomon Islands

Genus	Species	Subspecies	Specimen Registration	ABTC No.	Locality	State	Country
<i>Acontias</i>	<i>percivali</i>		HERR013918	—	—	—	—
<i>Eugongylus</i>	<i>rufescens</i>		UMMZ 242515	—	—	—	—
<i>Eremiascincus</i>	<i>fasciolatus</i>		SAMA R60807	—	—	—	—
<i>Sphenomorphus</i>	<i>solomonis</i>		BPBM 38999	—	—	—	—
<i>Amphiglossus</i>	<i>splendidus</i>		RAN40350	—	—	—	—
<i>Brachymeles</i>	<i>gracilis</i>		ACD4586	—	—	—	—
<i>Feylinia</i>	<i>polyplepis</i>		CAS233433	—	—	—	—
<i>Pygomeles</i>	<i>sp.</i>		RAN64845	—	—	—	—
<i>Scincus</i>	<i>scincus</i>		CTMZ12617	—	—	—	—
<i>Trachylepis</i>	<i>quinquetaeniata</i>		UMMZ227725	—	—	—	—
<i>Gallus</i>	<i>gallus</i>		SAMN15960293	—	—	—	—
<i>Varanus</i>	<i>komodoensis</i>		SAMN10967258	—	—	—	—
<i>Hydrophis</i>	<i>elegans</i>		SAMN35787919	—	—	—	—
<i>Salvator</i>	<i>merianae</i>		SAMN09273531	—	—	—	—
<i>Cryptoblepharus</i>	<i>egeriae</i>		SAMN32772511	—	—	—	—
<i>Heteronotia</i>	<i>binoei</i>		CCM8104	—	—	—	—
<i>Dibamus</i>	<i>novaeguineae</i>		ABTC062295	—	—	—	—
<i>Sphenodon</i>	<i>punctatus</i>		SAMN08038466	—	—	—	—
<i>Pogona</i>	<i>vitticeps</i>		SAMEA2300447	—	—	—	—

Table S2. Fossil ages and divergence dating calibrations as implemented in BEAST and MCMCTree. The root divergence between lepidosaurs (*Sphenodon* + squamates) is based on the fossil taxa *Sophineta cracoviensis* (Evans & Bialynicka, 2009), *Megachirella wachtleri* (Renesto & Posenato, 2003), and the Vellberg Jaw (Jones et al., 2013). These taxa represent stem squamates and rhynchocephalians, and so provide a soft lower bound on the crown divergence of Lepidosauria, with a soft upper bound provided by *Protosaurus speneri* (von Meyer, 1832). Fossil *Egernia*, *Proegernia*, and *Tiliqua* samples were implemented as tip calibrations in the combined evidence BEAST analysis shown in Fig.S7. Node calibrations A–J implemented in our MCMCTree analysis are shown in Fig.S1. All node priors as applied in MCMCTree are soft, allowing estimated ages to pull beyond priors if driven by the data.

Node	Fossil Information	Calibration (Tip or Node)	Split/Position	Source
-	<i>Egernia gillespieae</i>	14.17–15.11 myo	—	37
-	<i>Proegernia mikebulli</i>	25.50–25.70 myo	—	31
-	<i>Proegernia palankarinnensis</i>	25.50–25.70 myo	—	31
-	<i>Tiliqua frangens</i>	0.01–5.86 myo	—	38
-	<i>Tiliqua pusilla</i>	14.47–16.86 myo	—	31
A	Uniform— <i>Sophineta</i> & Vellberg Jaw	'B(2.380,2.550)'	Lepidosauria (<i>Sphenodon</i> + Squamata)	
B	Skew-T—Secondary from Combined Evidence	'ST(0.76,0.08,-1.49,213.71)'	Lygosominae (Tiliquini + (Mabuyini + Eugongylini))	
C	Skew-T—Secondary from Combined Evidence	'B(0.5,0.8)'	Crown Tiliquini (<i>Tribolonotus</i> + all others)	
D	Skew-T—Secondary from Combined Evidence	'ST(0.33,0.04,1.09,98.26)'	<i>Corucia</i> + Australian Tiliquini	
E	Skew-T—Secondary from Combined Evidence	'ST(0.23,0.04,2.86,20.53)'	Crown Australian Tiliquini	
F	Skew-T—Secondary from Combined Evidence	'ST(0.17,0.05,1.64,58.08)'	<i>L. coventryi</i> + <i>Liopholis</i>	
G	Skew-T—Secondary from Combined Evidence	'ST(0.20,0.04,3.29,73.91)'	(<i>Tiliqua</i> + <i>Cyclo</i>) + (<i>Bellatorias</i> + <i>Egernia</i>)	
H	Skew-T—Secondary from Combined Evidence	'ST(0.16,0.02,1.40,14.89)'	<i>Cyclodomorphus</i> + <i>Tiliqua</i>	
I	Minimum—Primary <i>Tiliqua pusilla</i>	'>0.153'	Crown <i>Tiliqua</i>	
J	Skew-T—Secondary from Combined Evidence	'ST(0.16,0.04,2.82,58.53)'	<i>Bellatorias</i> + <i>Egernia</i>	31

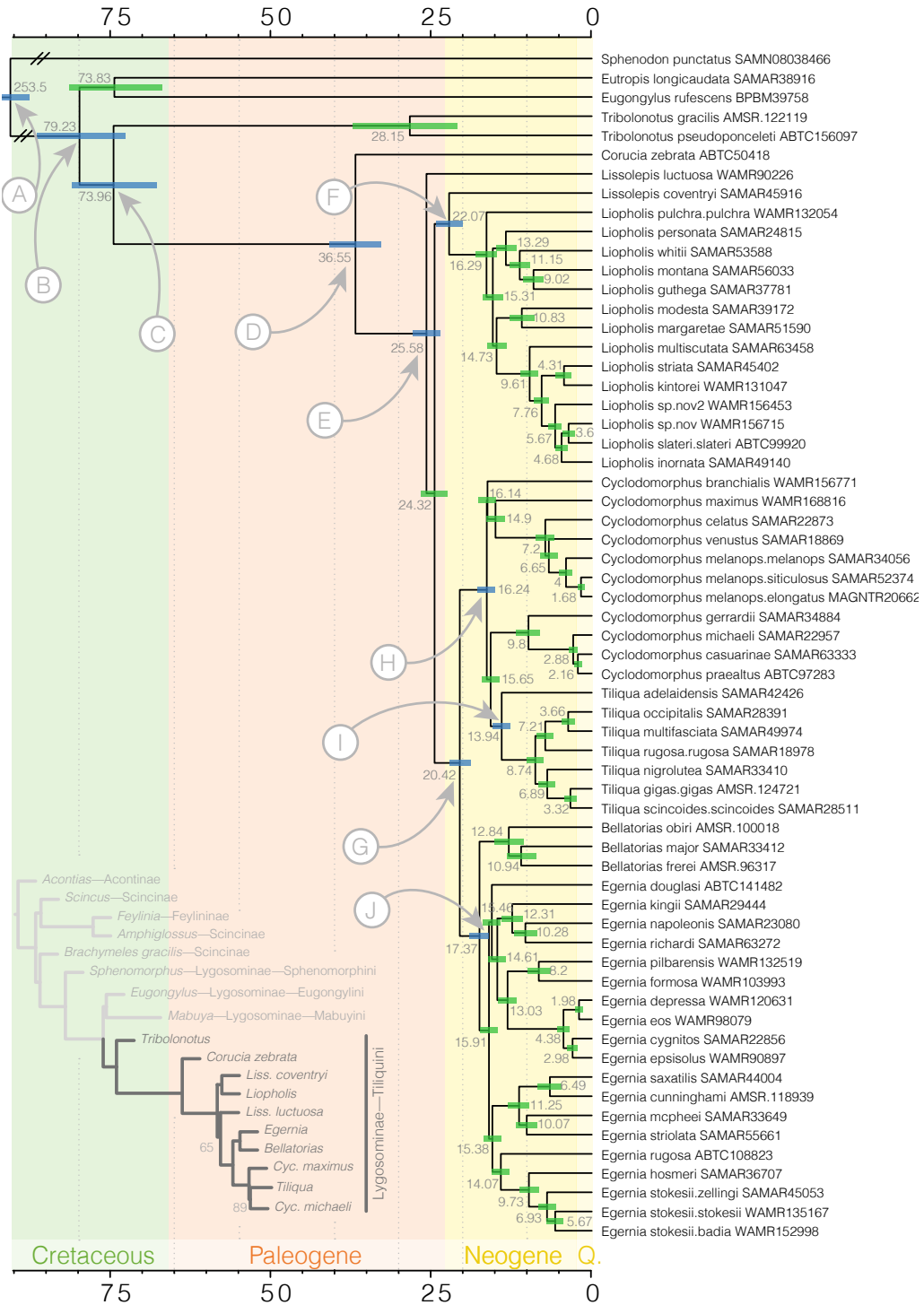


Figure S1: Reduced sampling Tiliquini species tree estimated with ASTRAL from IQTREE2 genetrees and time-calibrated with MCMCTree. Shaded bars at nodes indicate 95% confidence estimates on ages. Nodes labelled by letters A–F correspond to fossil calibrations listed in Table S2. Inset tree depicts the scincid phylogeny estimated from AHE data showing the placement of the Tiliquini among the Lygosominae.

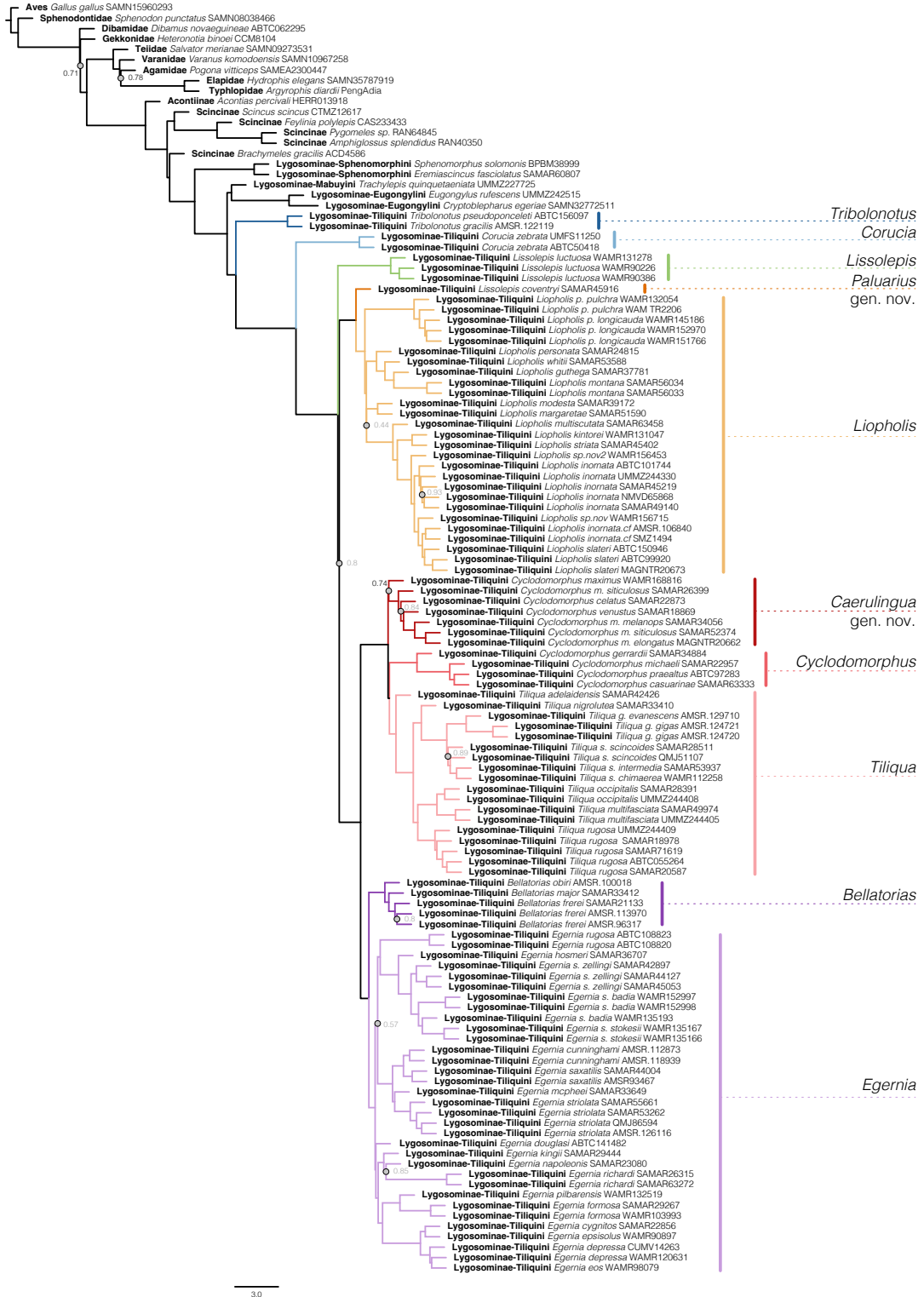


Figure S2: Fully sampled Tiliquini species tree estimated with hASTRAL from 379 IQTRE2 genetrees. Presentation of this full tree highlights intraspecific sampling, including several taxonomic issues discussed in the [Appendix](#). Annotations at right include proposed new generic names *Caerulingua* and *Paluarius*. Support values (local posterior probabilities) are 1 for all nodes except those marked by a grey circle and text.

Alignment Specifications

- 715 We downloaded the complete CDS of *Anolis carolinensis* and used a reciprocal blast to identify unique exonic targets in our AHE dataset (n=358). 25 targets appear to be separate exons of shared genes (APOB, DSP, DST, FAT4, HIVEP2, IRS1, KAT6B, PLXNA1, RBM15, SHANK2, USF3, ZNF536). We then downloaded additional squamate genomes as well as *Sphenodon* and *Gallus*, extracted these targets, and aligned them in correct reading frame using MACSE. We added our Tiliquini sampling to these alignments using MAFFT.
- 720 Input MAFFT/MUSCLE alignments were refined with MACSE using the following call:

```
$ java -jar /Applications/macse_v2.03.jar \
    -prog refineAlignment -align [rough alignment path] \
    -optim 1 -local_realign_init 0.1 -local_realign_dec 0.1 \
    -fs 10 -stop 10
```

Additional samples were added to MACSE alignments using MAFFT:

```
$ /Applications/mafft-mac/mafft.bat \
    --quiet --add <input_alignment> \
    --keeplength --reorder <existing_alignment> \
    > <combined_alignment>
```

Investigating Data Completeness and Informativeness

- 725 Below we visualize data completeness and informativeness on a per sample and per locus basis, as well as provide some insight into our data cleaning and sample selection.

Many valuable statistics of our molecular data are summarized in the *Alignments/Tiliquini_PerLocus_Summary.csv*. This file is the output of the AMAS command *summary*. For brevity, we provide some basic statistics below:

- Average alignment length was 1884 bp (min=332; max=2708).
- Average site coverage was 1837 (+/- 930).
- Average number of reads per sample was 6,465,416 (min=340,302; max=18,867,860)
- Average percent missing data per locus was 8% (min=0.93%; max=19%)

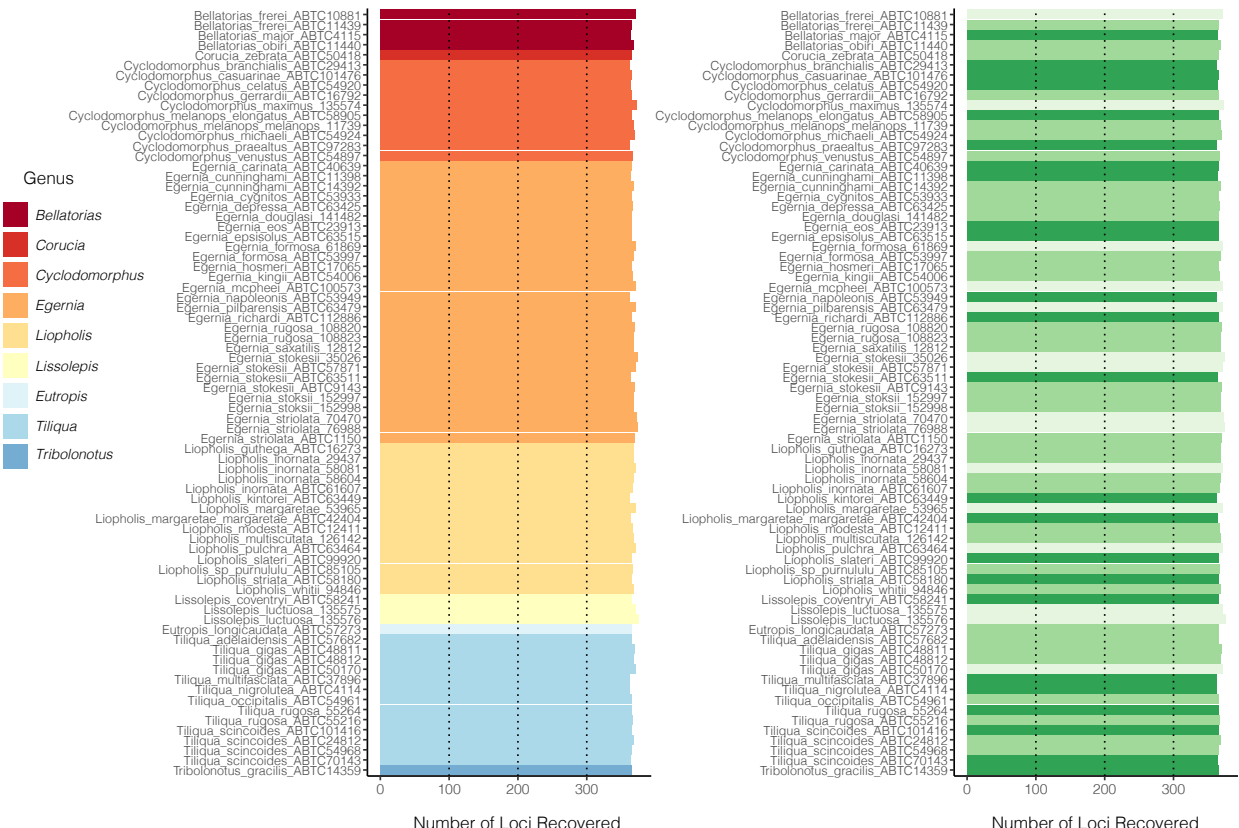


Figure S3: Number of loci recovered per sample for all Tiliquini and outgroup taxa included in the molecular data. Samples are colored by Genus (left) and coverage (right).

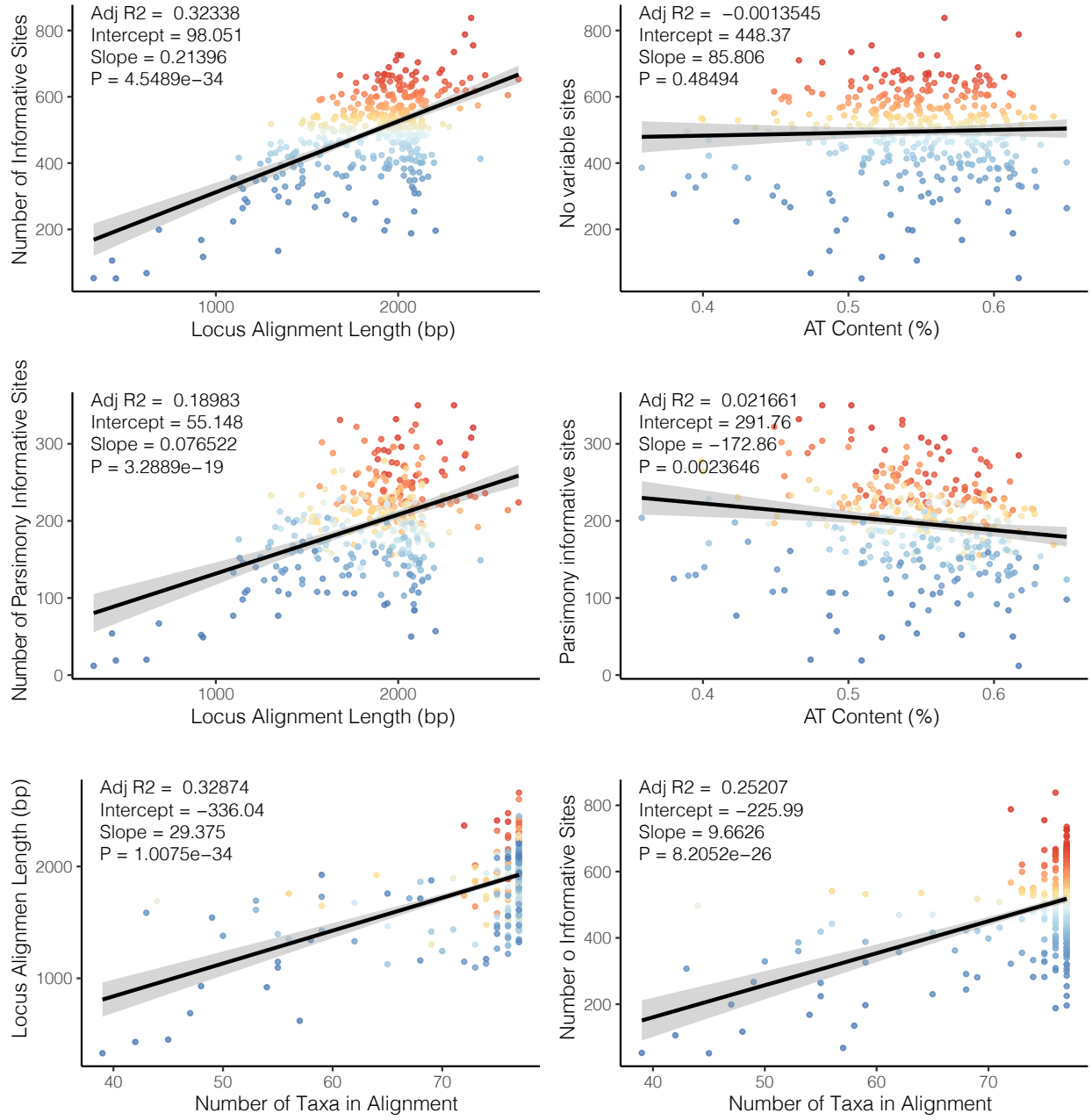


Figure S4: Plots of individual locus completeness and informativeness. Points are colored according to number of informative (variable) sites (blue—few, red—many). Top row shows the number of variable sites in each alignment as a function of alignment length and AT content. The middle row shows the number of parsimony informative sites as a function of alignment length and AT content. The bottom row shows alignment length and number of variable sites as a function of completeness.

Morphological Measurements

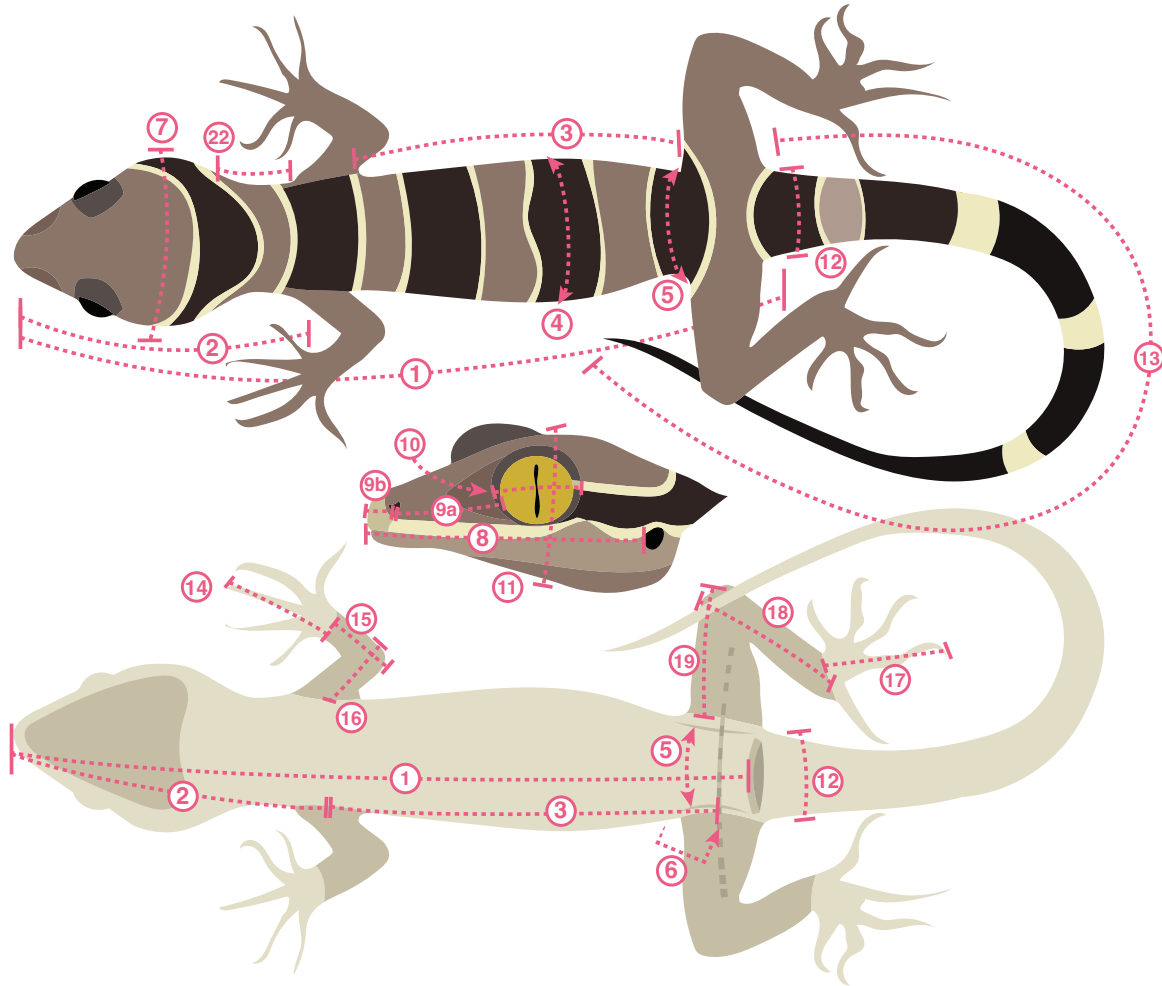


Figure S5: The 21 linear measurements collected.

Table S3

735 Initial morphological measurements used for data investigation:

No.	Measurement	Abbreviation	Method
1	Snout-vent length	SVL	From the tip of the snout to the vent.
2	Snout-axilla length	SAL	From the tip of the snout to the midpoint of the crease between the fore-limb and the body on the ventral surface.
3	Inter-limb length	ILL	Midpoint of the crease on the ventral surface where the fore-limb connects to

No.	Measurement	Abbreviation	Method
4	Body width	BW	the body, to the midpoint of the crease on the ventral surface where the hind-limb connects to the body.
5	Pelvic width	PW	From one lateral side of the body to the other, where possible at the midpoint of the ILL.
6	Pelvic height	PH	From the midpoint of the crease on the ventral surface where the left hind limb connects to the body, to the midpoint of the crease on the ventral surface where the right hind limb connects to the body.
7	Head width	HW	From the top of the dorsal surface were the PW was measured, to the bottom of the ventral surface where the PW was measured.
8	Head length	HL	Widest part of the head from one dorsal-lateral edge to the other edge.
9	Snout length	SN	From the nose tip, to the anterior of the ear.
10	Eye diameter	ED	From the nasal opening to the anterior of the eye.
11	Head depth	HD	From one side of the eye to the other.
12	Tail width	TW	From the top of the tallest part of the head on the dorsal surface, to the bottom of the ventral surface under the jaw.
13	Tail length	TL	Measured at the vent, from one dorsal-lateral edge to the other edge.
14	Fore-limb length	FLL	Measured from the vent to the tip of the tail.
15	Front foot	FFOOT	Measured fully extended from the midpoint of the crease on the ventral surface where the front limb connects to the body, to the end of longest toe (claw included).
16	Lower front limb	LFL	From the base of the foot to the end of the longest toe (claw included).
17	Upper front limb	UFL	Measured from the base of the lower fore limb to the juncture where the limb meets the front foot.
18	Hind-limb length	HLL	Measured from the crease on the ventral surface where the fore limb connects to the body, to the end of the lower front limb.
19	Hind foot	HFOOT	From the midpoint of the crease on the ventral surface where the hind limb connects to the body, to the end of longest toe (claw included)
20	Lower hind limb	LHL	From the base of the hind foot to the end of the longest toe (claw included)
			Measured from the top of the knee joint

No.	Measurement	Abbreviation	Method
21	Upper hind limb	UHL	to the heel juncture where the limb meets the front foot. Measured from the crease on the ventral surface where the hind limb connects to the body, to the end of the knee.

Table S4

Final morphological traits used for phenotypic analyses:

No.	Measurement	Shorthand	Method
3	Interlimb length	Interlimb	see above
4	Body width	Body_Width	see above
5	Pelvic width	Pelvic_Width	see above
6	Pelvic height	Pelvic_Height	see above
7	Head width	Head_Width	see above
9	Snout length	Snout_Eye	see above
10	Eye diameter	Eye_Diameter	see above
11	Head depth	Head_Depth	see above
12	Tail width	Tail_Width	see above
13	Tail length	Tail_Length	see above
17	Upper front limb	Upper_Arm	see above
16	Lower front limb	Lower_Arm	see above
15	Front foot	Hand	see above
21	Upper hind limb	Upper_Leg	see above
20	Lower hind limb	Lower_Leg	see above
19	Hind foot	Foot	see above
22	Neck length	Neck	Snout_Axilla - Head_Length
23	Posterior skull	Pos_Skull	Head_Length - (Snout_Eye + Eye_Diameter)
24	Pelvic gap	Pelvic_Gap	Snout_Vent - (Interlimb + Snout_Axilla)

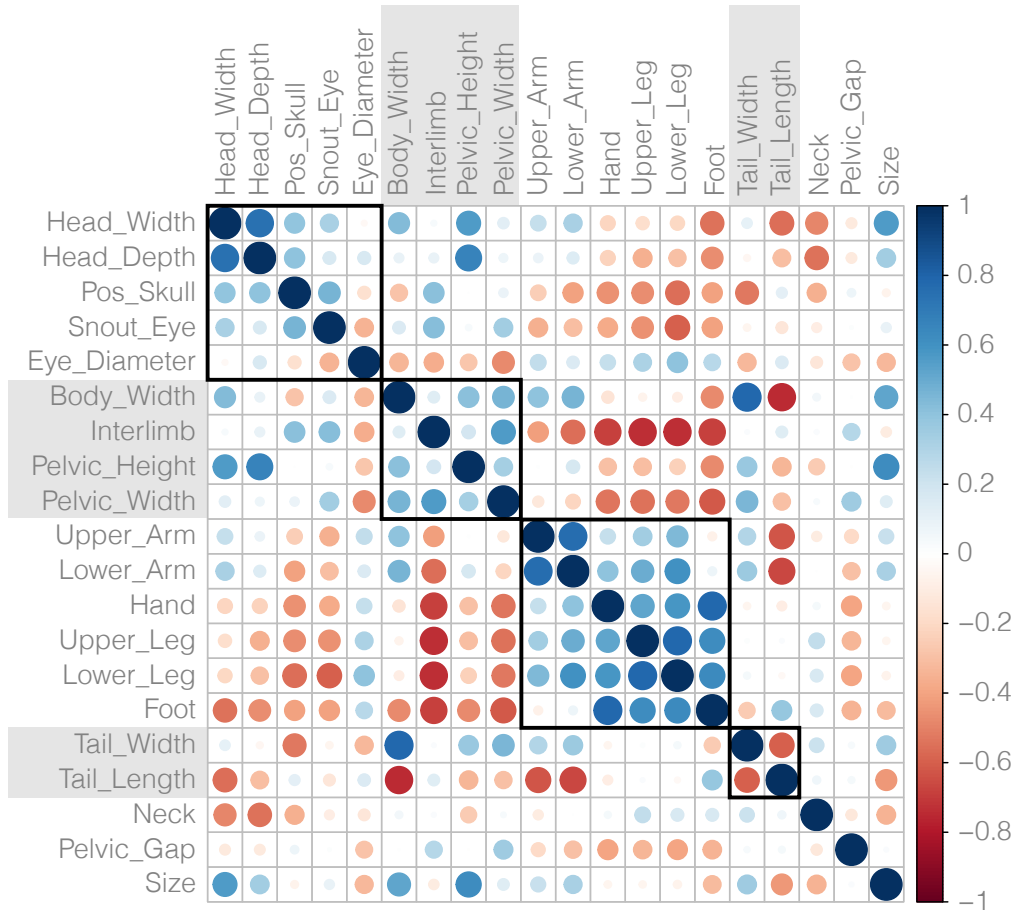


Figure S6: Correlation plot of all morphological traits after removing size via log-shape ratios. Some traits retain strong correlations despite removing the effect of size. Traits are organized according to the morphological module they belong to. Plot generated using *corrplot* [Wei & Simko 2021] using the Pearson (parametric) correlation.

Phylogenetic Analyses and Timetree Estimation

Specifics of alignment are covered [above](#).

740 We estimated individual genetrees (n=379) under maximum-likelihood in IQ-TREE 2⁵⁸,
allowing the program to assign the best fitting substitution model using ModelFinder⁵⁹, then
perform 1,000 ultrafast bootstraps⁶⁰. We then estimated the species tree using the shortcut
coalescent method ASTRAL III⁶¹, with IQ-TREE gene trees as input.

745 For each exonic locus we started by estimating raw genetic distances from alignments to
use as a proxy for evolutionary rate. We removed the fastest 5% and slowest 5% of loci to
avoid issues with extreme rate heterogeneity then partitioned the remaining loci into three
partitions using AMAS⁶⁶ to remove third codon positions.

```
python3 /Applications/AMAS-master/amas/AMAS.py concat  
-d dna -f fasta -t GeneClump1_CP12.fasta -n 12 -i ...  
-u fasta -c 8 -t GeneClump1_CP12.fasta -p GeneClump1_CP12_parts.txt
```

750 To incorporate fossil information in a cohesive way we modified the combined-evidence
BEAST xml file of³⁸ to include our phylogenomic data and additional fossil taxa. We started
by reducing the molecular data to our three AHE partitions and applied a GTR model to
each. We removed the continuous morphological data which had shown to cause spurious
results³⁸ and added in the newly redescribed Plio/Pleistocene species *Tiliqua frangens*. We
ran four independent runs for 100 million generations, inspected log files for convergence
755 and stationarity in TRACER, combined runs with LOGCOMBINER, and generated a max-
imum clade credibility tree with median node heights using TREEANNOTATOR (Fig.[S7](#)).
Phylogenetic analyses of Tiliquini skinks based on morphology alone can generate unreliable
topologies³¹ but are buffered by the inclusion of molecular data. Our combined-evidence tree
is mostly consistent with our molecular tree, but molecular and morphological partitions ex-
hibit some differences in behavior. The morphological partition in particular appears to show
760 extreme rate variation among taxa, particularly along the lineage leading to *Cyclodomorphus*
and *Tiliqua* (Fig.[S8](#)). We anticipate that this rate variation may inflate estimated ages, and
as such used the estimated 95% confidence intervals to generate wide Skew-T priors for our
subsequent MCMCTree analysis.

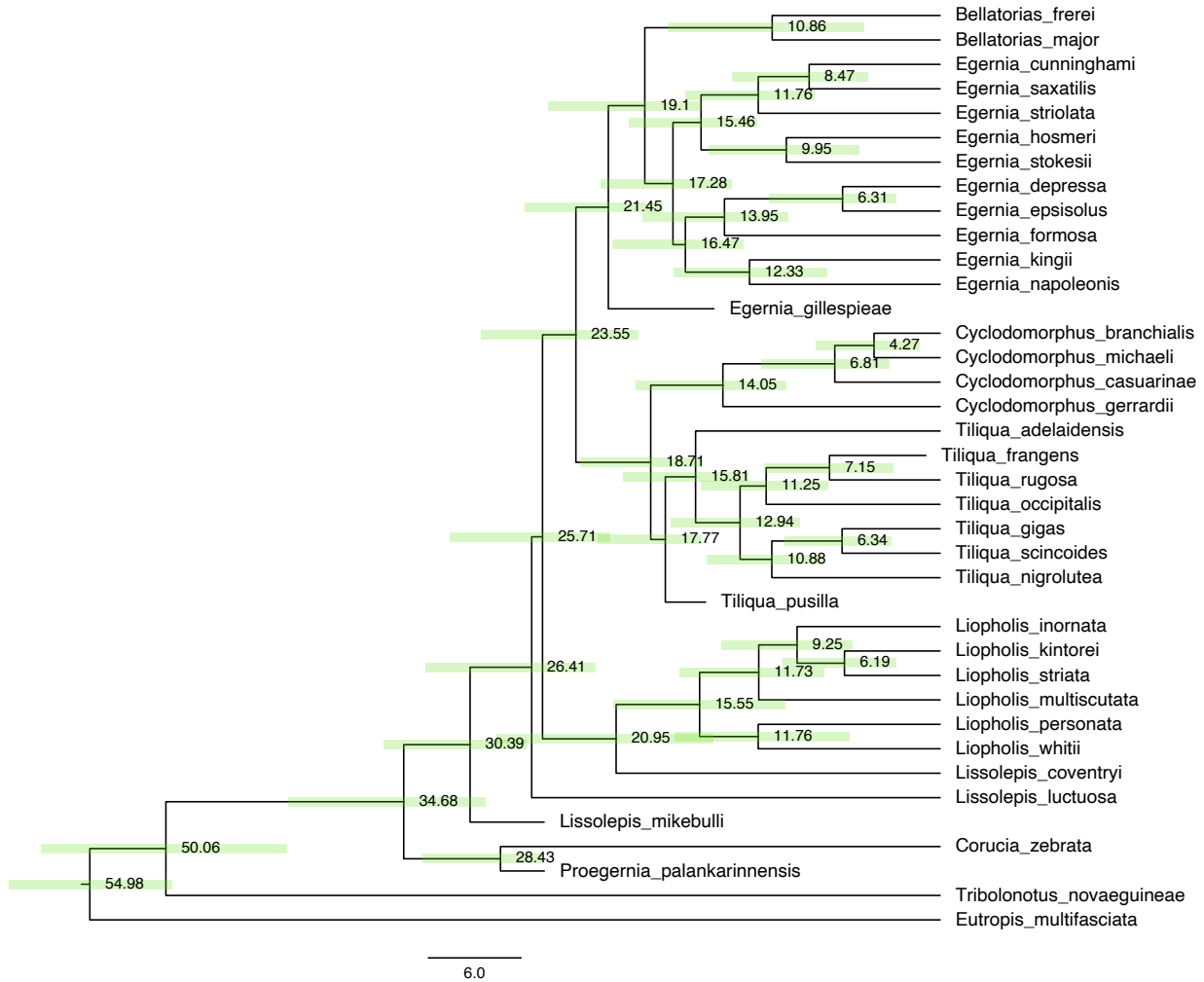


Figure S7: Combined evidence analysis of morphological and molecular data in BEAST 1.8.4, incorporating morphological data from Thorn et al. (2019), Thorn et al. (2021), Thorn et al. (2023). This analysis recovers a topology largely consistent with our molecular data, but provides insight into the phylogenetic placement of fossil taxa. Notably, we do not recover a monophyletic *Proeugenia*, with *P. mikebulli* (in tree as *Lissolepis mikebulli*) placed as a stem Australian tiliquine, and we identify *Tiliqua pusilla* as a likely stem *Tiliqua*, and *Egernia gillespieae* as a stem lineage leading to *Bellatorias* and *Egernia*. As a result of the inclusion of morphological data, all *Cyclodomorphus* are drawn into a single clade, likely as a result of shared plesiomorphic characters. Estimated divergence dates are likely inflated by severe rate heterogeneity in morphological characters (see Fig. S8).

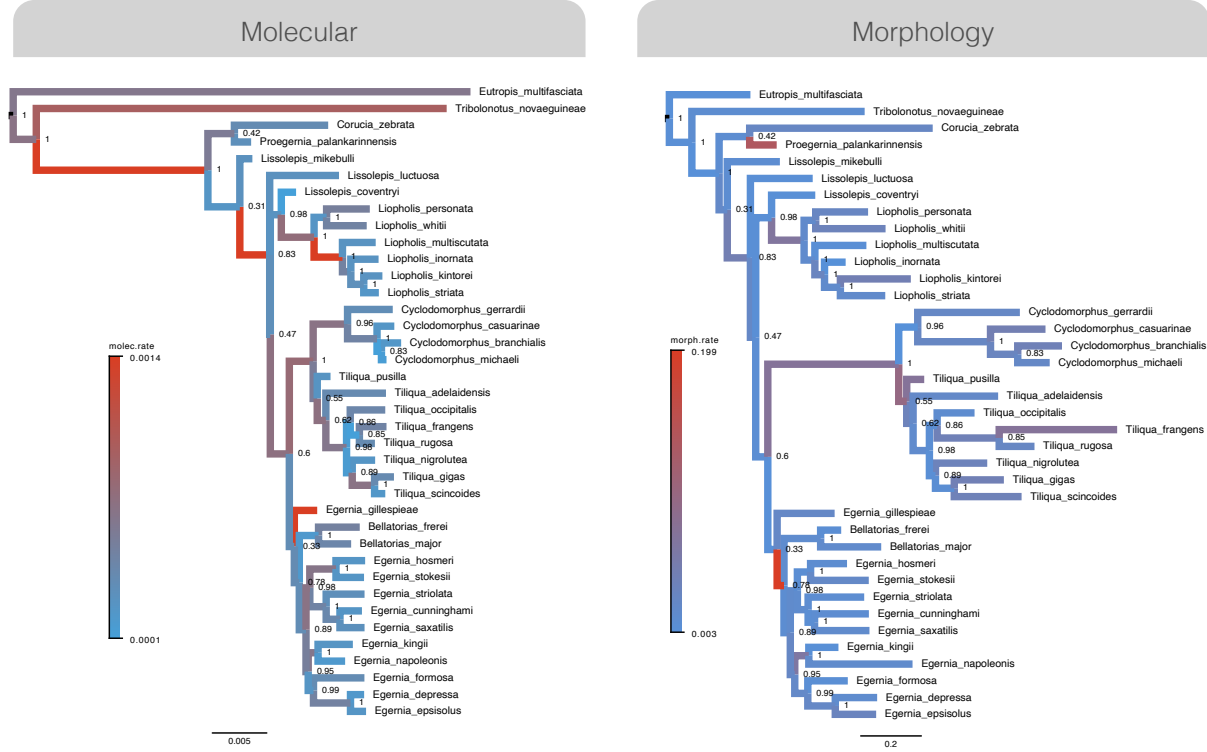


Figure S8: Maximum clade credibility trees based on molecular (left) and morphological (right) estimated in a combined-evidence BEAST analysis. The morphological tree shows strong rate heterogeneity in the lineage leading to *Cyclodomorphus/Tiliqua*.

For each partition we ran MCMCTree with `usedata = 3` to get the approximate likelihoods and branch lengths using `baseml`⁶⁷, then concatenated the `out.BV` files together. We then ran four replicate `mcmctree` analyses on the gradient and Hessian (`in.BV` file; `usedata = 2`), each for 20k burnin generations before collecting 20k samples at a sampling frequency of 100 generations (2,020,000 total generations). We compared `mcmc` files for stationarity and convergence (ESS of all parameters > 300), combined them using `logCombiner`, and used this combined `mcmc` file to summarize divergence times on our tree (`print = -1` in `.ctl` file). To investigate our priors we ran an additional analysis `usedata = 0` to run explicitly from the prior calibrations and determine our effective priors for comparison against our posterior age estimates. We then plotted the applied priors (Table S2), against effective priors (priors as a result of multiple interacting priors from `usedata = 0`), and posterior estimates to ensure the appropriate behavior of the MCMCTree analyses (Fig.S9). Our summarized MCMCTree output is show in Figure S1.

To take advantage of all available morphological and phylogenetic information we incorporated two additional *Tribolonotus* species into our dated tree used for trait evolution analyses. *T. blanchardi* and *T. ponceleti* were added using `bind.tip` in *phytools*, based on the topology and ages estimated from a recent phylogenomic investigation of Squamata by Title & Singhal et al. (2024).

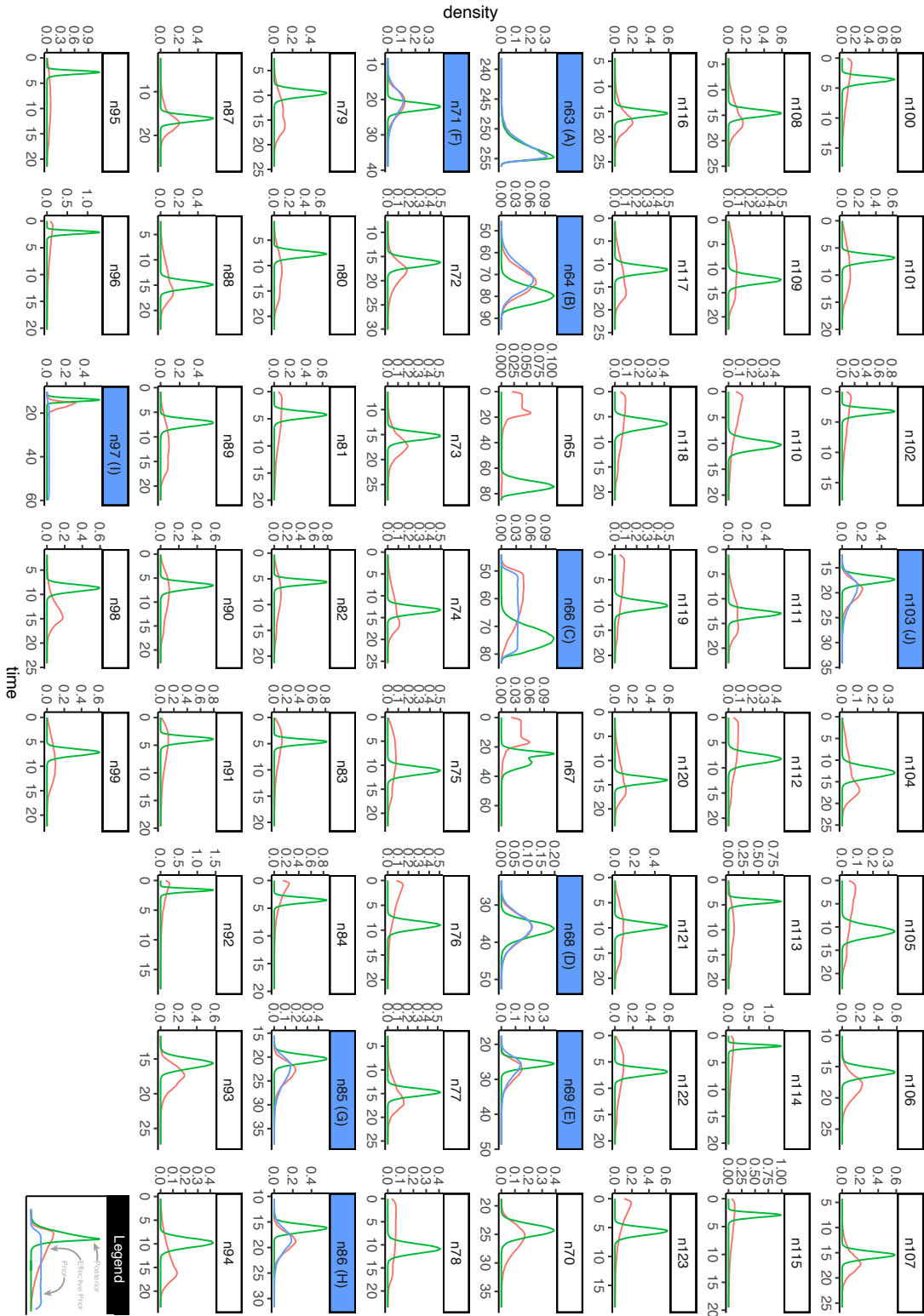


Figure S9: Plots of priors (blue), effective priors (pink), and posteriors (green) from MCMCTree analyses show reasonable behavior. Node numbers correspond to the phylogeny in *Trees/Tiliquini_MCMCTree.tre* and plotted with *ape*, where *n63* is the root node. Nodes with a blue header indicate those which included a prior.

Table S6: A set of morphological models for testing modularity with *EMMLi*. Each column represents a model and each row represents the occupancy of a given trait in that model. Module numbering scheme follows that required for *EMMLi*.

Trait	m0a	m0b	m1a	m1b	m2a	m2b	m3a	m3b	m4a	m4b	m5a	m5b
Interlimb	1	1	1	1	1	1	1	1	1	1	1	1
Body_Width	1	1	1	1	1	1	1	1	1	1	1	1
Pelvic_Width	1	1	1	1	1	1	1	1	1	1	1	1
Pelvic_Height	1	1	1	1	1	1	1	1	1	1	1	1
Head_Width	1	1	4	4	1	1	1	1	2	2	1	1
Snout_Eye	1	1	4	4	1	1	1	1	2	2	1	1
Eye_Diameter	1	NA	4	NA	1	NA	1	NA	2	NA	1	NA
Head_Depth	1	1	4	4	1	1	1	1	2	2	1	1
Tail_Width	1	1	2	2	2	2	1	1	3	3	2	2
Upper_Arm	1	1	3	3	3	3	2	2	3	3	2	2
Lower_Arm	1	1	3	3	3	3	2	2	3	3	2	2
Hand	1	1	3	3	3	3	2	2	3	3	2	2
Upper_Leg	1	1	3	3	3	3	2	2	3	3	2	2
Lower_Leg	1	1	3	3	3	3	2	2	3	3	2	2
Foot	1	1	3	3	3	3	1	2	3	3	2	2
Neck	1	NA										
Pos_Skull	1	1	4	4	1	1	1	1	2	2	1	1
Pelvic_Gap	1	NA										
Tail_Length	1	1	2	2	2	2	1	1	3	3	2	2

Modelling Trait Evolution and Disparity

The below methodology is accompanied by a series of scripts found in `/Scripts` which will run on the included `/Data` files. These steps can be followed chronologically and are scripts indicated as such `<Number>_<Process>.R` e.g. `00_Data_Preparation.R`.

We started by generating mean trait values per species ([Scripts/00_Data_Preparation.R](#)). To remove the effect of size on individual traits (allometry) we then calculated the geometric mean of all traits by species and used this to transform trait measurements into log-shape ratios. This also provided an additional trait *size*. To investigate integrated and modular evolution we estimated correlations among traits and provided this as input for the package *EMMLi*³³. *EMMLi* also requires *a priori* hypotheses of the assignment of traits to modules. We provided five general hypotheses for model comparison with the most specialized model allowing traits of the head, limbs, body, and tail to evolve as independent modules, and the most restrictive null model lumping all traits into a single module. *EMMLi* also allowed us to compare models in which the correlation coefficient among modules and among traits within modules is either similar or different (see Goswami & Finarelli Fig.2). Once we established the preferred model (head, body, limbs, tail as separate modules with differing inter- and intramodule correlations) we split our traits into module-specific datasets.

We designed six models of modular evolution for the Tiliquini skink body plan to test integration and modularity via *EMMLi*. (1) a four-module model (`m1:Body_Tail_Limbs_Head`) in which each of the major body regions is isolated as an independent module; (2) a three-module model (`m2:BodyHead_Tail_Limbs`) where traits of the head and body are combined into a single module; (3) a two-module model (`m3:BodyHeadTail_Limbs`) in which traits of the head, body, and tail are combined into a single module; (4) a three-module model (`Body_Head_TailLimbs`) where tail and limb traits make up a single module; and (5) a two-module model (`m4:BodyHead_TailLimbs`) where body and head traits are one module

and tail and limb traits another. We compared these to one another and to a null model
810 where all traits exist as part of a single module (m0). For model specifications shown see
Table S5 and Fig.[S10](#).

We fit the Variable Rates model via the comparative methods software *BayesTraits V4*
which implements a reversible-jump MCMC sampler. We began by fitting the VR model
815 (burnin 10 million generations, 110 million total generations) to each individual trait and
summarizing the output to check for convergence with *Scripts/processBTVarRates.R* veri-
fying that all parameters had reached effective sample sizes (ESS) >200. We summarized
model parameters and used these to provide informed priors (*Data/BayesTraits/...*) for full
analyses of individual modules (multi-trait). To verify model fit and consistency among runs
820 we ran four separate runs for each module (burnin 100 million generations, 200 million total
generations). Individual model outputs ... *VarRates.txt* were summarized using the *PPPost-
Processor* script. We then summarized runs for each module accepting shifts that occurred
in >70% of the sampled posterior in **all four** runs ([01_Process_BayesTraits_Output.R](#)).
Trees were transformed, colored, and plotted with evolutionary rate and shift information
825 using custom scripts ([02_VarRates_Trees.R](#))

To investigate the effect fossil taxa may have on our evolutionary inferences we analyzed
a dataset of head length of extinct and extant Tiliquini species by fitting the Variable Rates
model. We used the age and relationships of extinct species as inferred in our BEAST analysis
830 and added these taxa to our MCMCTree timetree. We used the trait “head length” which
in extant taxa was measured from the nose tip to the anterior of the ear opening, and for
extinct taxa was measured as the full extent of the mandible length. These measurements
are comparable in this group of skinks. Results are qualitatively identical with the same
number and positions of shifts (Fig.[S12](#)).
835

To estimate ancestral trait values we transformed our timetrees by scaling branches
by the mean rate scalar estimated by BayesTraits (*mean.scalar.trees*), using [plotting_BayesTraits.R](#). We then extrapolated trait values linearly along branches given start
840 and end values at nodes and a constant evolutionary rate. We did this from the root to the
tips in 0.1 million year windows across all branches [03_Extract_Ancestral_Traits.R](#).

To summarize the standing morphological variation across the same temporal windows we
calculated disparity as both the variance and the average squared Euclidean distance among
all pairs of contemporaneous taxa [04_Disparity_Through_Time_TRAITS.R](#). Similarly we
845 extracted the mean evolutionary rate in 0.1 million year windows for each trait and module
[05_Rate_Through_Time_TRAITS.R](#).

To determine if our observed patterns follow a null expectation of the accumulation of
disparity through time we simulated univariate and uncorrelated and correlated multivari-
850 ate datasets for each trait and module applying parameter estimates from observed data
for theta, sigma, and covariance. We carried out the same disparity and rate through
time extraction methods in 0.1 million year windows. To understand the relative con-
tribution of niche expansion and niche packing to the accumulation of disparity through

time we compared slopes of the accumulation of variance of observed traits and modules to simulated data. We plotted the trends in variance, rate, and slopes [06_Disparity_Rate_Through_Time_MODULES.R](#).

To visualize how rate heterogeneity contributes to great changes in the evolution of trait space we generated *rate trajectory* plots. These variations on classical traitgrams/phenograms incorporate the estimated ancestral trait values and color branches according to their evolutionary rate

To visualize rate heterogeneity among individual branches we generated *

To summarize the major avenues of morphological change we started with our dataset of all traits including estimated trait values at ancestral nodes which were inferred using our rate-transformed BayesTraits trees (see Materials and Methods section *Phenotypic Analyses* in the main text). We then ran PCA on (1) all traits jointly across all species and across (2) individual modules and (3) clades separately, then fit linear models to the first 2 PC axes (always accounting for $\geq 90\%$ of variance). This allowed us to identify the major axes of elaboration (PC1) and innovation (PC2) following the language of¹² and¹³ [11_Innovate_Elaborate.R](#). We then identify change between parent and child node pairs as primarily elaborative or innovative by estimating the angle/slope of change of the line connecting them in Euclidean space (Fig.[S15](#)) and indicated by color. For branches which exhibit both elaborative and innovative change (likely most branches exhibit some combination of both), the primary trend is a discrete binary state described by the angle of change (innovation: $>45^\circ < 135^\circ, >225^\circ < 315^\circ$; elaboration: $>135^\circ < 225^\circ, >315 < 360^\circ$). Further, we identify the strength of this change as the distance between the points and indicated by color saturation.

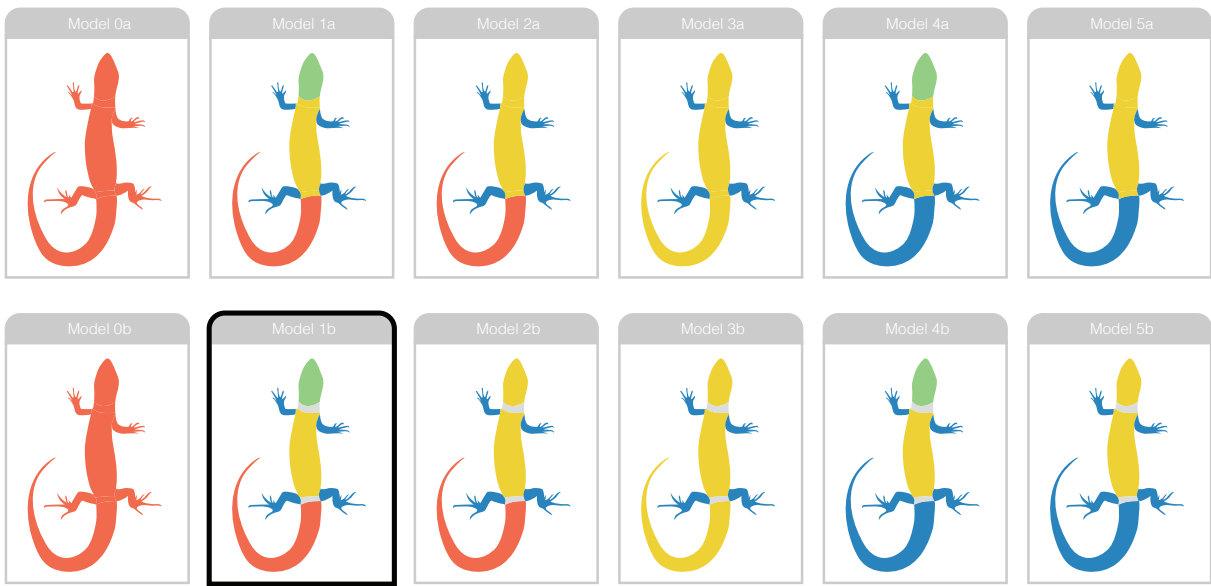


Figure S10: Diagram indicating the models for testing morphological modularity with *EMMLi*. Top and bottom rows indicate slight variations on the same basic model, with the bottom model ('b') treating three traits (neck length, pelvic gap length, eye diameter) that did not fit into modules neatly as 'unintegrated'. The preferred model *Model 1b* is highlighted with a black outline. Trait occupancy in specific models are indicated in Table S5.

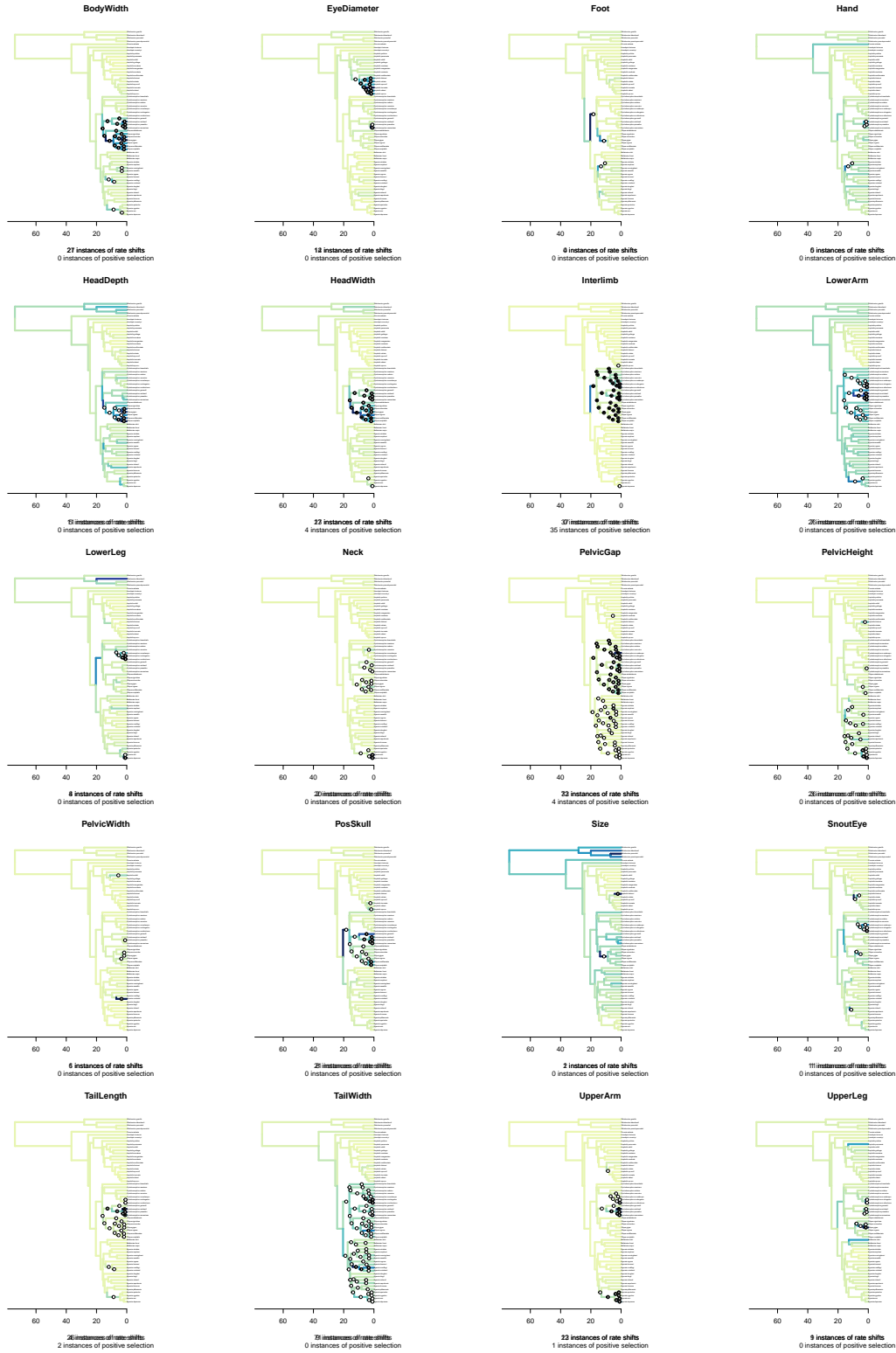


Figure S11: Pulses in rates of phenotypic evolution are common across tiliquine morphological traits. Species tree branches are colored according to mean estimated sigma value. Circles indicate significant rate shifts: empty circles represent shifts which appeared in > 70% of the posterior samples and in which the mean estimated scalar > 2; black circles represent shifts which appeared in >95% of the posterior samples and in which the mean estimated scalar > 2 corresponding to instances of “positive phenotypic selection” per Baker et al. 2017.

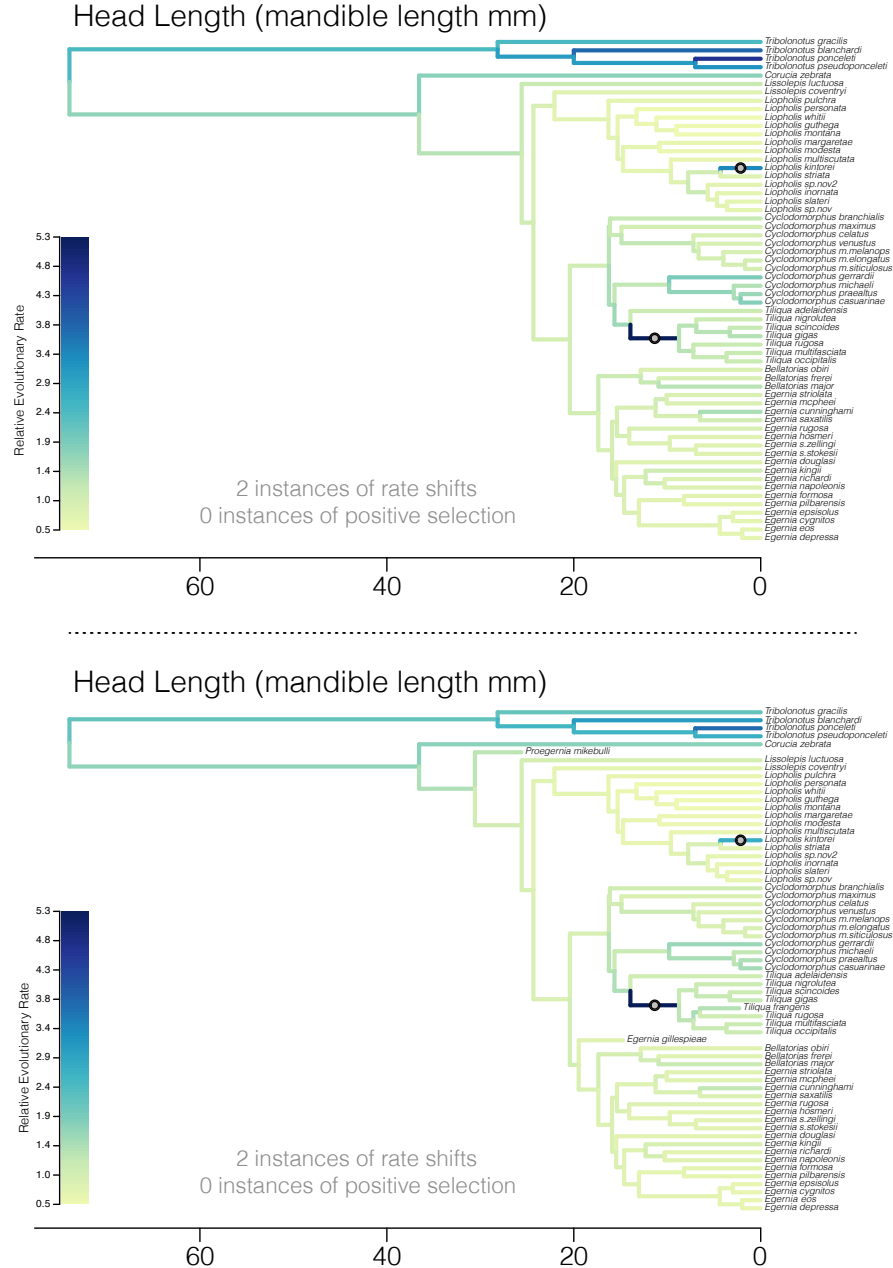


Figure S12: Incorporating extinct *Tiliquini* species does not change inferences of trait evolution. Trees show the estimated pattern of evolution of head length in *Tiliquini* skinks, with branches colored according to relative evolutionary rate and shifts indicated by circles on branches. (Top) Phylogenetic tree of extant *Tiliquini* and (bottom) phylogenetic tree of extinct and extant species return the same inferred shifts and qualitatively similar evolutionary rates. Additional fossil information may elucidate additional shifts in trait evolution, but are unlikely to erase inferred shifts. This is highlighted by the inclusion of *Tiliqua frangens* in the additional head length analysis. *T.frangens* has been estimated (Thorn et al. 2023) to have been more than twice the size of its close relative *T.rugosa* (SVL: 250 mm vs. 590 mm). In order to achieve this disparity in size, however, it is only necessary to increase the estimated evolutionary rate marginally. In comparison, a far higher evolutionary rate (5x the mean/background rate) is required to generate the comparatively huge heads of *Tiliqua* as shown on the dark blue branch in both trees.

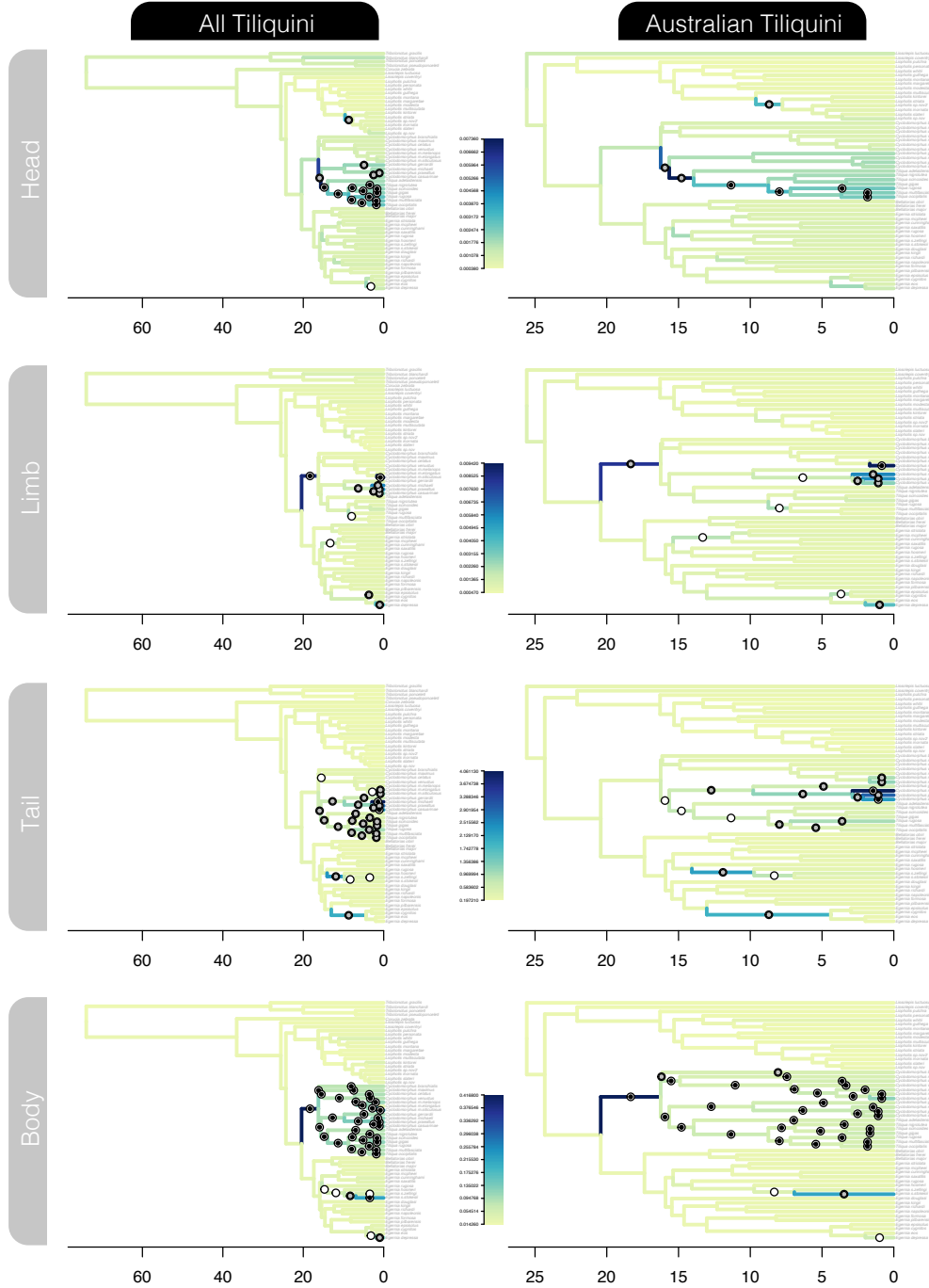


Figure S13: The inclusion of taxa on long branches (*Tribolonotus*, *Corucia*) does not bias the estimation of evolutionary rates across the rest of the tree. (left column) Analyses including non-Australian tiliquine taxa *Tribolonotus* and *Corucia*, and (right column) including **only** Australian tiliquine taxa. Trees show the output of the VR model applied to each labelled module (rows), with branches colored according to common color scales shown in the middle, plotted using `plot.VarRates.tree` in `Scripts/plotting_BayesTraits.R`. Estimated rates and inferred shifts are highly consistent across sampling strategies.

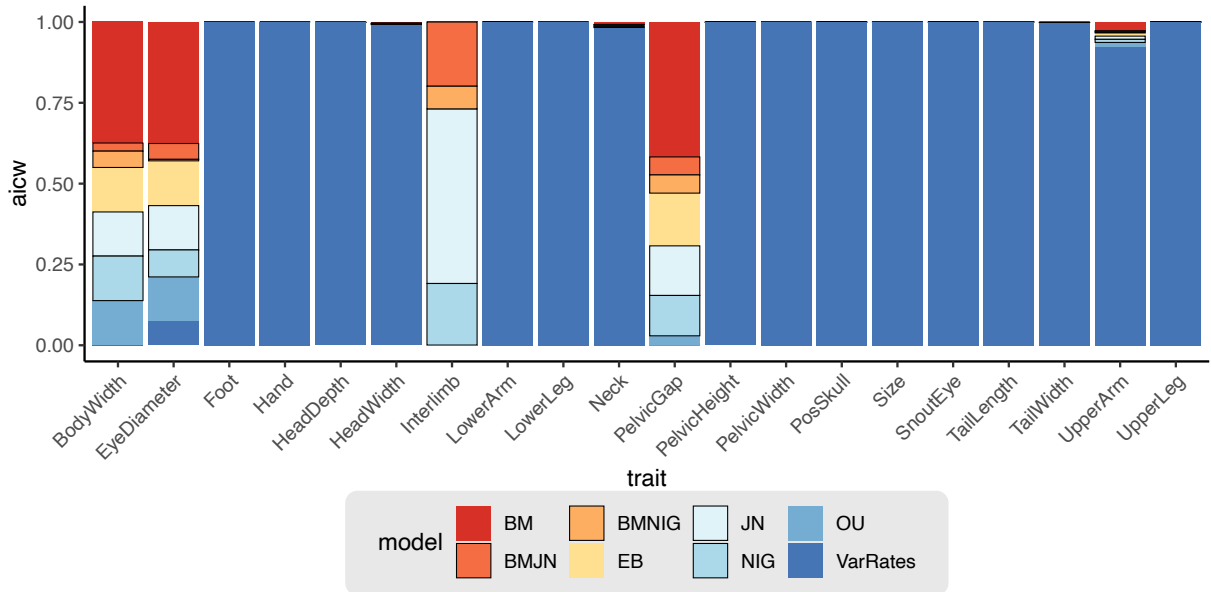
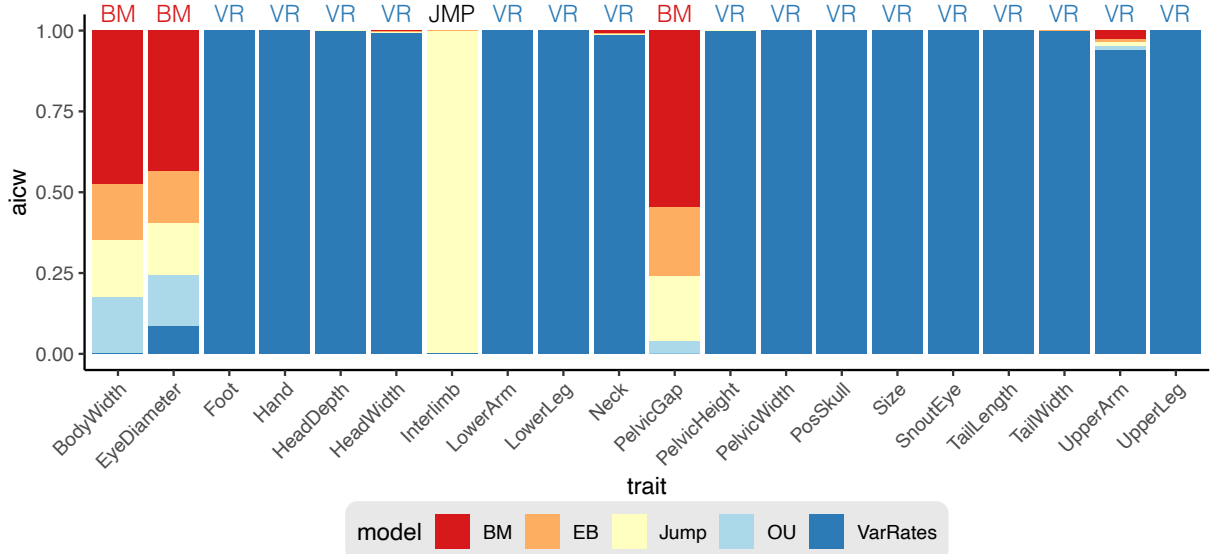


Figure S14: Comparative model fits for each of 19 morphological traits and the summary trait ‘Size’. Upper figure summarizes AICw by model type (BM, EB, ‘Jump’, OU, or VarRates), with the preferred model indicated above the column. Model preference required AICw of the best fitting model to be at least twice that of the next best fitting model. Bottom figure similarly shows model preference but with ‘Jump’ models expanded into their four alternative models (BMJN, BMNIG, JN, NIG) indicated by black outlines.

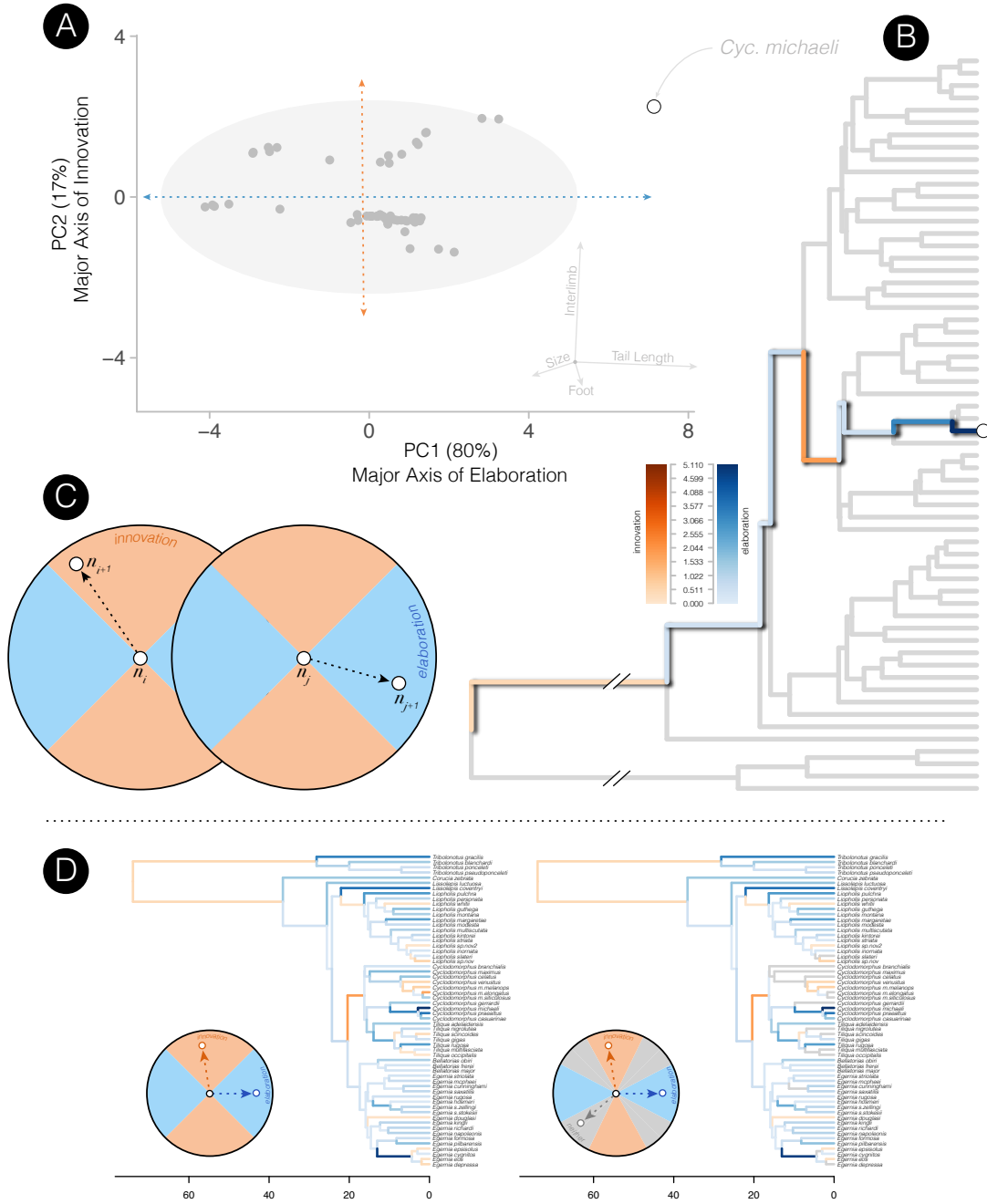


Figure S15: Diagram of method design and discretization of elaboration and innovation across Tiliquini skinks. (A) PCA biplot of first two axes indicating the path from root node to a specific tip, this path corresponds to the colored branches in the tree in (B). In (C) we show thresholds for designating elaborative and innovative trends, with parent node indicated at the center of the polar plot (n_i , n_j) and child nodes (n_{i+1} , n_{j+1}) plotted in either elaborative or innovative positions. Changing the threshold to a more conservative coding (D) does not change the overall inferences.

880 Concatenation and the Anomaly Zone

To investigate topological differences between coalescent and concatenated species trees we assessed the likelihood that discordant branches fall into the anomaly zone, where concatenation may be positively mislead. To identify anomalous branches we used *Anomaly Finder*³², using the script from Chafin et al. 2021.

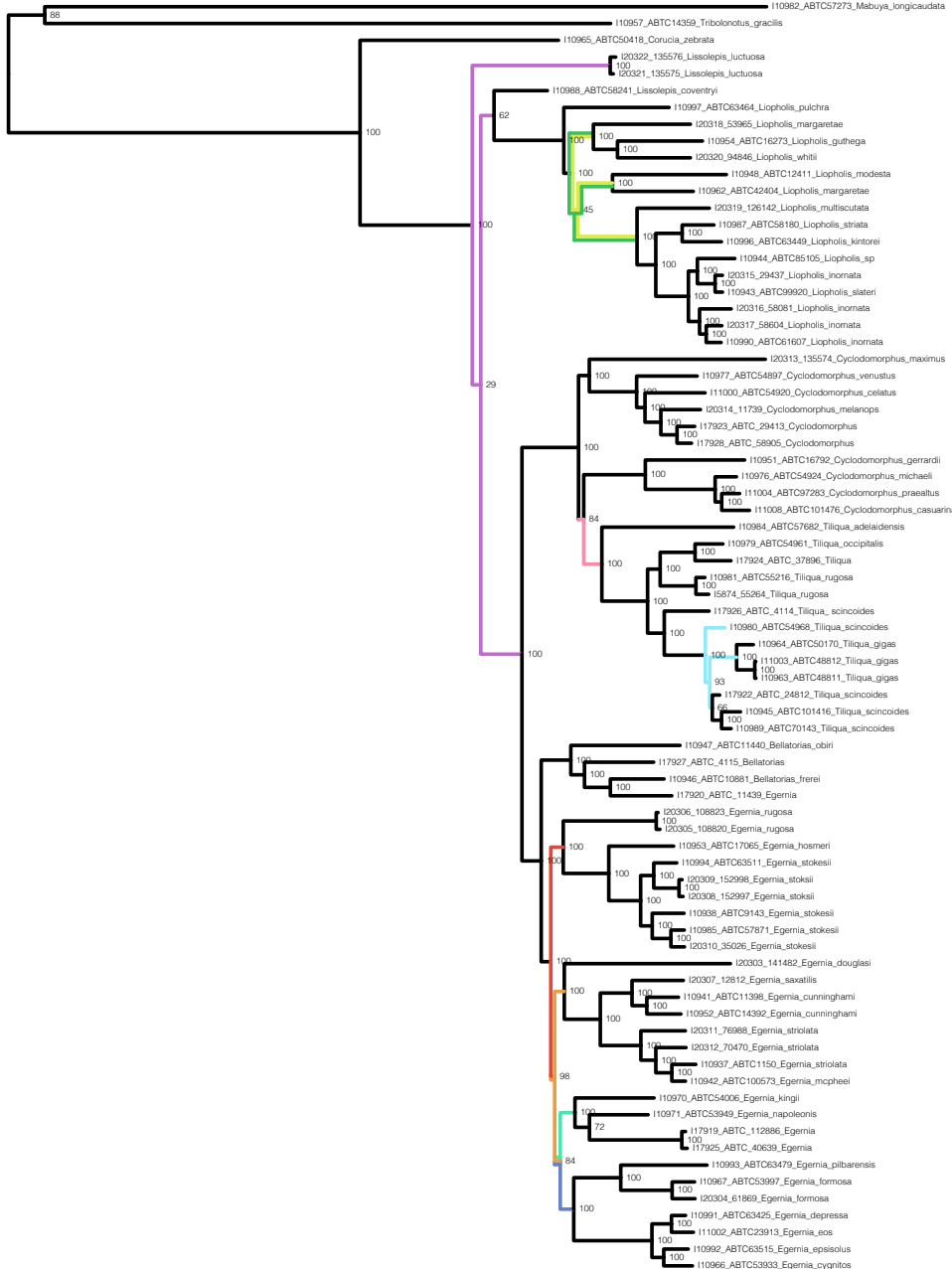


Figure S16: The Tiliquini phylogeny estimated from a concatenated and locus-partitioned alignment is likely misled by branches which fall into the anomaly zone. Colored branches correspond to the anomaly zone cladogram below and indicate edges which differ from the coalescent species tree.

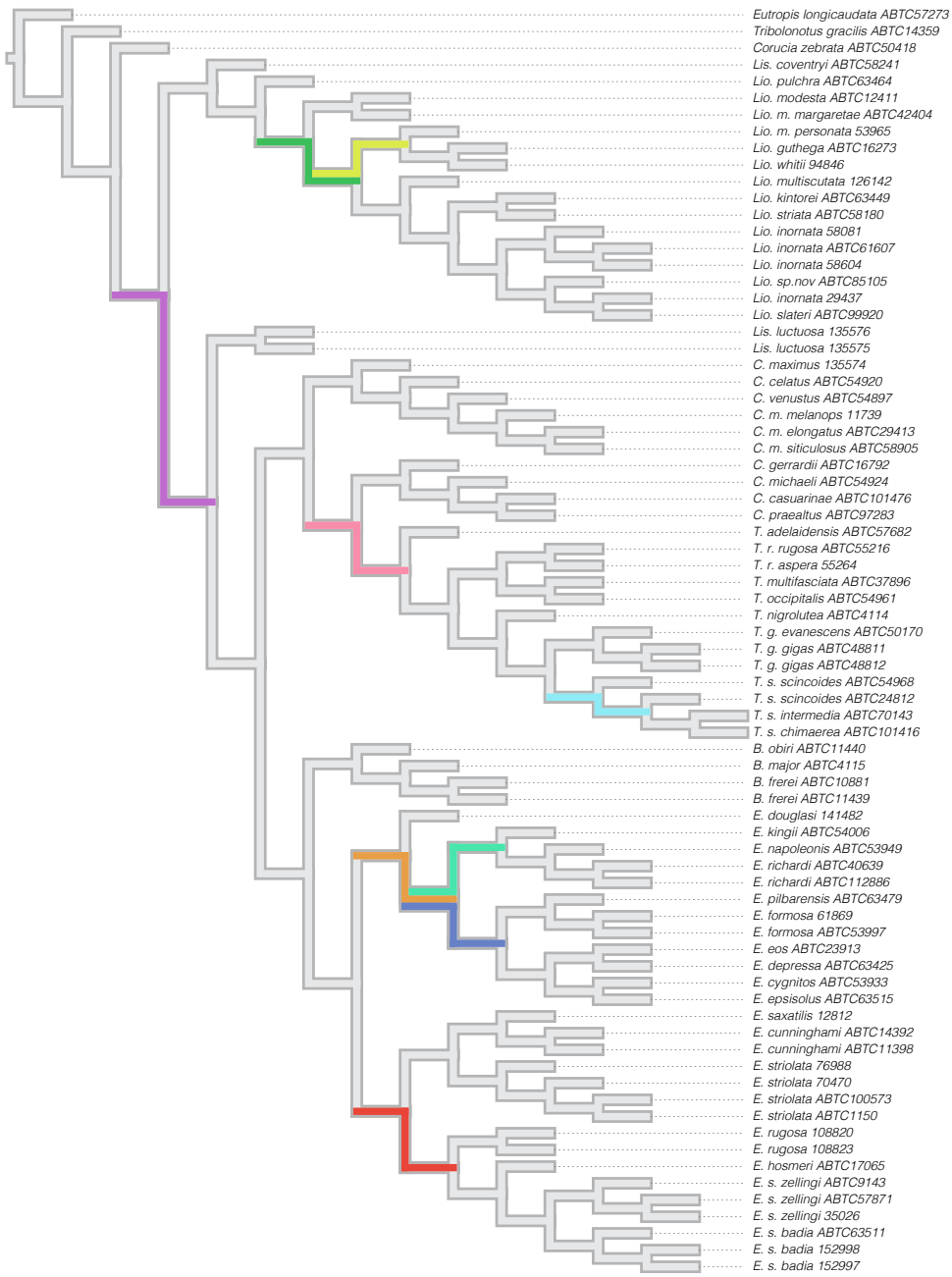


Figure S17: Colored branches indicate edges that fall within the anomaly zone and may provide misleading results under concatenation.

885 **Topology Tests**

We used a series of topology tests in IQ-TREE to investigate two nodes which bear taxonomic implications. We used the concatenated alignment and simplified phylogenies as the input. In each case the preferred topology is presented first followed by the two alternative resolutions to the bipartition. Significant differences are denoted by (-), and show decisive preference 890 for the coalescent species tree topology in comparison to alternative resolutions, reinforcing molecular phylogenetic evidence for the paraphyly of both *Cyclodomorphus* and *Lissolepis*.

Topology test for the paraphyly of *Cyclodomorphus* with regards to *Tiliqua*.

Tree topologies:

- 895 1. (Egernia,(C.maximus,(T.gigas,C.michaeli)); : coalescent/concatenated species trees
 2. (Egernia,(C.michaeli,(T.gigas,C.maximus)); : alternative *Cyclodomorphus* paraphyly
 3. (Egernia,(T.gigas,(C.maximus,C.michaeli)); : *Cyclodomorphus* monophyly

Tree	logL	deltaL	bp-RELL	p-KH	p-SH	p-WKH	p-WSH	c-ELW	p-AU
1.	-1142007.338	0	0.97(+)	0.98(+)	1(+)	0.98(+)	0.993(+)	0.971(+)	0.981(+)
2.	-1142067.499	60.161	0.03(-)	0.02(-)	0.026(-)	0.02(-)	0.039(-)	0.0294(-)	0.021(-)
3.	-1142110.488	103.15	0(-)	0(-)	0(-)	0(-)	0(-)	2.08e-10(-)	1.79e-05(-)

Topology tests for the paraphyly of *Lissolepis*.

Tree topologies:

- 900 1. (Outgroup,((Lis.luctuosa,E.striolata),(Lis.coventryi,Lio.inornata))); : coalescent species tree
 2. (Outgroup,(Lis.luctuosa,(E.striolata,(Lis.coventryi,Lio.inornata)))); : concatenated species tree
 3. (Outgroup,((Lis.coventryi,Lis.luctuosa),(Lio.inornata,E.striolata))); : *Lissolepis* monophyly

Tree	logL	deltaL	bp-RELL	p-KH	p-SH	p-WKH	p-WSH	c-ELW	p-AU
1.	-1326723.218	0	1(+)	1(+)	1(+)	1(+)	1(+)	1(+)	0.995(+)
2.	-1326798.358	75.141	0(-)	0(-)	0.122(+)	0(-)	0(-)	8.47e-07(-)	0.00491(-)
3.	-1327315.329	592.11	0(-)	0(-)	0(-)	0(-)	0(-)	1.9e-174(-)	3.58e-05(-)

Additional Supplementary Figures

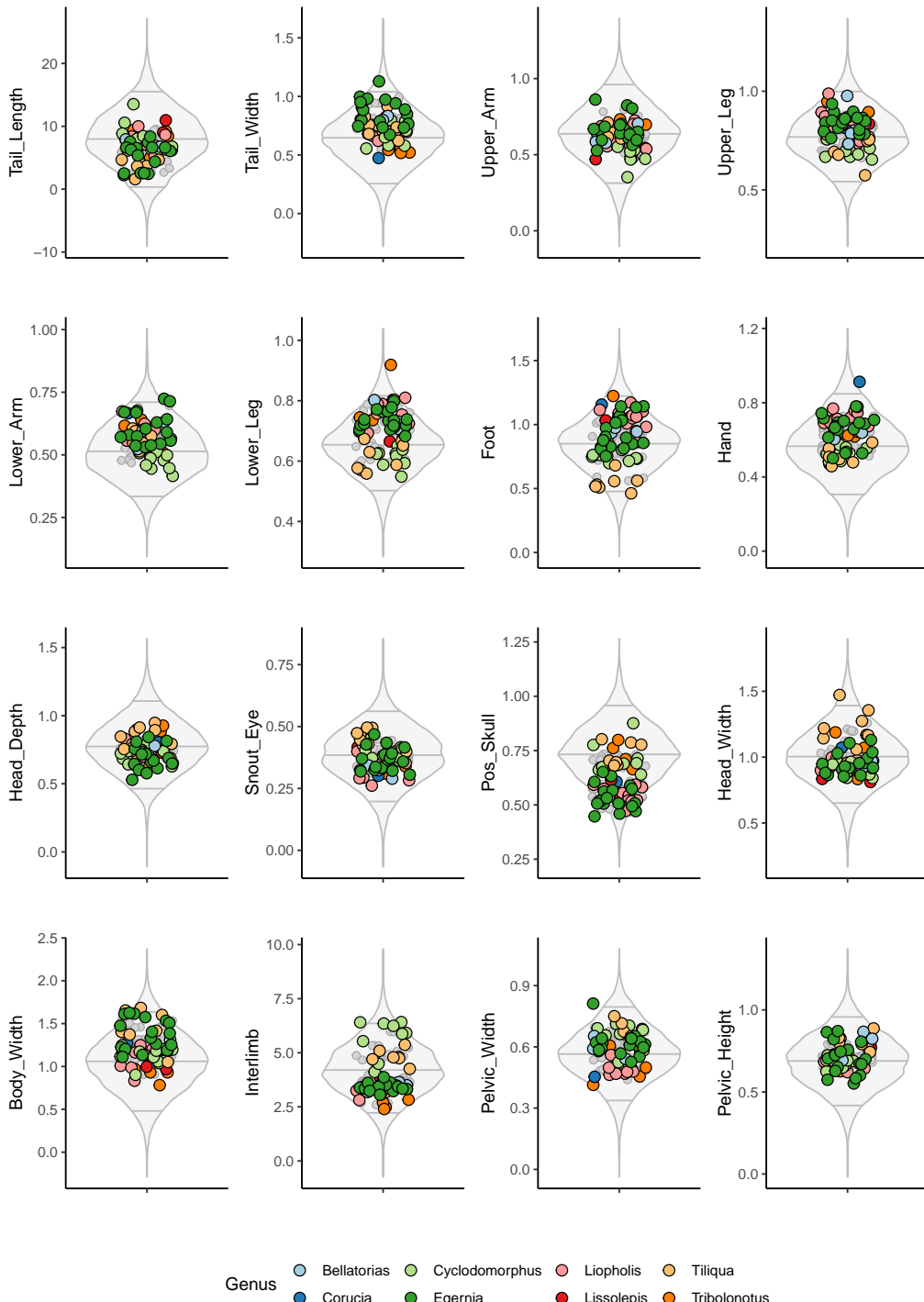


Figure S18: Empirical phenotypes generally conform to expected trait values of data simulated under uncorrelated evolution, showing limited ability of selection to exceed null expectations in Tiliquini skinks. Circles represent empirical trait values per species, colored by genus, with grey representing ancestral states. Transformed traits size corrected by log-shape ratios are plotted against 500 simulated datasets for each trait. Simulated traits are plotted as a grey violin plot summarizing the distribution of trait values, with 65%, 50%, and 95% quantiles plotted as horizontal lines. Simulations were generated with MVMORPH using as input the theta–root and sigma values estimated by MVMORPH assuming a constant-rate Brownian Motion model.

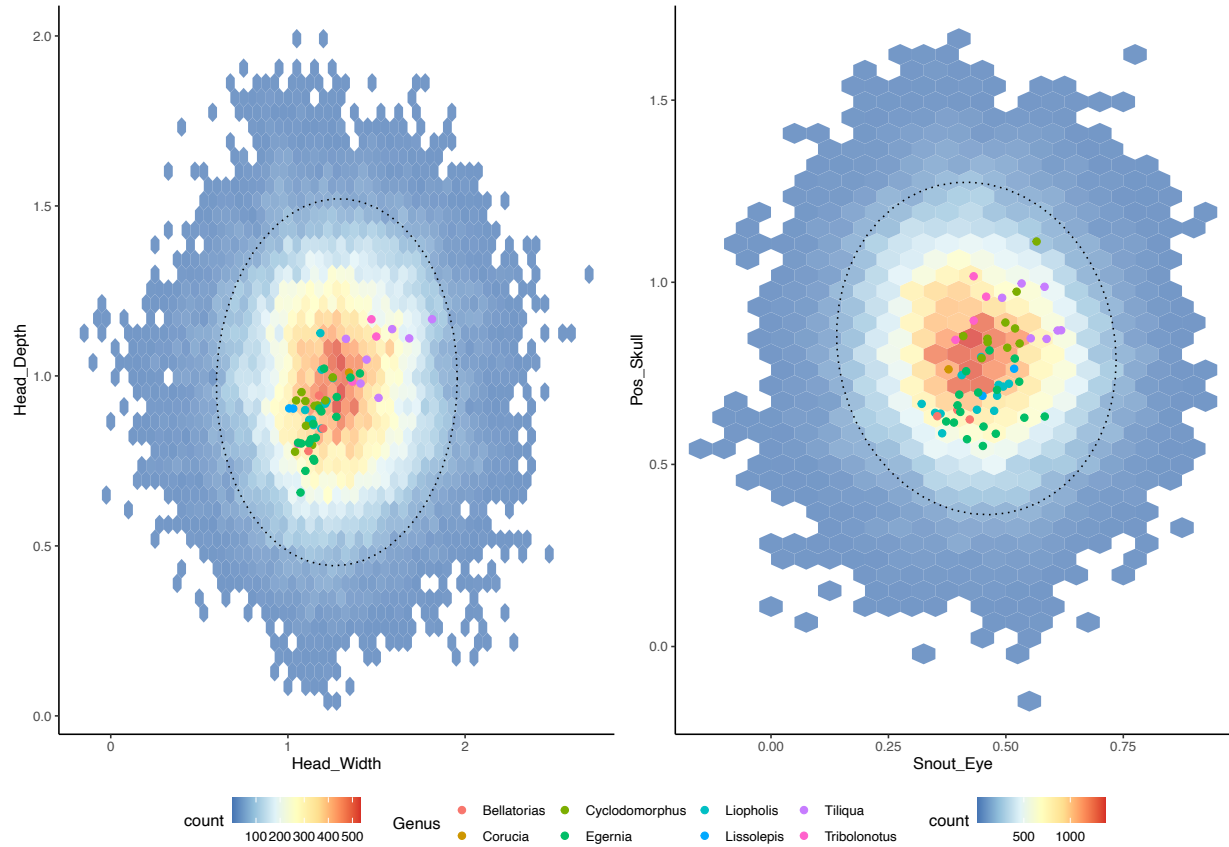


Figure S19: Empirical phenotypes generally conform to expected trait values of data simulated under uncorrelated evolution, showing limited ability of selection to exceed null expectations in Tiliquini skinks. Hexagonal heatplot in background shows the distribution of trait values from 500 datasets simulated under rates from empirical estimates. Warmer colors indicate greater density of simulated points. Circular points indicate empirical trait values and are colored according to the genus the belong to. The dotted ellipse contains 95% of the simulated data (95% confidence interval).

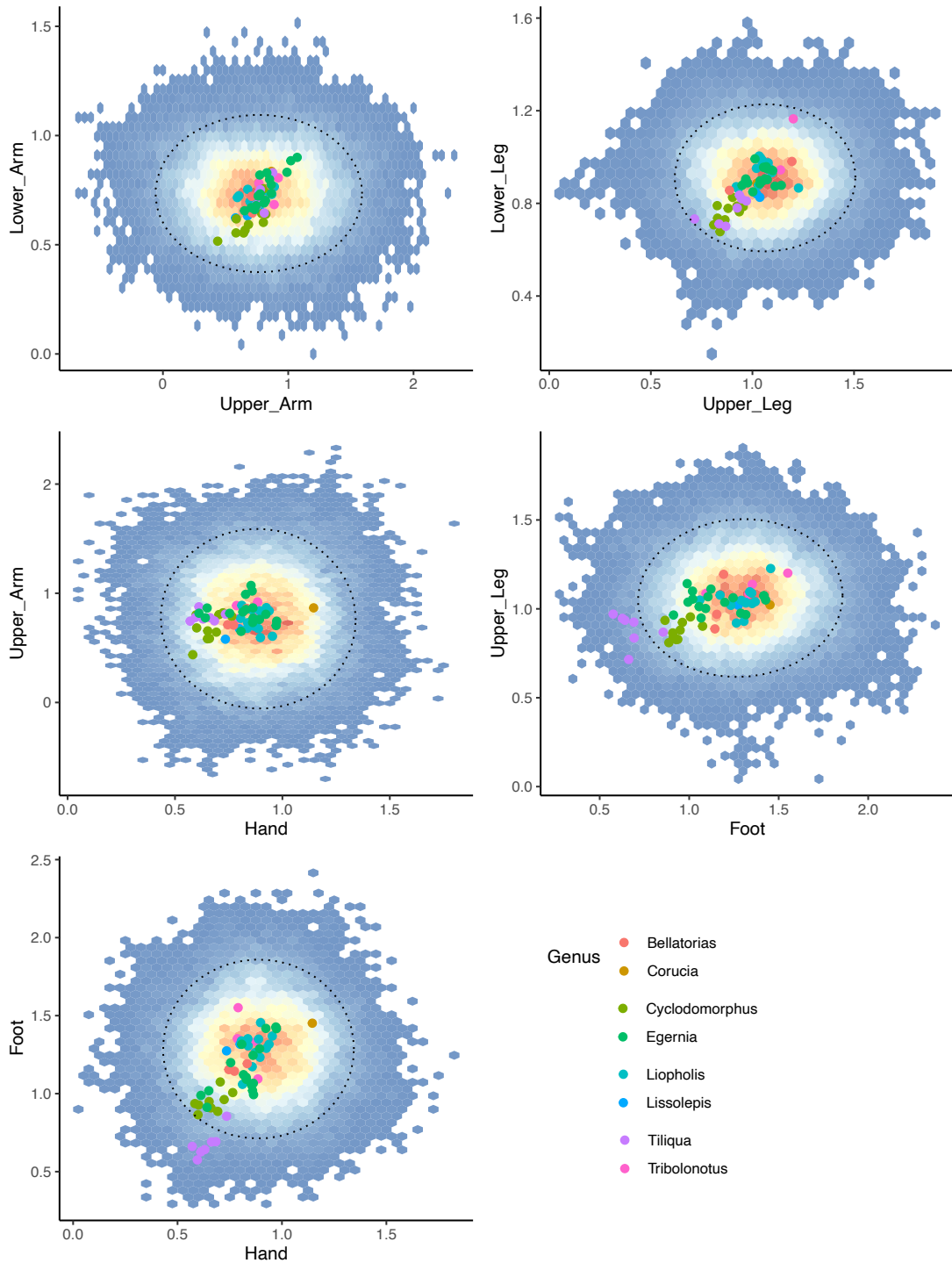


Figure S20: Empirical phenotypes generally conform to expected trait values of data simulated under uncorrelated evolution, showing limited ability of selection to exceed null expectations in *Tiliquini* skinks. Hexagonal heatplot in background shows the distribution of trait values from 500 datasets simulated under rates from empirical estimates. Warmer colors indicate greater density of simulated points. Circular points indicate empirical trait values and are colored according to the genus they belong to. The dotted ellipse contains 95% of the simulated data (95% confidence interval).

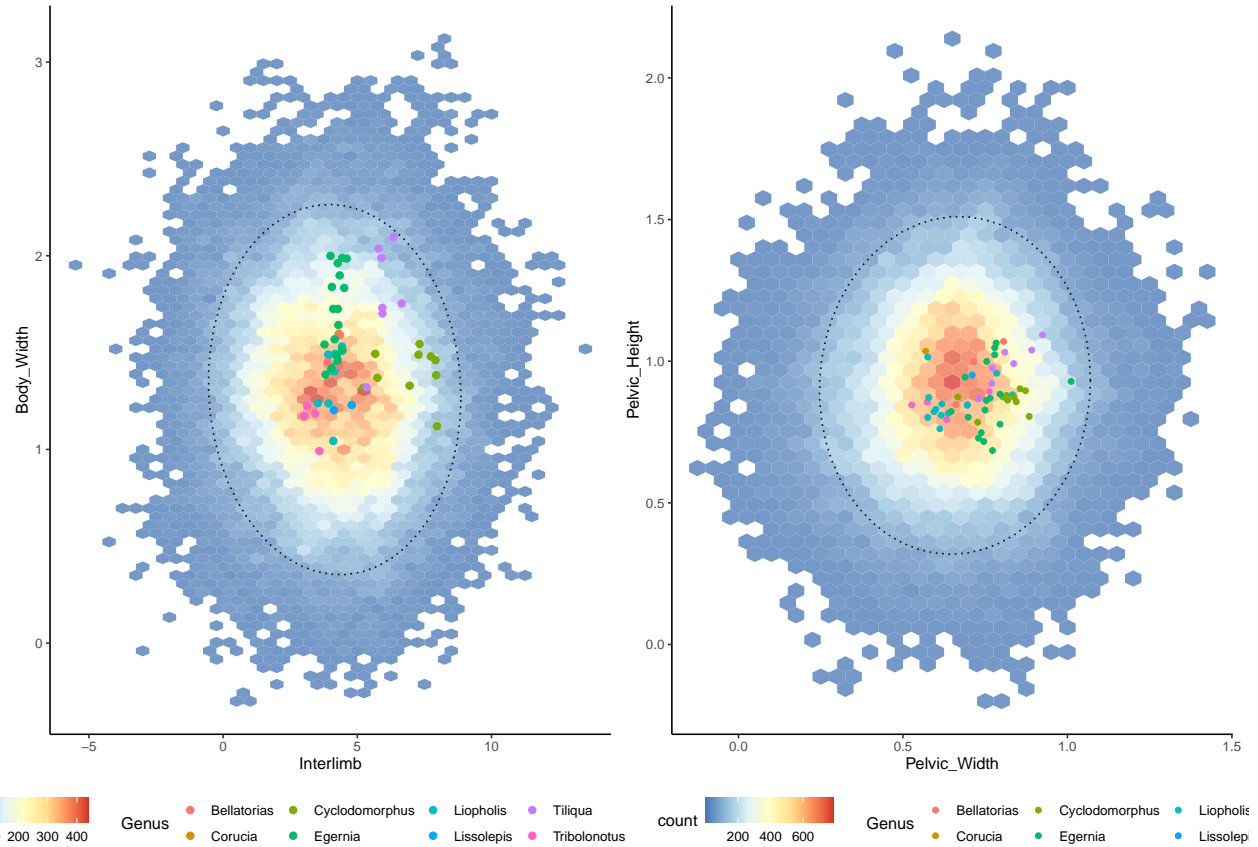


Figure S21: Empirical phenotypes generally conform to expected trait values of data simulated under uncorrelated evolution, showing limited ability of selection to exceed null expectations in Tiliquini skinks. Hexagonal heatplot in background shows the distribution of trait values from 500 datasets simulated under rates from empirical estimates. Warmer colors indicate greater density of simulated points. Circular points indicate empirical trait values and are colored according to the genus they belong to. The dotted ellipse contains 95% of the simulated data (95% confidence interval).

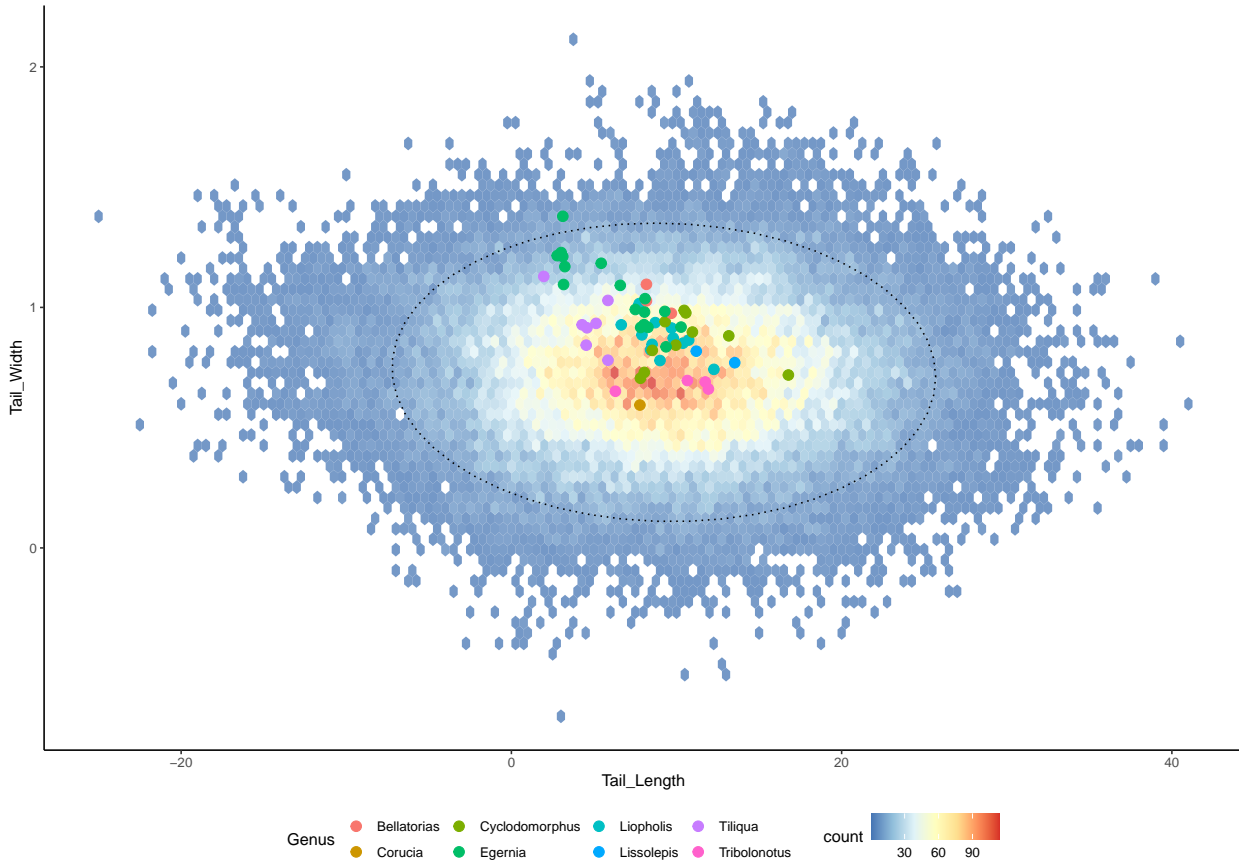


Figure S22: Empirical phenotypes generally conform to expected trait values of data simulated under uncorrelated evolution, showing limited ability of selection to exceed null expectations in Tiliquini skinks. Hexagonal heatplot in background shows the distribution of trait values from 500 datasets simulated under rates from empirical estimates. Warmer colors indicate greater density of simulated points. Circular points indicate empirical trait values and are colored according to the genus they belong to. The dotted ellipse contains 95% of the simulated data (95% confidence interval).

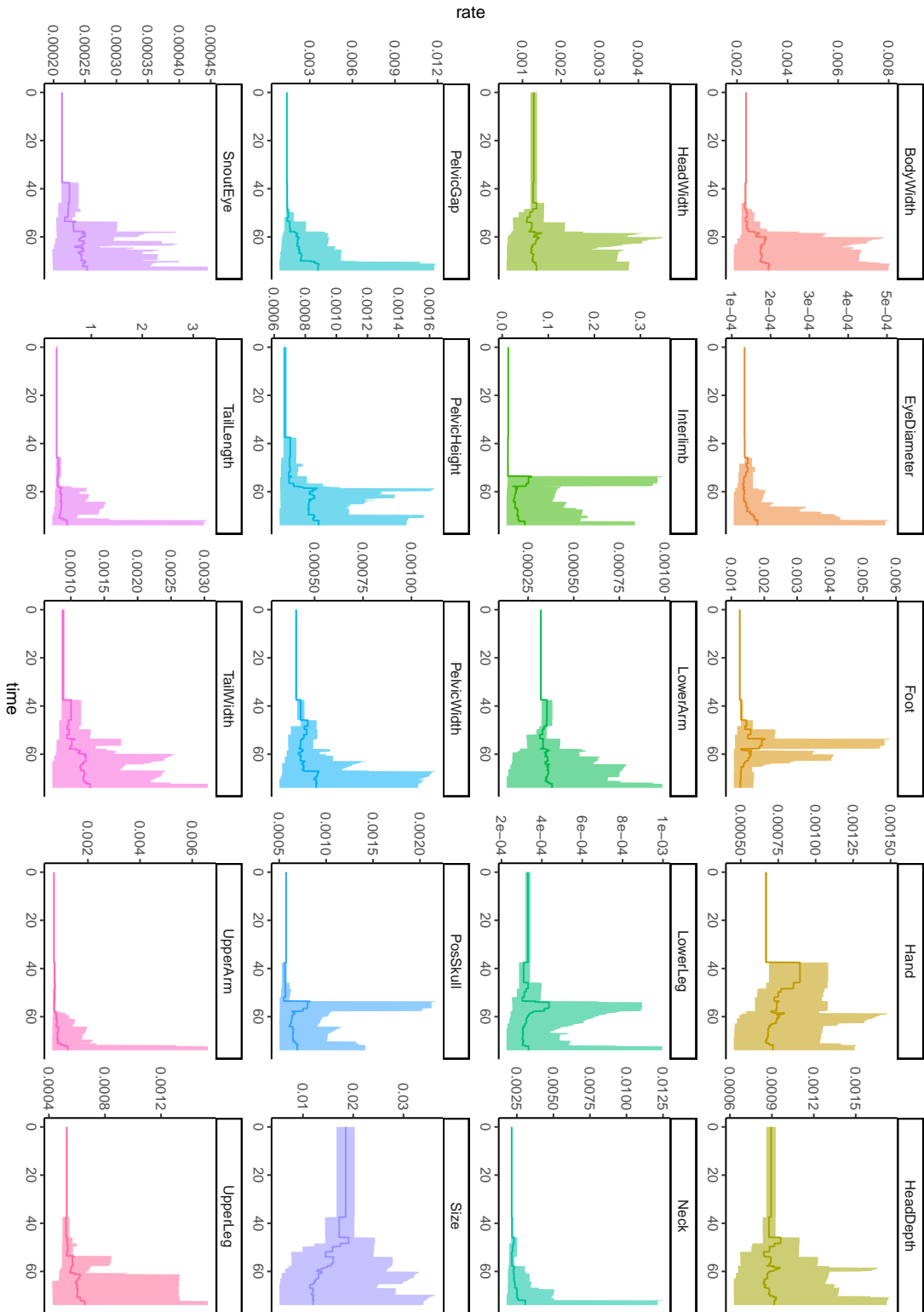


Figure S23: Mean evolutionary rates through time for all morphological traits with envelopes containing 95% quantiles.

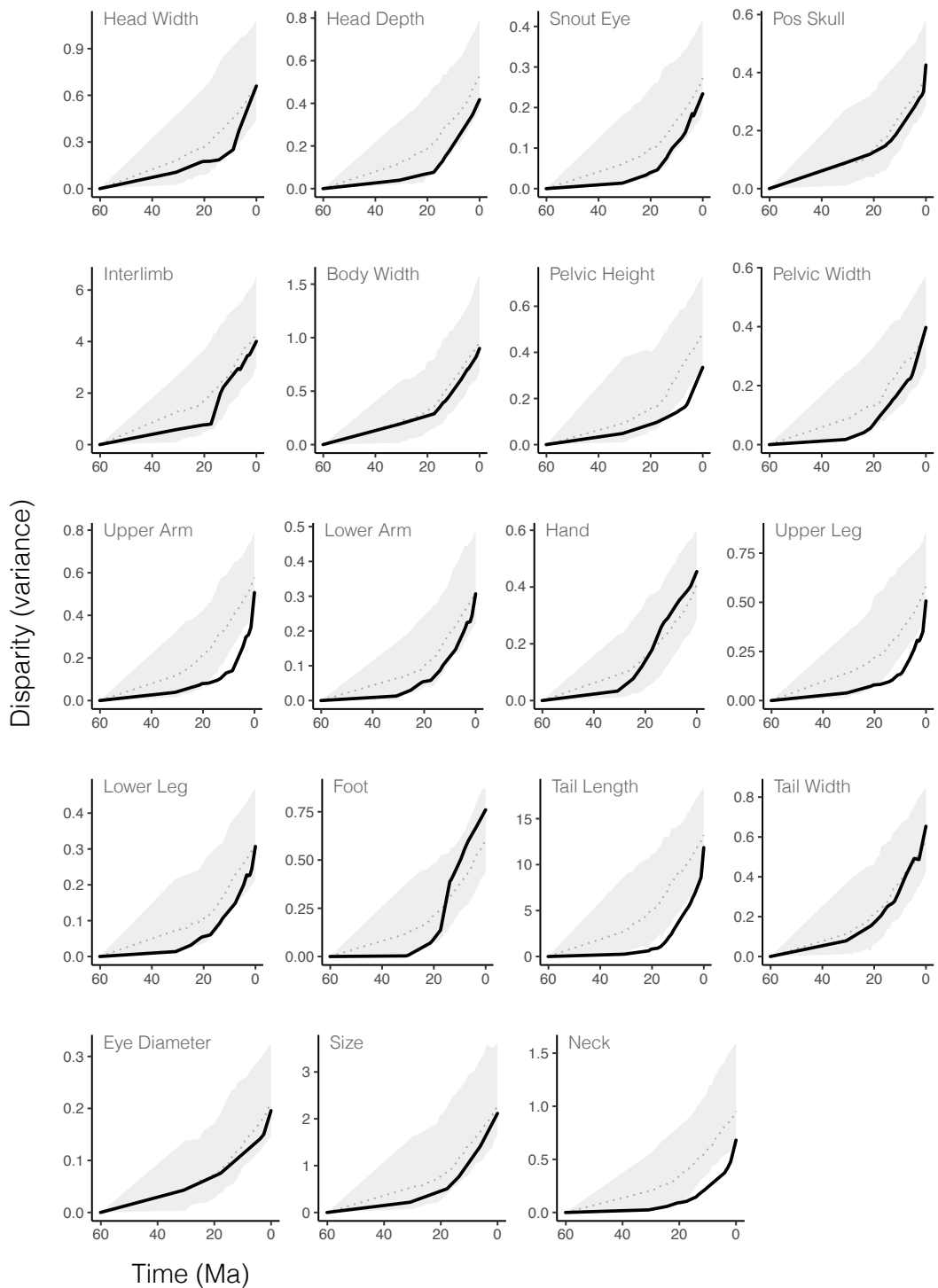


Figure S24: Disparity (variance) through time for morphological traits is often lower than expected under BM for long periods of time early in the evolution of this group. Empirical trends are shown in black with 95% quantiles of disparity for simulated datasets in grey.

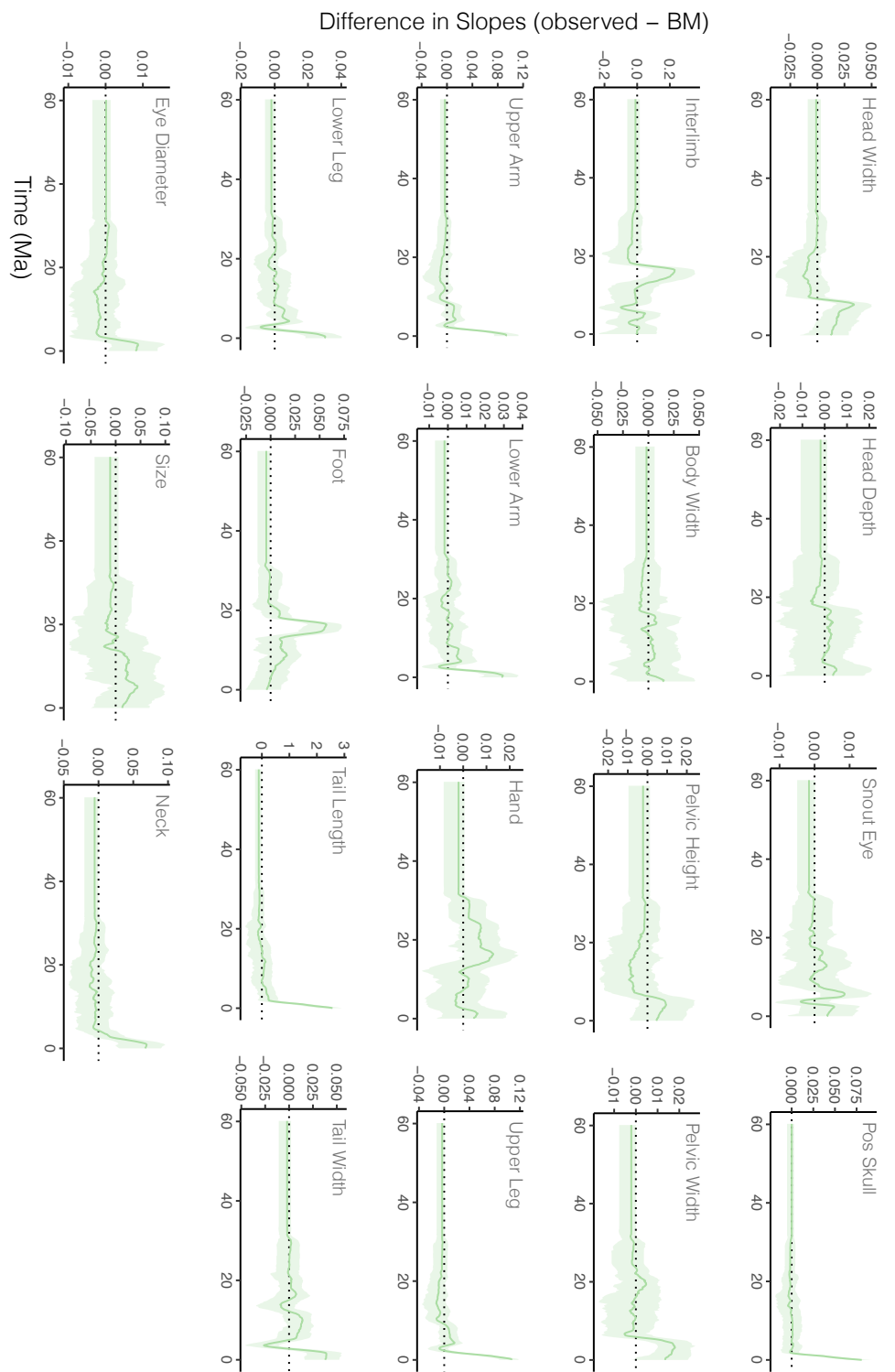


Figure S25: Individual traits show varied temporal patterns of morphological expansion and niche packing. Solid green line shows the mean trend and green envelope shows the 95% quantiles.

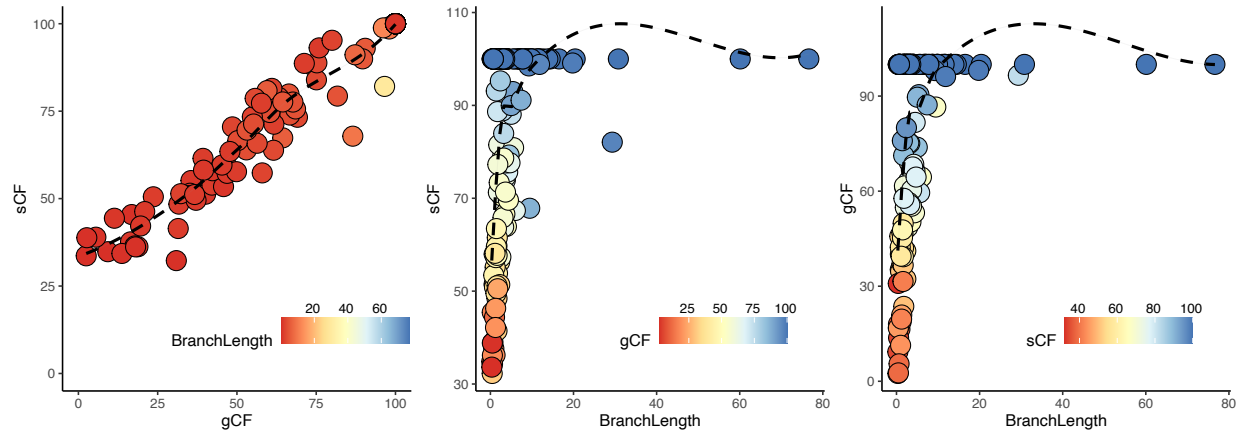


Figure S26: Concordance factors show a positive relationship with increasing branch length. Both site- and gene concordance factors increase support with increasing branch lengths (time), but show saturation ($sCF=100$, $gCF=100$) on branches ≥ 10 million years long.

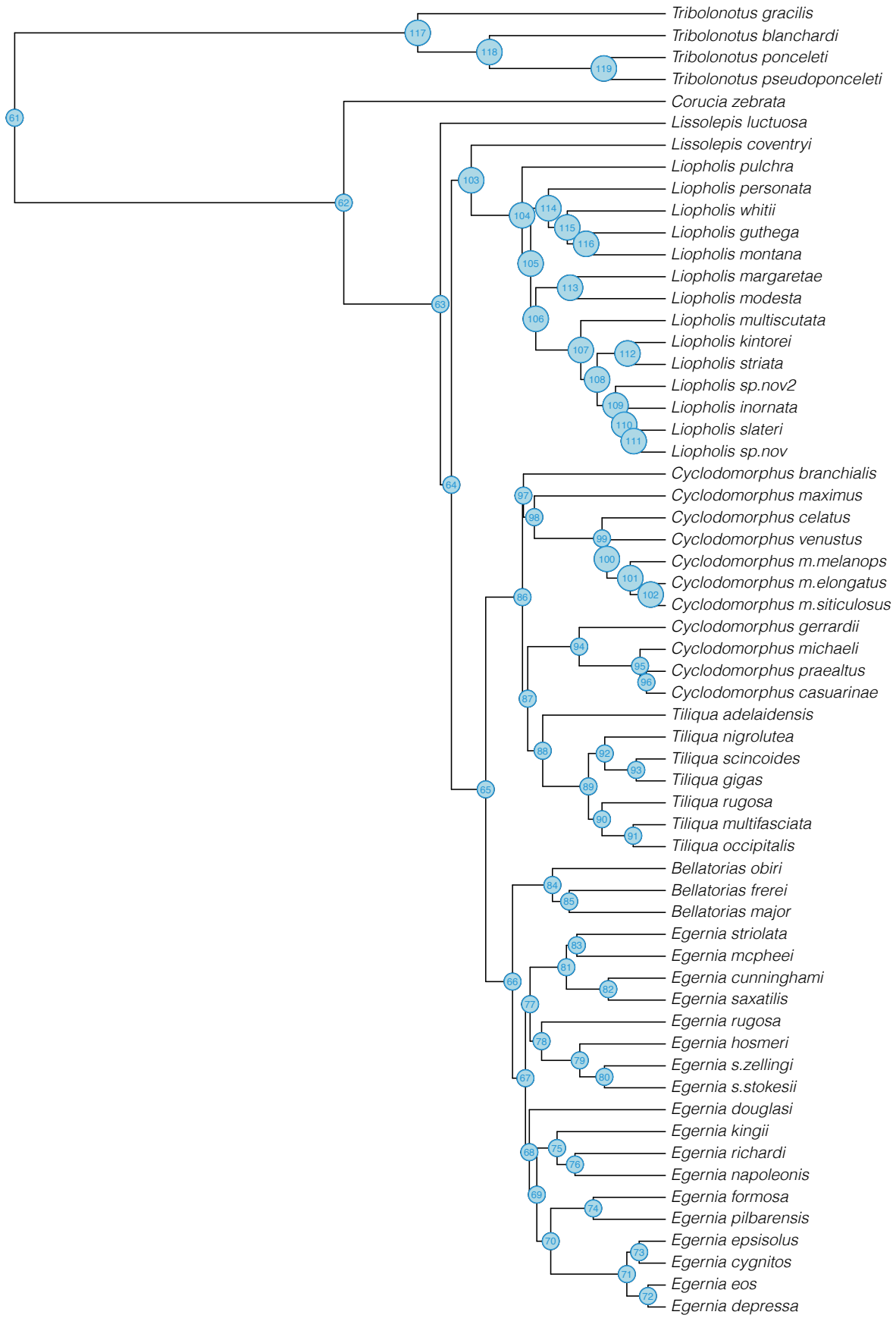


Figure S27: Node numbers of MCMCtree species tree used for analyses.

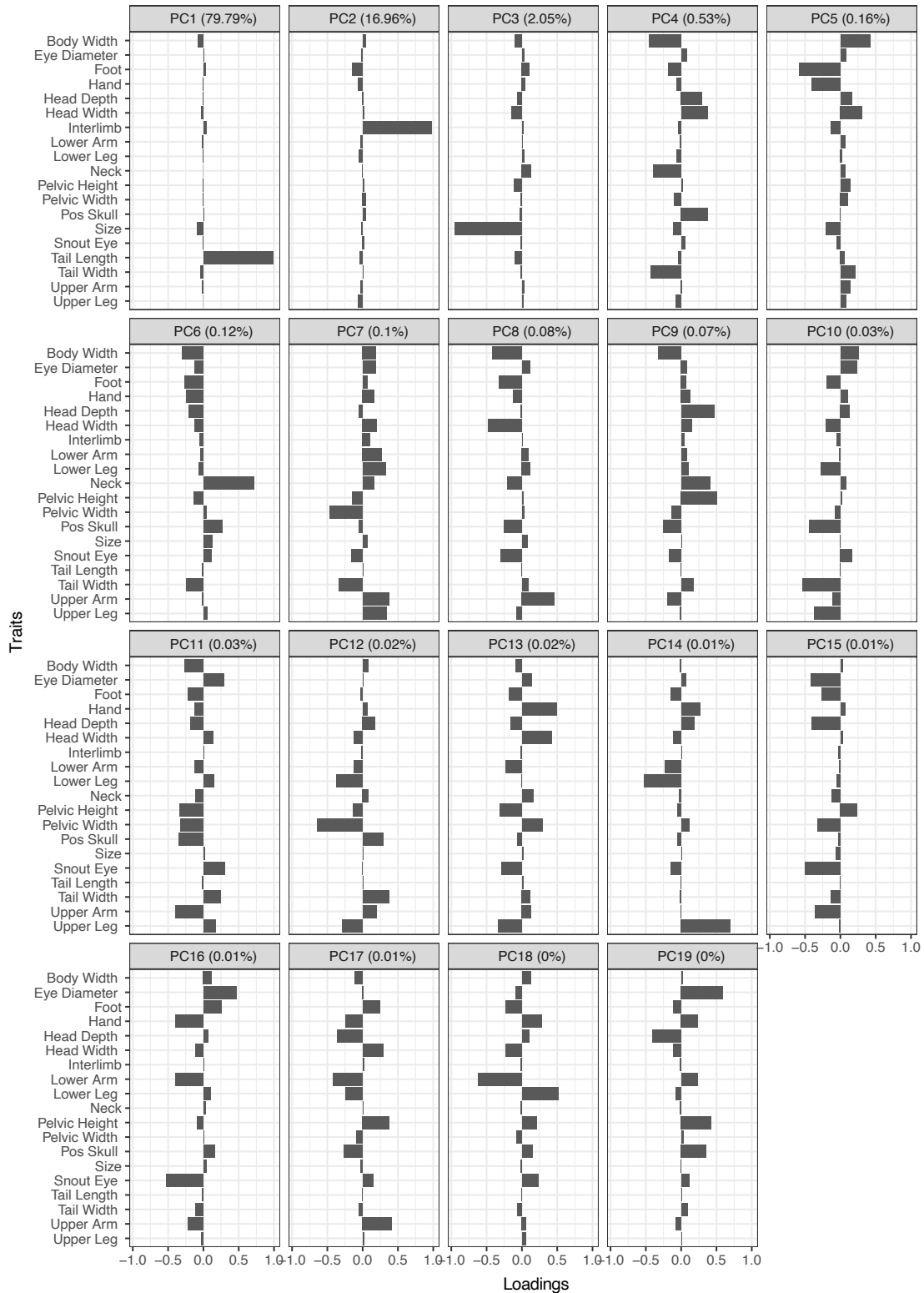


Figure S28: PCA loadings for 19 focal traits across all *Tiliquini* skinks. The first three principal components account for >98% of the variance, and are primarily explained by tail length, interlimb length, and size.

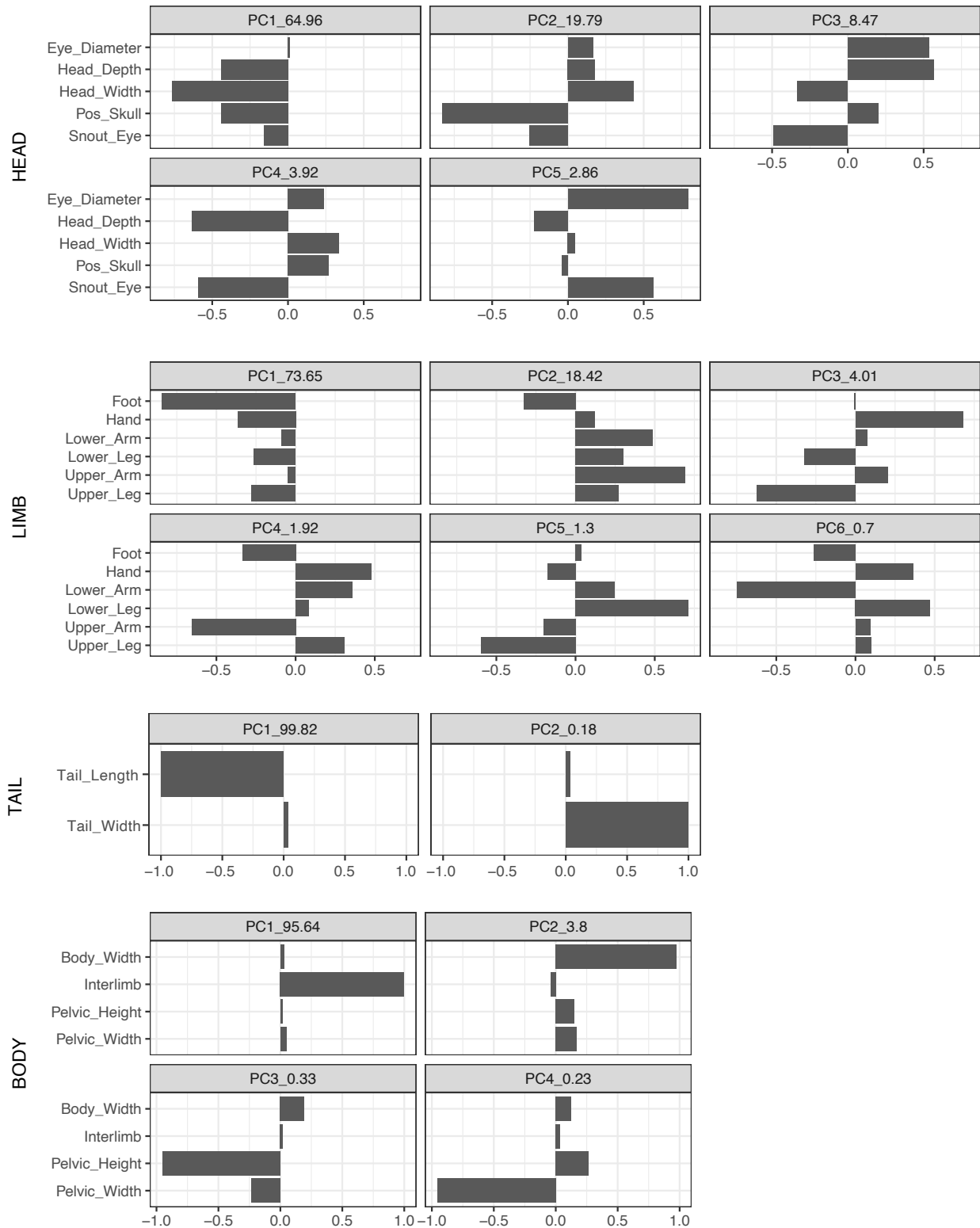


Figure S29: PCA loadings for 19 focal traits analyzed by module across all Tiliquini skinks.

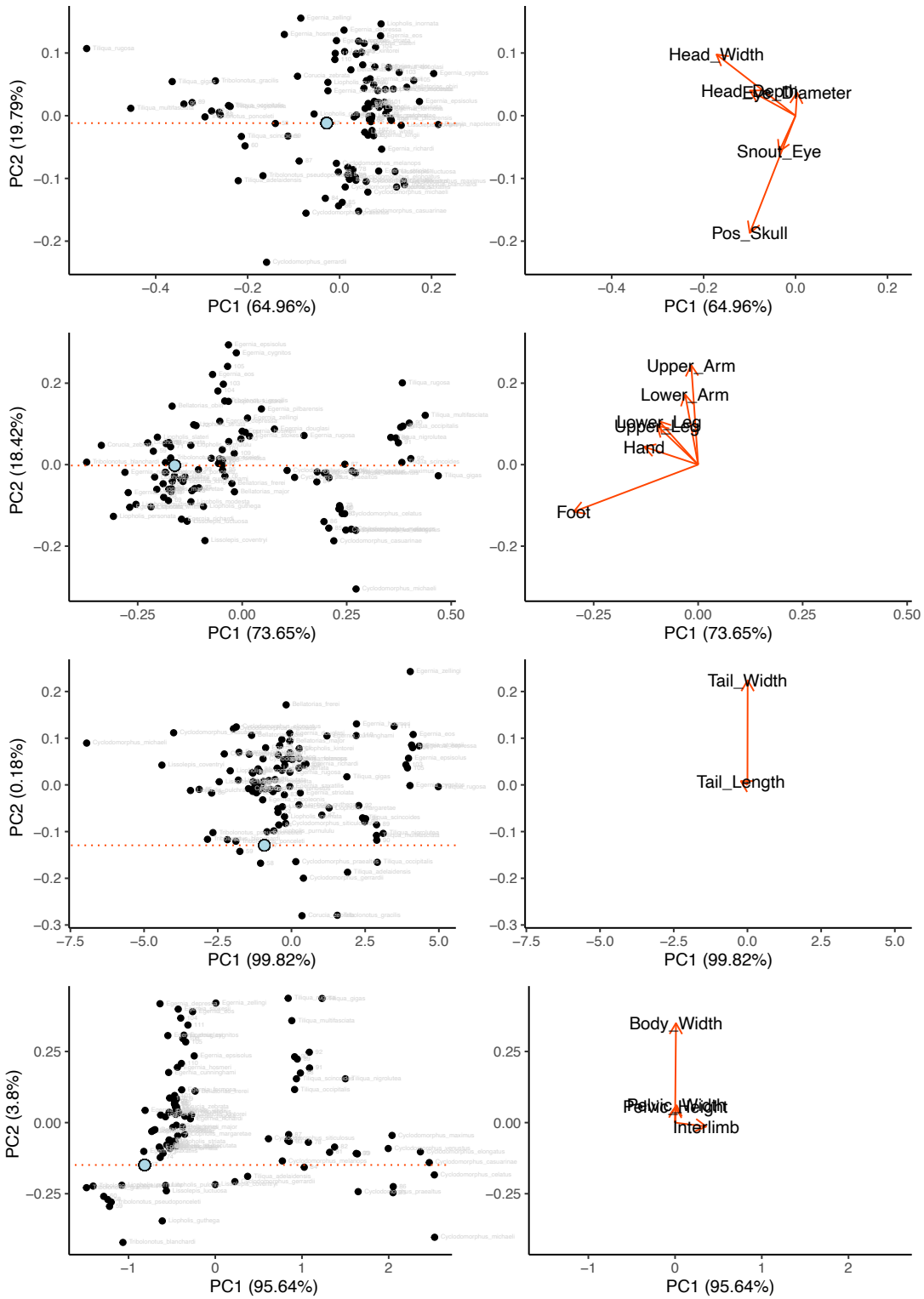


Figure S30: Biplots of the first two PC axes from analyses of modules.

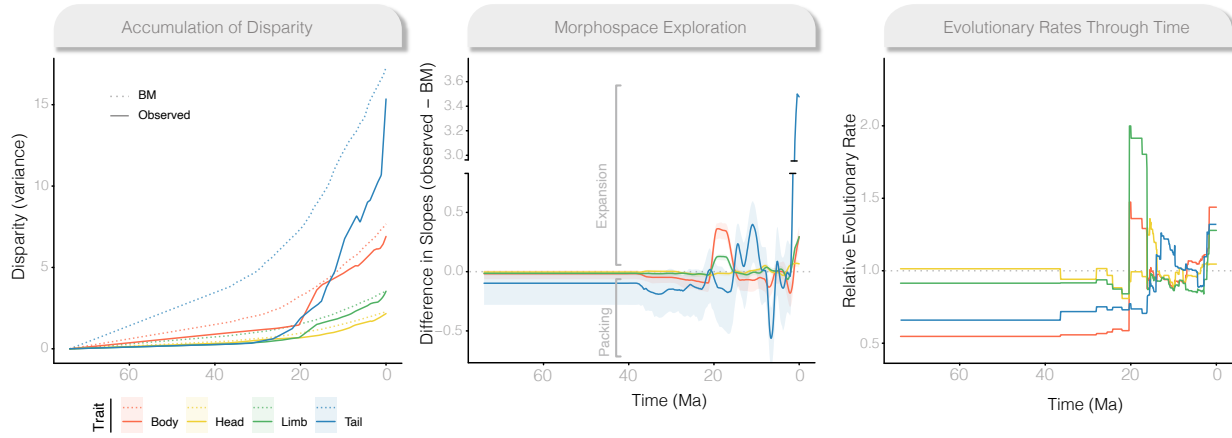


Figure S31: Evolutionary trajectories vary widely across modules and through time. (left) Accumulation of multivariate disparity (as variance) through time for each module (solid lines) compared to Brownian Motion (dotted lines). (center) The comparison of slopes of each module to BM highlights periods of morphological expansion (values greater than 0) and conservatism (values less than 0). (right) Evolutionary rates across modules are highly heterogeneous (see three different scales for y axis), showing periods of temporal variability, as well as high variances within modules and among traits (Fig.S23–S25). Figures represent analyses of all samples, and show some differences from Fig.3. Differences can likely be attributed to the underestimation of mean rates resulting from the long bare branches leading to *Corucia* and *Tribolodonotus*.